

THESE EN COTUTELLE

Ecole Centrale de Lyon - Université Polytechnique de Lodz

présentée devant

L'ECOLE CENTRALE DE LYON

pour obtenir le titre de **DOCTEUR**

spécialité : **MATERIAUX**

par

Tomasz LIŚKIEWICZ

MSc, Eng Université Polytechnique de Lodz

HARD COATINGS DURABILITY UNDER VARIABLE FRETTING WEAR CONDITIONS

**ENDURANCE DES DEPOTS DURS
SOUS SOLLICITATIONS VARIABLES
DE FRETTING WEAR**

Soutenue le 29 Novembre 2004 devant la commission d'examen

MM. P. KAPSA, Directeur de Recherche CNRS
J.P. CELIS, Professeur
S. MISHLER, Docteur
C. DONNET, Professeur
B. WENDLER, Professeur
S. FOUVRY, Docteur
P. KULA, Professeur
S. DEYBER

Président du jury
Rapporteur
Rapporteur
Membre
Dir. de Thèse
Dir. de Thèse
Invité
Invité

To Monika and Wiktor

To my Parents

ECOLE CENTRALE DE LYON

Liste des personnes habilitées à diriger des recherches

A	ALLARD Bruno	maître de conférence	CEGELY	INSA
	AIT-EL-HAJD Smaïl	professeur	GRESTI	ECL
	ARQUES Philippe	professeur		ECL
	AURIOL Philippe	professeur	CEGELY	ECL
B	BAILLY Christophe	professeur	LMFA	ECL
	BATAILLE Jean	professeur	LMFA	UCBL
	BAYADA Guy	professeur	MAPLY	INSA
	BEN HADID Hamda	professeur	LMFA	UCBL
	BERGHEAU Jean-Michel	professeur	LTDS	ENISE
	BEROUAL Abderrahmane	professeur	CEGELY	ECL
	BERTOGLIO Jean-Pierre	directeur de recherche	LMFA	CNRS
	BLAIZE Alain	maître de conférence	LTDS	UCBL
	BLANC-BENON Philippe	directeur de recherche	LMFA	CNRS
	BLANCHET Robert	professeur	LEOM	ECL
	BUFFAT Marc	professeur	LMFA	UCBL
	BUREAU Jean-Claude	professeur	CEGELY	INSA
C	CAMBON Claude	directeur de recherche	LMFA	CNRS
	CAMBOU Bernard	professeur	LTDS	ECL
	CARRIERE Philippe	chargé de recherche	LMFA	CNRS
	CHAMBAT Michèle	professeur	MAPLY	UCBL
	CHAMPAGNE Jean-Yves	maître de conférence	LMFA	INSA
	CHAMPOUSSIN J-Claude	professeur	LMFA	ECL
	CHANTE Jean-Pierre	professeur	CEGELY	INSA
	CHEN Liming	professeur	ICTT	ECL
	CLERC Guy	professeur	CEGELY	UCBL
	COMTE-BELLOT Geneviève	professeur émérite	LMFA	ECL
	COQUILLET Bernard	maître de conférence	IFOS	ECL
	CREPEL Pierre	chargé de recherche	MAPLY	CNRS
D	DAVID Bertrand	professeur	ICTT	ECL
	DUBUJET Phillipe	maître de conférence	LTDS	ECL
E	ESCODIE Dany	directeur de recherche	LMFA	CNRS
F	FERRAND Pascal	directeur de recherche	LMFA	CNRS
	FOUVRY Siegfried	chargé de recherche	LTDS	CNRS
G	GAFFIOT Frédéric	professeur	LEOM	ECL
	GAGNAIRE Alain	maître de conférence	LEOM	ECL
	GALLAND Marie-Annick	maître de conférence	LMFA	ECL
	GARRIGUES Michel	directeur de recherche	LEOM	CNRS
	GAY Bernard	professeur	LMFA	UCBL
	GENCE Jean-Noël	professeur	LMFA	UCBL
	GENDRY Michel	chargé de recherche	LEOM	CNRS
	GEORGES Jean-Marie	professeur émérite	LTDS	ECL
	GRENET Geneviève	directeur de recherche	LEOM	CNRS
	GUIRALDENQ Pierre	professeur émérite	IFOS	ECL

ECOLE CENTRALE DE LYON

Liste des personnes habilitées à diriger des recherches

H	<i>HAMADICHE Mahmoud</i>	<i>maître de conférence</i>	LMFA	UCBL
	<i>HEIBIG Amaud</i>	<i>professeur</i>	MAPLY	INSA
	<i>HELLOUIN Yves</i>	<i>maître de conférence</i>		ECL
	<i>HENRY Daniel</i>	<i>chargé de recherche</i>	LMFA	CNRS
	<i>HERRMANN Jean-Marie</i>	<i>directeur de recherche</i>	IFOS	CNRS
	<i>HOLLINGER Guy</i>	<i>directeur de recherche</i>	LEOM	CNRS
J	<i>JAFFREZIC-RENAULT Nicole</i>	<i>directeur de recherche</i>	IFOS	CNRS
	<i>JEANDEL Denis</i>	<i>professeur</i>	LMFA	ECL
	<i>JEZEQUEL Louis</i>	<i>professeur</i>	LTDS	ECL
	<i>JOSEPH Jacques</i>	<i>professeur</i>	LEOM	ECL
	<i>JUVE Daniel</i>	<i>professeur</i>	LMFA	ECL
	<i>JUVE Denyse</i>	<i>ingénieur de recherche</i>	IFOS	ECL
K	<i>KAPSA Philippe</i>	<i>directeur de recherche</i>	LTDS	CNRS
	<i>KRÄHENBÜHL Laurent</i>	<i>directeur de recherche</i>	CEGELY	CNRS
	<i>KRAWCZYK Stanislas</i>	<i>directeur de recherche</i>	LEOM	CNRS
L	<i>LACHAL Aimé</i>	<i>PRAG</i>	MAPLY	INSA
	<i>LANCE Michel</i>	<i>professeur</i>	LMFA	UCBL
	<i>LANGLADE-BOMBA Cécile</i>	<i>maître de conférence</i>	IFOS	ECL
	<i>LE BOT Alain</i>	<i>chargé de recherche</i>	LTDS	CNRS
	<i>LE HELLEY Michel</i>	<i>professeur</i>		ECL
	<i>LE RIBAUT Catherine</i>	<i>chargé de recherche</i>	LMFA	CNRS
	<i>LEBOEUF Francis</i>	<i>professeur</i>	LMFA	ECL
	<i>LOEHAC Jean-Pierre</i>	<i>maître de conférence</i>	MAPLY	ECL
	<i>LOUBET Jean-Luc</i>	<i>directeur de recherche</i>	LTDS	CNRS
	<i>LYONNET Patrick</i>	<i>professeur</i>	LTDS	ENISE
M	<i>MAITRE Jean- François</i>	<i>professeur émérite</i>	MAPLY	ECL
	<i>MARION Martine</i>	<i>professeur</i>	MAPLY	ECL
	<i>MARTELET Claude</i>	<i>professeur</i>	IFOS	ECL
	<i>MARTIN Jean-Michel</i>	<i>professeur</i>	LTDS	ECL
	<i>MARTIN Jean-René</i>	<i>professeur</i>	IFOS	ECL
	<i>MASSON Jean-Pierre</i>	<i>professeur</i>	CEGELY	UCBL
	<i>MATHIA Thomas</i>	<i>directeur de recherche</i>	LTDS	CNRS
	<i>MATHIEU Jean</i>	<i>professeur émérite</i>	LMFA	ECL
	<i>MAZUYER Denis</i>	<i>professeur</i>	LTDS	ECL
	<i>MIDOL Alain</i>	<i>maître de conférence</i>	LTDS	UCBL
	<i>MOREL Hervé</i>	<i>chargé de recherche</i>	CEGELY	CNRS
	<i>MOREL Robert</i>	<i>professeur</i>	LMFA	INSA
	<i>MOUSSAOUI Mohand</i>	<i>professeur</i>	MAPLY	ECL
	<i>MUSY François</i>	<i>maître de conférence</i>	MAPLY	ECL
N	<i>NICOLAS Alain</i>	<i>professeur</i>	CEGELY	ECL
	<i>NICOLAS Laurent</i>	<i>directeur de recherche</i>	CEGELY	CNRS
P	<i>PERKINS Richard</i>	<i>professeur</i>	LMFA	ECL
	<i>PERRET-LIAUDET Joël</i>	<i>maître de conférence</i>	LTDS	ECL

ECOLE CENTRALE DE LYON

Liste des personnes habilitées à diriger des recherches

	PERRIN Jacques	professeur		INSA
	PHANER-GOUTORBE Magali	maître de conférence	LEOM	ECL
	PICHAT Pierre	directeur de recherche	IFOS	CNRS
	POUSIN Jérôme	professeur	MAPLY	INSA
	PONSONNET Laurence	maître de conférence	IFOS	ECL
	PREVOT Partick	professeur	ICTT	INSA
R	REBOUX Jean-Luc	professeur	LTDS	ENISE
	RETIF Jean-Marie	maître de conférence	CEGELY	INSA
	ROBACH Yves	professeur	LEOM	ECL
	ROGER Michel	professeur	LMFA	ECL
	ROJAT Gérard	professeur	CEGELY	UCBL
	ROUSSEAU Jacques	professeur émérite	LTDS	ENISE
	ROUY Elisabeth	professeur	MAPLY	ECL
S	SALVIA Michelle	maître de conférence	IFOS	ECL
	SANDRI Dominique	maître de conférence	MAPLY	UCBL
	SCHATZMAN Michelle	directeur de recherche	MAPLY	CNRS
	SCOTT Julian	professeur	LMFA	ECL
	SIDOROFF François	professeur	LTDS	ECL
	SIMOENS Serge	chargé de recherche	LMFA	CNRS
	SOUTEYRAND Eliane	directeur de recherche	IFOS	CNRS
	STREMSDOERFER Guy	professeur	IFOS	ECL
	SUNYACH Michel	professeur	LMFA	UCBL
T	TARDY Jacques	directeur de recherche	LEOM	CNRS
	THOMAS Gérard	professeur	LAGEP	UCBL
	THOUVEREZ Fabrice	maître de conférence	LTDS	ECL
	TREBINJAC Isabelle	maître de conférence	LMFA	ECL
	TREHEUX Daniel	professeur	IFOS	ECL
V	VANNES André-Bernard	professeur	IFOS	ECL
	VIKTOROVITCH Pierre	directeur de recherche	LEOM	CNRS
	VINCENT Léo	professeur	IFOS	ECL
	VOLPERT Vitaly	directeur de recherche	MAPLY	CNRS
Z	ZAHOUANI Hassan	professeur	LTDS	ENISE

ACKNOWLEDGEMENTS

This dissertation has been realised in a close collaboration between Institute of Materials Engineering at the Technical University of Lodz (Poland) and Laboratoire de Tribologie et Dynamique des Systèmes at Ecole Centrale de Lyon (France). I render best thanks to the directors of these centres: Professor Piotr KULA and Directeur de Recherche Phillipe KAPSA for the possibility of working on the very topical research problem in their leading laboratories.

I express my sincere gratitude to the supervisors of the thesis: in Poland – Prof. Bogdan WENDLER and in France – Dr. Siegfried FOUVRY. I had this great opportunity to benefit from their wide knowledge in the field of surface engineering and fretting damage, which has broadened my research experience. I would like to thank for the help in completion of this work, mobilisation, support and valuable remarks.

I want to warmly thank both reviewers of the thesis: Prof. Jean-Pierre CELIS and Dr. Stefano MISCHLER for the deep analysis of the manuscript, relevant remarks and exciting discussion.

My special thanks are addressed to the staff of Laboratoire de Tribologie et Dynamique des Systèmes for all the great and unforgettable moments at the laboratory. Particularly I wish to thank to Thomas MATHIA, Hassan ZAHOUANI, Gérard MEILLE, Jean-Christophe ABRY, Vincent FRIDRICI, Krzysztof KUBIAK and Cécile REVOL. Finally, exceptional thanks are directed to David PHILIPPON for effective cooperation and significant help in conduction of fretting test programme.

I wish to thank all the employee of Institute of Materials Engineering, which have been involved in the realisation of this research work, especially to Leszek KLIMEK, Krzysztof JAKUBOWSKI, Bartłomiej JANUSZEWICZ and Łukasz KACZMAREK.

RESUME DE LA THESE

1. Introduction

Les dégradations générées par les processus tribologiques (usures des surfaces) sont un problème majeur pour l'industrie mécanique. Elles impliquent souvent la réparation voire le remplacement des systèmes. L'usure est un processus complexe qui suppose une approche multidisciplinaire incluant différentes sciences comme la mécanique, la physique, la chimie. La sollicitation de fretting est un cas particulier des endommagements tribologiques, elle est caractérisée par des déplacements alternés de très faibles amplitudes, inférieures à la largeur du contact. Les sollicitations de fretting sont habituellement observées dans les assemblages serrés soumis à des vibrations. Considérées comme une "calamité" dans de nombreux secteurs industriels on retrouve des endommagements par fretting dans différents secteurs tels que le transport, l'énergie, la connectique... On peut citer le cas des contacts frettés de roulement, des roues de TGV, des rivets, des boulons, des aubes de turbines, des contacts électriques etc.

La sélection des matériaux pour ce type de sollicitation est en général très difficile en raison de la complexité des phénomènes mis en jeu. En réalité, la stratégie souvent appliquée consiste à réaliser des traitements de surfaces spécifique anti-usure. En effet, un même matériau ne peut répondre à toutes les spécificités mécaniques, anti-corrosion voire esthétiques requises. La solution consiste alors à combiner différents matériaux au travers de traitements de surface. Les plus classiques, impliquent une transformation mécanique des surfaces (grenaillage) mais restent limités vis-à-vis de la résistance à l'usure. Depuis quatre décennies, de nouveaux traitements de surface associés à l'application de couches minces et dures (dépôts physiques par phase vapeur et dépôts chimiques par phase vapeur) ont démontré de très bonnes performances vis-à-vis de la résistance à l'usure. Induisant de plus faibles coefficients de frottement et surtout de très fortes duretés, ces revêtements ont permis une augmentation conséquente de la durée de vie de très nombreux composants et en particulier des outils de coupe et d'usinage.

Si de nombreuses études ont démontré la pertinence des dépôts durs contre l'usure, il existe malheureusement très peu de développements concernant la modélisation de la durée de vie de ces traitements de surface. L'objectif de cette

recherche est, au travers de systèmes tribologiques modèles, de développer un formalisme prédictif, basé sur une description énergétique des processus d'usure.

2. Objectifs de la Thèse

Les objectifs de cette thèse sont de développer et d'optimiser des traitements de surface (TiC, VC, etc...) et de développer au travers d'un contact modèle de fretting wear, un modèle prédictif de l'endurance de ces traitements de surface pour des sollicitations variables et constantes de fretting wear.

Cette recherche a été réalisée dans le cadre d'une thèse en co-tutelle entre l'Université Polytechnique de Lodz (Pologne) pour la réalisation et la caractérisation physique des dépôts durs et d'autre part le Laboratoire de Tribologie et Dynamique des Systèmes de l'Ecole Centrale de Lyon (France) pour l'étude expérimentale et la modélisation du comportement sous sollicitations de fretting.

3. Les différents aspects traités de cette thèse

- Revue et analyse de la littérature concernant l'élaboration, des dépôts durs par voies PVD et CVD et dans le domaine de la caractérisation en usure par fretting;
- Elaboration de dépôts durs par dépôts physiques CVD;
- Analyse et caractérisation mécanique et physico-chimique des dépôts étudiés;
- Etude expérimentale et modélisation de l'endurance des dépôts durs soumis aux sollicitations de fretting wear;
- Analyse et synthèse des résultats obtenus.

4. Méthodologie mise en place

4.1. Elaboration des dépôts durs

Un acier rapide HSS Vanadis23 steel a été choisi comme substrat pour l'élaboration de plusieurs séries de dépôts durs : TiN, TiCN, TiC, VC, TiC/VC, (TiC/VC)_{x2}. Ces dépôts ont été réalisés dans l'unité de dépôt PVD de l'Université Technologique de Lodz au travers d'un réacteur "magnetron" *B90* pour les dépôts TiC, VC, TiC/VC, (TiC/VC)_{x2}, et d'un réacteur Arc-PVD *WUIB* pour les dépôts TiN et TiCN.

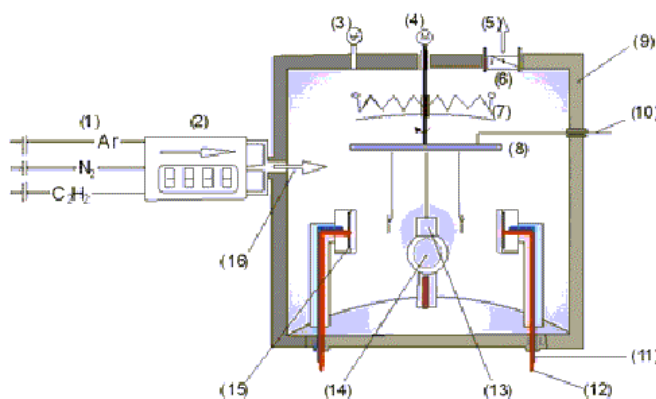
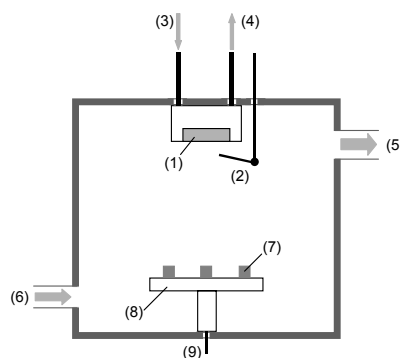


Figure 1. Réacteur PVD utilisé pour le dépôt des couches Ti et V.

1– alimentation en gaz inertes et réactifs; 2– contrôleur par masse des débits de gaz; 3– mesure du vide; 4– moteur de la platine; 5– connexion à la pompe à vide; 6– valve de fermeture; 7– chauffage par IR; 8– table rotative; 9– chambre de vide; 10– application des potentiels; 11– refroidissement par eau; 12– alimentation du canon magnétron; 13– échantillons suspendus sous la table; 14 et 15– canons magnétron; 16– entrée des gaz (inertes et réactifs).

Figure 2. Réacteur arc-PVD pour dépôts de TiN et TiCN. 1– cathode; 2 – décharge de l'arc; 3,4 – refroidissement de la cathode; 5 – connexion à la pompe à vide; 6 – entrée des gaz; 7 – échantillons; 8 – table rotative; 9 – table du potentiel.



Les dépôts réalisés ont été caractérisés du point de vue de leurs propriétés mécaniques et physico-chimiques. Des mesures de dureté, d'adhésion et de rugosité ont été réalisées (Tableau 1). L'analyse de la composition en phase a été conduite au travers de clichés de diffraction X. La structure et la morphologie des dépôts furent caractérisées par des observations au MEB.

Tableau 1. Propriétés mécaniques et de surface des dépôts étudiés.

Dépôts	Module de Young E (GPa)	Coefficient de Poisson ν	Dureté (HV _{0.05})	Epaisseur (μm)	Adhésion (N)	Rugosité Ra (μm)
TiC	510	0.2	1300	1.6	45	0.2
VC	460		2500	2.0	35	
TiN	600	0.25	2000	4.0	35	
TiCN	550		1700	2.5	40	
TiC/VC	580	0.2	1450	2.5	35	
(TiC/VC)x2			2300	4.0	40	

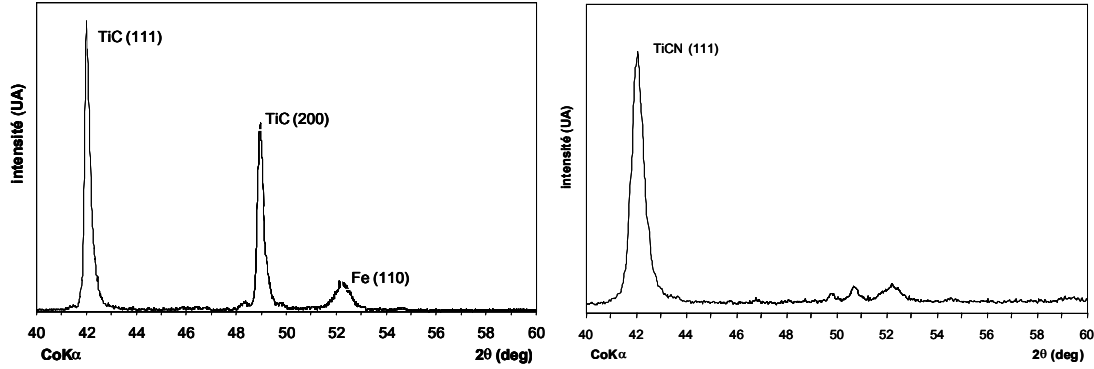


Figure 3. Clichés de diffraction X : (a) TiC; (b) TiCN.

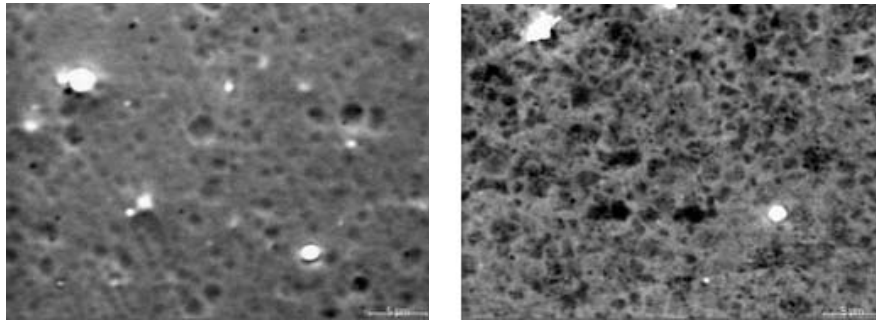


Figure 4. Observation au MEB des surfaces des dépôts : (a) TiN; (b) VC.

4.2. Approche expérimentale de l'étude en Fretting Wear des dépôts

Les dépôts ainsi réalisés ont été testés à l'aide d'un tribomètre du LTDS (Ecole Centrale de Lyon) permettant d'appliquer des glissements alternés de très faibles amplitudes, caractéristiques des sollicitations de fretting. Le principe de cet essai, développé en collaboration avec la société Delta-Lab, consiste à produire un déplacement alterné entre les deux pièces en contact à l'aide d'un vérin électromagnétique. Le contact est constitué d'une sphère, représentée par une bille en alumine polycristalline de 12.7 mm de rayon, contre un plan. On retiendra que l'essai est instrumenté de façon à permettre l'acquisition de l'évolution de la force tangentielle ($Q(t)$) en fonction du débattement imposé ($\delta(t)$) et ainsi, de mesurer les variables de chargement utilisées par la suite pour quantifier la cinétique de l'usure (Fig. 5) :

δ^* (μm) – amplitude de débattement;

Q^* (N) – amplitude de la force tangentielle;

P (N) – force normale (constante);

Ed (J) – énergie dissipée du cycle de fretting;

δg (μm) – amplitude de glissement identifiée pour une valeur nulle de la force tangentielle.

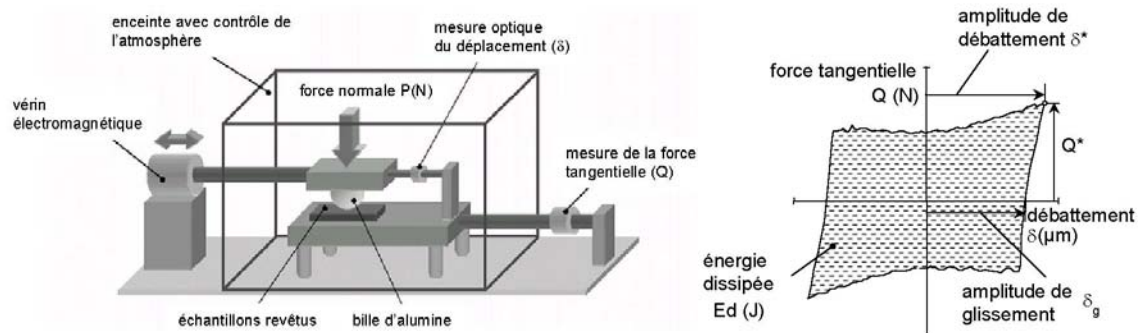


Figure 5. (a) Schéma de l'essai de fretting; (b) illustration des variables de chargement déduites du cycle de fretting.

Les essais de fretting ont été réalisés à fréquence (f) constante de 5 Hz, les autres paramètres de chargement comme l'amplitude de débattement, et la force normale sont détaillés dans le Tableau 2. Le nombre de cycles imposés varie entre 1000 et $2.5 \cdot 10^5$ cycles. Les essais ont été systématiquement réalisés pour des conditions de température et d'humidité relative contrôlées et asservies. Trois niveaux d'humidité ont été plus spécifiquement étudiés 5%, 50% et 90%.

Tableau 2. Conditions de chargement étudiées :

◆ TiC, ◇ VC, ■ TiC/VC, □ (TiC/VC)x2, ▲ TiCN, △ TiN.

$P \backslash \delta$	50	75	100	125	150	200
50	▲	▲	▲	▲	▲	▲
100	◆ △	△	◆ □ ▲ ◇ ■ △	▲ △	◆ △ ▲	◆
150	▲	▲	▲	▲	▲	▲

Il est important de souligner que cette recherche expérimentale a non seulement été conduite pour des amplitudes de débattement constantes, mais aussi variables. En effet, si la plupart des recherches sur l'usure par fretting sont réalisées à amplitudes de débattement constantes, un aspect original de ce travail a été d'introduire un nouveau formalisme permettant de caractériser des cycles variables de glissement. Ainsi, s'inspirant d'une démarche classiquement appliquée en fatigue, des blocs de grands et

petits cycles de fretting ont été imposés et les endommagements associés étudiés (Fig. 6). Cette démarche reste relativement éloignée des conditions réelles de fonctionnement impliquant de fortes variations de fréquence, d'amplitudes de glissement et de charges normales. Cependant, l'application de cette approche permet pour la première fois d'évaluer la stabilité de modèles d'usure pour des sollicitations tribologiques variables. Limitée à l'impact d'amplitudes variables de débattement durant l'essai, l'étude consiste à alterner des blocs de $\pm 50\mu\text{m}$ et $\pm 100\mu\text{m}$. Ainsi, la durée totale des essais est divisée en une, deux, et quatre séquences de durées identiques soit respectivement $(50/100)\mu\text{m}_{x1}$, $(50/100)\mu\text{m}_{x2}$ et $(50/100)\mu\text{m}_{x4}$.

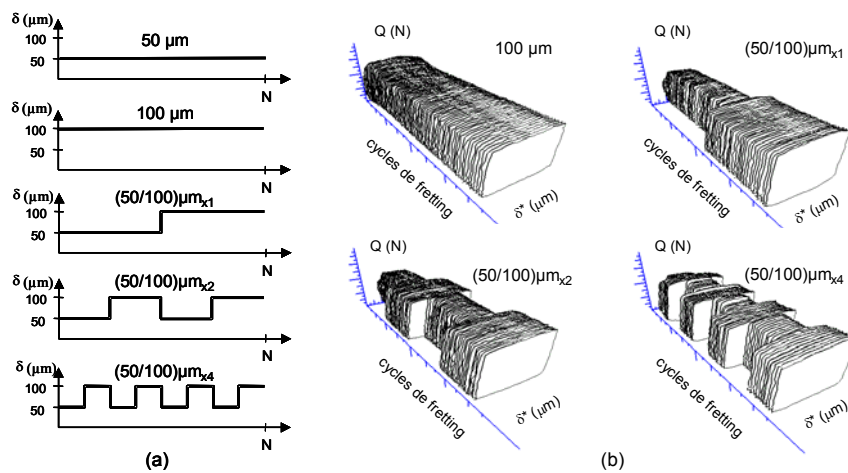


Figure 6. Illustration de la démarche mise en œuvre pour étudier l'impact d'amplitudes variables de glissement (TiC/alumine, $RH=50\%$, $f=5\text{Hz}$, $P=100\text{N}$) : (a) définition des séquences de chargement (constantes et variables); (b) Illustration via les bûches de fretting des séquences étudiées.

5. Résultats des recherches

5.1 Impact de l'humidité relative

Cette thèse a pour objectif d'établir une formalisation de l'endurance des dépôts c'est pour cela que nous nous sommes orientés sur la mise en place d'un système tribologique modèle. Ainsi nous avons choisi une bille d'alumine pour limiter l'impact des effets d'adhésion, classiquement observés avec un contre corps en acier. Un autre paramètre difficile à maîtriser dans les systèmes tribologiques est l'impact de l'environnement et en particulier l'humidité relative. Cet aspect a largement été développé par les travaux de Celis et al. La Figure 7 qui montre l'évolution du

coefficient de frottement du contact TiC/alumine en fonction de l'humidité relative imposée confirme cet aspect.

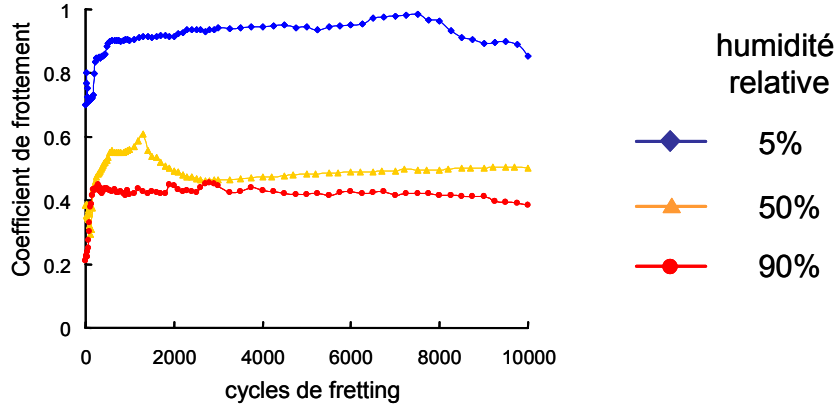


Figure 7. Impact de l'humidité relative sur l'évolution du coefficient de frottement du contact TiC/ alumine.

De façon à s'affranchir de cet effet, nous avons choisi de conduire l'ensemble de l'étude pour une humidité relative de 50%.

5.2 Comparaison des cinétiques de l'usure à partir de l'approche classique de Archard

Dans un premier temps nous avons cherché à quantifier la cinétique d'usure à partir de la démarche classique de Archard. Celle-ci consiste à comparer l'évolution du volume d'usure (W_v) en fonction du produit de la force normale (P) par la distance totale de glissement (S). Pour des conditions de glissement total en fretting, l'expression de ce facteur est exprimé par la relation suivante :

$$PS = \sum_{i=1}^N 4 \cdot \delta_g(i) \cdot P(i) \quad (Nm)$$

On détermine ainsi le coefficient d'usure d'Archard tel que :

$$K = \frac{W_v}{W} = \frac{W_v}{\sum_{i=1}^N 4 \cdot \delta_g(i) \cdot P(i)} \quad (\mu m^3/Nm)$$

La Figure 8 compare l'évolution des cinétiques d'usure des différents traitements de surface étudiés. On remarque que le dépôt le plus résistant est le VC alors que celui qui présente la plus faible résistance à l'usure est le TiN. Le comportement à l'usure semble vérifier une loi de mélange fonction des compositions chimiques des dépôts sans obéir toute fois à une relation linéaire. En effet, si on compare la cinétique d'usure des

composants TiN, TiC et TiCN on remarque que la cinétique d'usure du composant TiCN ($207.9 \mu\text{m}^3/\text{Nm}$) est bien comprise entre les cinétiques d'usure des composants TiC ($130.5 \mu\text{m}^3/\text{Nm}$) et TiN ($2770 \mu\text{m}^3/\text{Nm}$) mais n'est pas égale à la moyenne des deux. On retrouve ce comportement pour les dépôts issus des combinaisons des composants VC et TiC. Ainsi l'ordre des résistances à l'usure vérifie celui des proportions des éléments *V* et *Ti* sans cependant obéir à une fonction linéaire (lois de mélange).

$$\text{VC} (24\mu\text{m}^3/\text{Nm}) < \text{TiC/VC} (43\mu\text{m}^3/\text{Nm}) \approx (\text{TiC/VC})_{x2} (58\mu\text{m}^3/\text{Nm}) < \text{TiC} (130.5\mu\text{m}^3/\text{Nm})$$

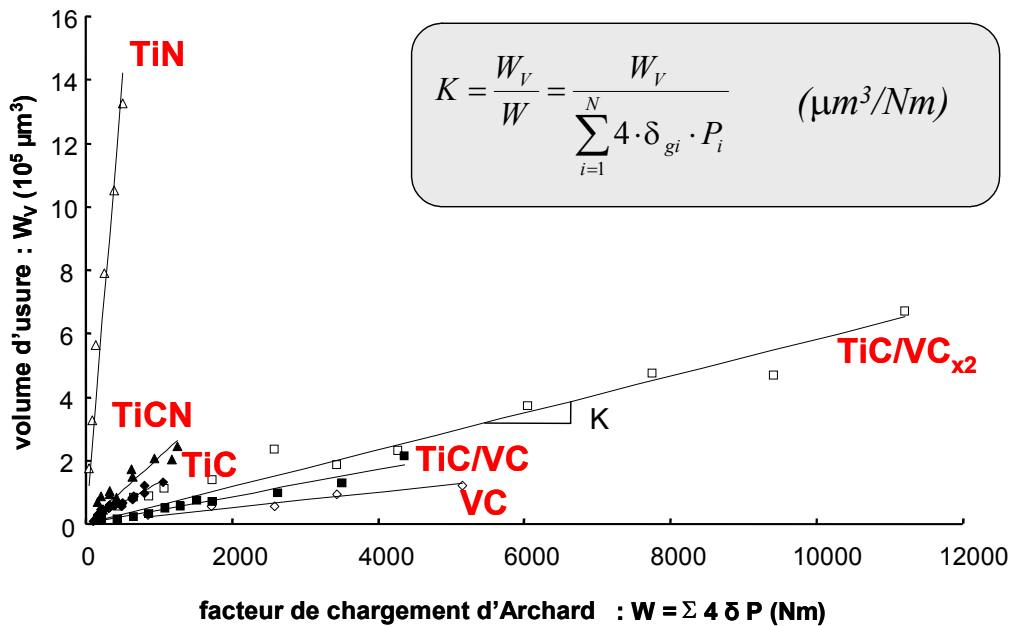


Figure 8. Evolution des cinétiques d'usure identifiées à partir du spectre de chargement établi dans le Tableau 2 : comparaison des différents dépôts.

On démontre une corrélation entre la composition chimique des dépôts étudiés et les cinétiques d'usure observées. Une première démarche considérée pour expliquer ces évolutions de cinétique d'usure a été de corréler les coefficients d'usure en fonction de la dureté des couches obtenues. En effet, de nombreuses recherches montrent une réduction de la cinétique de l'usure avec l'augmentation de la dureté des matériaux.

La Figure 9 compare l'évolution des cinétiques d'usure en fonction des duretés mesurées des différents dépôts étudiés. On remarque deux tendances en fonction des constituants considérés. En effet, si on compare les systèmes associés aux deux composants VC et TiC on confirme bien la tendance d'une réduction de la cinétique d'usure avec l'augmentation de la dureté. On confirme pour ce système la corrélation résistance à l'usure – dureté. L'analyse du système Ti-C-N montre une évolution très

différente. En effet, alors que ce système présente une dureté pratiquement équivalente, on remarque une très forte variation de la cinétique d'usure avec un comportement très mauvais du TiN. On démontre donc, que pour ce système, la corrélation résistance à l'usure – dureté n'est pas vérifiée.

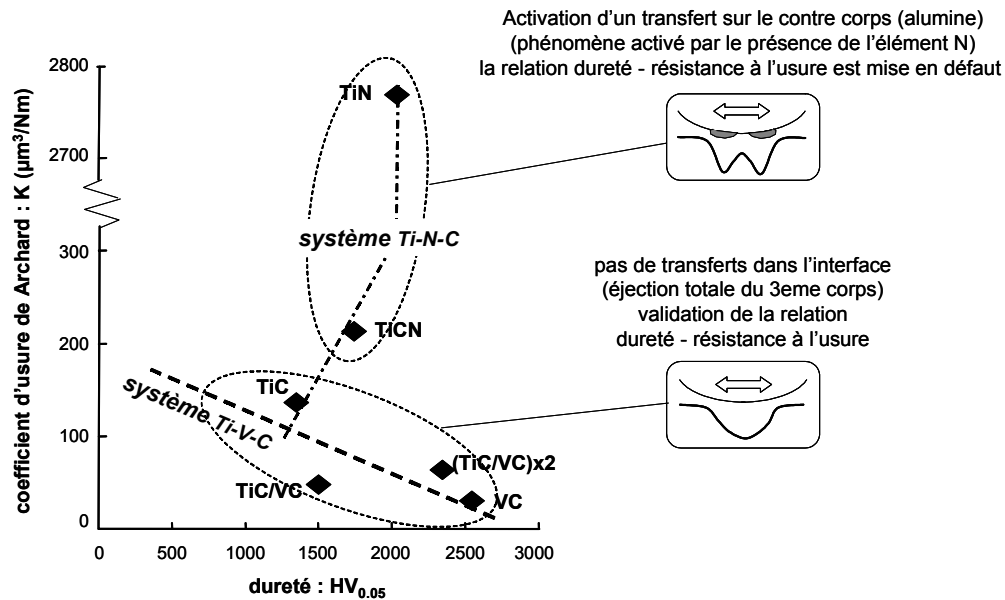


Figure 9. Illustration de la corrélation résistance à l'usure – dureté : mise en évidence de l'impact de l'effet du troisième corps associé aux compositions chimiques des systèmes étudiés.

Cette recherche nous a donc permis de démontrer que la corrélation résistance à l'usure – dureté n'est pas absolue du moins pour les sollicitations de fretting wear.

Ainsi, elle semble être validée pour le système Ti-V-C, système impliquant différent métaux mais un seul élément léger (C) alors que le système un seul métal et deux éléments légers (Ti, C, N) ne répond plus à cette corrélation. On montre que l'ajout de l'élément *N* modifie le système tribologique de telle sorte que la corrélation dureté-résistance à l'usure n'est plus vérifiée. Pour expliquer ce comportement nous avons conduit une expertise des interfaces des contacts en nous focalisant sur l'aspect 3^{ème} corps. On remarque que le système Ti-V-C ne présente pas de transferts au niveau du contre corps. Le troisième corps est totalement éliminé de l'interface. On observe un profil en *U* des faciès d'usure du TiC. En revanche, le système Ti-C-N (impliquant l'adjonction de l'élément *N*) favorise les phénomènes d'adhésion du troisième corps sur l'alumine. On observe alors un faciès en *W* de la trace d'usure du dépôt. Finalement, on peut postuler que la relation résistance à l'usure – dureté est vérifiée tant que le troisième corps et surtout les phénomènes d'adhésion sur le contrecorps n'interviennent pas (ou

peu) dans le système tribologique. C'est le cas du système Ti-V-C. En revanche, dès lors que le troisième corps joue un rôle prépondérant dans l'interface, cas observé dans les systèmes incluant l'élément *N*, alors la corrélation résistance à l'usure – dureté ne semble plus être vérifiée.

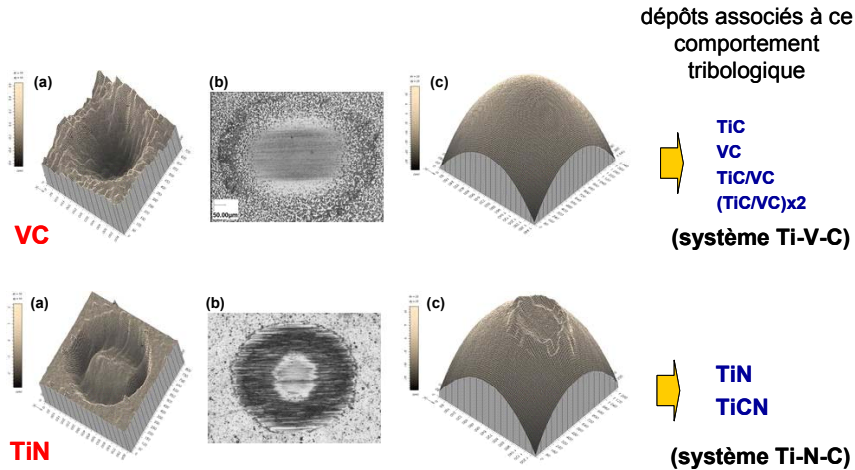


Figure 10. Evolution de la morphologie du contact en fonction des dépôts étudiés en fretting wear (contre corps en alumine) : (a) profil 3D de la surface des dépôts; (b) observation optique de la trace des dépôts; (c) profil 3D de la surface correspondante de la bille d'alumine.

Ceci est tout à fait cohérent avec une interprétation physique du comportement tribologique du contact. En l'absence de troisième corps, l'essentiel de la dissipation interfaciale est transmise aux premiers corps. En revanche, la présence d'un troisième corps aggloméré dans l'interface va considérablement modifier les processus énergétiques et donc invalider la relation usure-dureté. On montre aussi que l'activation des phénomènes de 3^{ème} corps est directement liée à la présence de l'élément *N*. Enfin, on montre ici que l'implication du troisième corps n'implique pas systématiquement une réduction de la cinétique d'usure. En effet, le TiN qui présente la plus forte densité de transferts montre l'usure la plus importante.

Une recherche future devra se concentrer pour expliquer pourquoi l'élément *N* favorise l'adhésion du 3^{ème} corps et engendre la modification du régime d'usure. Cette recherche, impliquant une analyse chimique poussée, intégrant différents constituants tels que les oxydes et hydrates formés qui n'a pu être finalisée durant cette recherche.

Ayant démontré l'interactivité cinétique d'usure – dureté troisième corps pour analyser le comportement de différents dépôts, nous nous sommes focalisés sur un système modèle ne mettant pas en jeu la problématique des transferts (dépôt TiC) de façon à voir comment à partir d'une approche énergétique, il était possible de rationaliser

et surtout prédire la cinétique d'usure et en particulier établir la prédiction de la durée de vie d'un dépôt.

5.3 Introduction de l'approche énergétique pour quantifier la cinétique d'usure des dépôts durs étudiés

Différents travaux ont démontré que l'approche Archard n'est à priori pas la plus adaptée pour quantifier l'usure et surtout établir une démarche thermodynamique. En effet, si on regarde sa formulation, le produit PS ne fait pas intervenir le coefficient de frottement. Or il est démontré par de nombreux auteurs (K.L. Johnson et co-auteurs) que le coefficient de frottement joue un rôle primordial dans l'activation des endommagements tant du point de vue de l'intensité que de la localisation des maximums de chargements. D'autre part, on retiendra aussi que le travail de la force normale considéré par Archard est un non sens physique, puisque le produit scalaire du vecteur glissement et force normale est nul dans la mesure où ses deux directions sont perpendiculaires. Ainsi, plutôt que de considérer ce formalisme, qui n'intègre pas le coefficient de frottement, nous avons choisi de considérer une analyse énergétique associée au travail de la force tangentielle. Développée par les équipes de Leuven et ECL, cette approche considère l'énergie de frottement dissipée dans l'interface comme critère d'endommagement par usure des matériaux.

La formulation de cette variable pour des sollicitations de fretting est donnée par l'expression suivante :

$$\sum E_d = \sum_{i=1}^N E_d(i) \quad (J), \text{ avec :}$$

N – nombre de cycles de fretting;

$Ed(i)$ – énergie dissipée par cycle i ;

ΣE_d – énergie dissipée cumulée.

Un premier résultat de cette thèse fut de démontrer la stabilité de l'approche énergétique pour décrire la cinétique d'usure du contact TiC/alumine sous amplitudes variables de fretting. En effet, la Figure 11 confirme une évolution linéaire du volume d'usure (W_V) en fonction de l'énergie dissipée cumulée (ΣE_d). Ainsi, le volume d'usure est exprimé à partir de la relation suivante quelques soient les cycles de chargement : $W_V = \alpha \cdot \Sigma Ed$ avec $\alpha = 415 \mu\text{m}^3/\text{J}$ (coefficient énergétique d'usure du TiC pour le contact étudié).

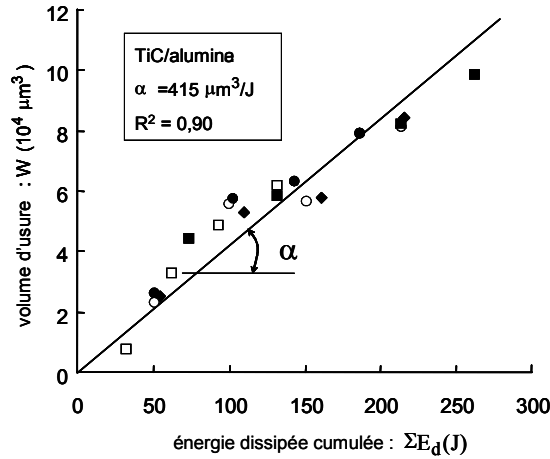


Figure 11. Evolution du volume d'usure du TiC en fonction de l'énergie dissipée cumulée. (TiC/alumine, $RH=50\%$, $f=5\text{Hz}$, $P=100\text{N}$, amplitude de débattement : ■ $50\mu\text{m}$, □ $100\mu\text{m}$, ◆ $(50/100)\mu\text{m}_{x1}$, ○ $(50/100)\mu\text{m}_{x2}$, ● $(50/100)\mu\text{m}_{x4}$).

Cependant, l'analyse en terme de volume d'usure, bien qu'indicative, n'est pas pertinente dans la mesure où la durée de vie du dépôt est associée au moment où le substrat est atteint. Ceci implique une analyse en terme de profondeur d'usure et donc une analyse locale de l'endommagement. Considérant l'approche énergétique comme stable on a donc cherché à dériver l'approche globale (volume) en une approche locale (profondeur d'usure) autrement dit à comparer l'évolution de la profondeur d'usure en fonction de la densité d'énergie dissipée cumulée (Fig. 12).

distribution de densité d'énergie en régime de glissement total ($\delta_g/a = 1.5$)

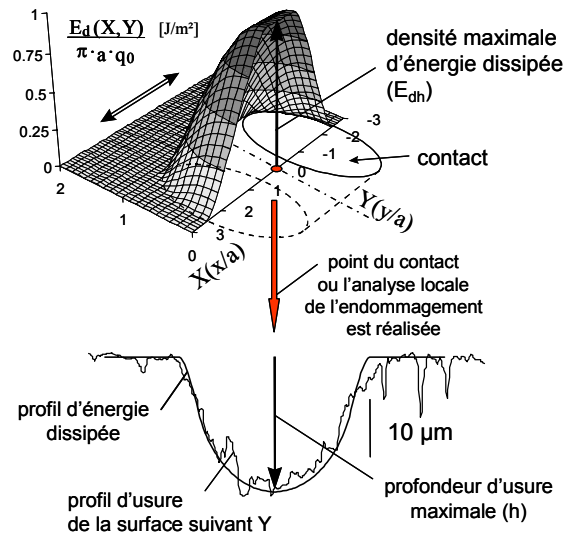


Figure 12. Illustration de la démarche locale associant l'évolution de la profondeur d'usure en fonction de la densité d'énergie dissipée : application au contact sphère/plan (a – rayon du contact Hertzien; q_0 – valeur maximale du cisaillement Hertzien).

Un des aspects très intéressant de l'approche énergétique est qu'elle permet, au travers d'une seule variable, d'inclure de multiples paramètres de sollicitations tribologiques, tels que la pression, le coefficient de frottement et l'amplitude de glissement. On retiendra cependant la difficulté de tenir compte de l'évolution de l'interface induite par l'usure pour calculer correctement les densités d'énergie dissipées dans l'interface. Cet aspect a été traité plus en détail dans le manuscrit en faisant intervenir indirectement l'énergie dissipée cumulée total comme facteur d'extension de l'aire de contact.

Une première application de cette démarche fut de relier l'évolution de la profondeur usée en fonction de la densité d'énergie cumulée maximale :

$$\sum E_{dh} = \sum_{i=1}^N E_{dh}(i) \cdot$$

Une évolution linéaire est encore une fois observée ce qui confirme la propriété d'additivité de l'énergie dissipée pour quantifier l'usure générée par fretting pour ce tribo-système (Fig. 13).

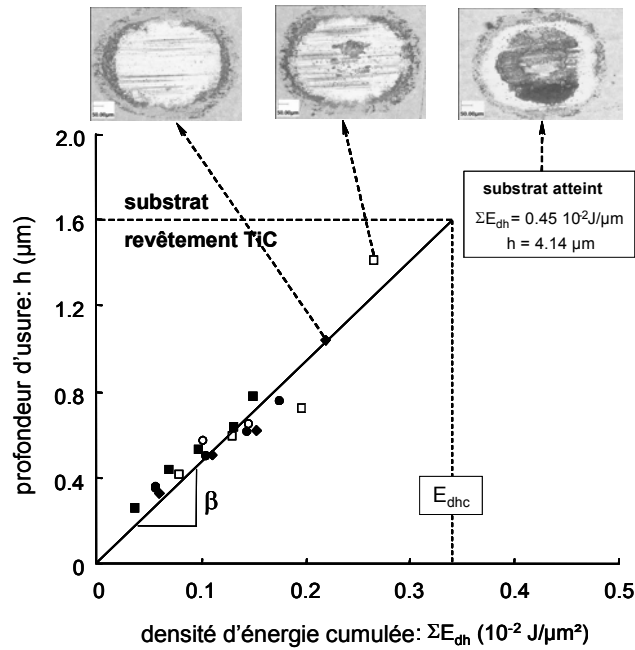


Figure 13. Evolution de la profondeur d'usure en fonction de la densité d'énergie cumulée, identification du paramètre énergétique d'usure $\beta = 474 \mu\text{m}^3/\text{J}$, $R^2 = 0.91$; amplitude de débattement : ■ $50 \mu\text{m}$, □ $100 \mu\text{m}$, ◆ $(50/100) \mu\text{m}_{x1}$, ○ $(50/100) \mu\text{m}_{x2}$, ● $(50/100) \mu\text{m}_{x4}$, (TiC/alumine, $RH=50\%$, $f=5\text{Hz}$, $P=100\text{N}$).

L'évolution de la profondeur d'usure (h) peut être quantifiée à partir de la densité cumulée d'énergie dissipée (ΣE_{dh}) au travers de la relation : $h = \beta \cdot \Sigma E_{dh}$. L'analyse de la

Figure 13 montre aussi que la durée de vie du dépôt, établie lorsque l'interface du contact atteint le substrat peut être associée à une densité d'énergie dissipée critique : E_{dhc} aussi définie comme capacité énergétique du dépôt. Cet aspect est fondamental puisque qu'à partir de ce formalisme on peut associer l'endurance d'un dépôt à une capacité énergétique spécifique. Autrement dit, le dépôt et son action protectrice seront maintenus tant que la densité d'énergie dissipée maximale dans l'interface restera inférieure à la valeur de capacité énergétique spécifique du dépôt étudié. On retiendra que cette capacité énergétique est fonction des propriétés intrinsèques du matériau ainsi que de l'épaisseur de la couche.

En combinant l'analyse locale énergétique avec la description en endurance des dépôts développée par C. Langlade et co-auteurs, on introduit une courbe unifiée ou courbe maîtresse d'endurance du dépôt étudié (Wöhler like coating endurance fretting wear chart). Cette représentation consiste à reporter la durée de vie du dépôt N_c en fonction de la valeur moyenne de la densité d'énergie dissipée dans l'interface par cycle au cours de l'essai considéré (\bar{E}_{dh}). On observe une évolution hyperbolique des résultats expérimentaux (Fig.14). Considérant le concept de capacité énergétique comme grandeur représentative de l'endommagement en usure du dépôt on formule la durée de vie à partir de la cinétique d'usure telle que : $N_c = \frac{E_{dhc}}{\bar{E}_{dh}}$

avec E_{dhc} la capacité énergétique du dépôt extrapolée à partir de la cinétique de l'évolution de la profondeur usée telle que : $E_{dhc} = t/\beta = 3.4 \cdot 10^{-3} \text{ J}/\mu\text{m}^2$ (avec t (épaisseur du dépôt) = $1.6 \mu\text{m}$ et $\beta = 475 \mu\text{m}^3/\text{J}$).

La comparaison des deux courbes expérimentale et théorique montre une évolution hyperbolique similaire qui confirme la démarche "densité d'énergie" (Fig. 14). Cependant, on observe un décalage en terme de durée de vie qui suppose que la durée de vie réelle du dépôt est inférieure à celle prédite par le modèle établi à partir de la cinétique de profondeur d'usure.

En réalité, l'expertise des traces d'usure révèle un phénomène d'écaillage lorsque l'épaisseur rémanente du dépôt est inférieure à une certaine valeur. On observe ainsi une compétition entre deux phénomènes d'endommagement. En premier lieu une usure progressive de l'interface et parallèlement une fatigue de l'interface induite par les sollicitations cycliques du contact. Lorsque l'épaisseur rémanente de dépôt devient égale à une valeur critique (t_r), il y a rupture brutale par décohésion de l'interface du substrat.

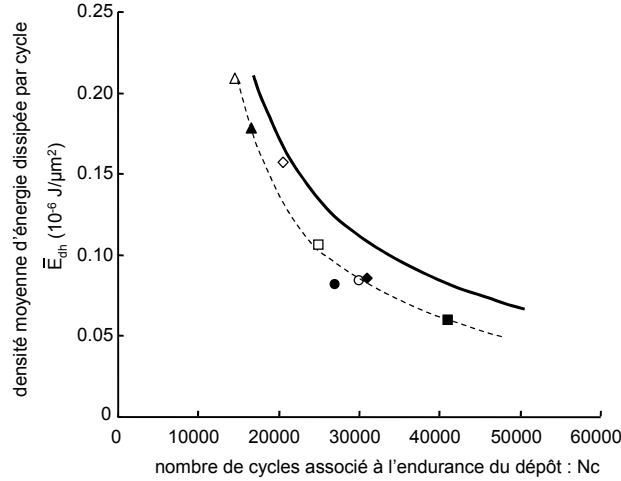


Figure 14. Comparaison entre l'analyse expérimentale de l'endurance du dépôt TiC et la prédiction de la durée de vie formulée à partir de la cinétique de profondeur d'usure :

Δ 200 μm , \blacktriangle (150/200) μm_{x1} , \diamond 150 μm , \blacksquare 50 μm , \square 100 μm , \blacklozenge (50/100) μm_{x1} ,

\circ (50/100) μm_{x2} , \bullet (50/100) μm_{x4} , (TiC/alumine, RH=50%, $f=5\text{Hz}$, $P=100\text{N}$);

— Prédiction théorique définie à partir du concept de capacité d'énergie admissible déterminée à partir de la quantification de la cinétique de profondeur d'usure

$$(N_C = \frac{E_{dhc}}{E_{dh}}, E_{dhc} = 3.4 \cdot 10^{-3} \text{ J}/\mu\text{m}^2).$$

On retiendra que la résistance à la décohésion du dépôt, caractérisée par la couche rémanente de dépôt (t_r), illustre les propriétés d'adhésion du dépôt. Ainsi, une mauvaise accroche du dépôt impliquera une épaisseur rémanente plus importante.

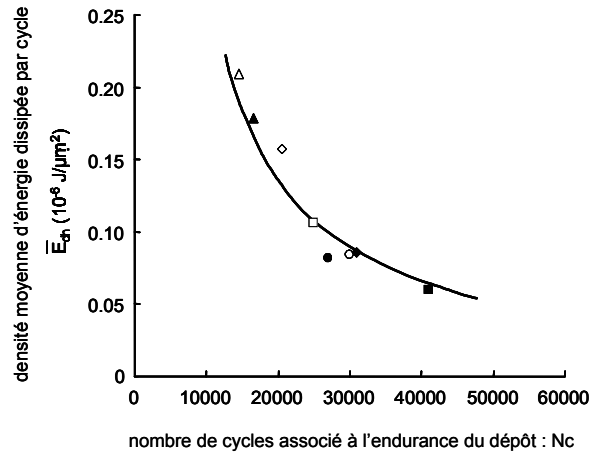


Figure 15. Prédiction de la durée de vie du dépôt en tenant compte des aspects compétitifs entre l'usure progressive activée par les processus énergétiques et la décohésion du dépôt rémanent par des phénomènes de fatigue de l'interface avec le substrat :

Δ 200 μm , \blacktriangle (150/200) μm_{x1} , \diamond 150 μm , \blacksquare 50 μm , \square 100 μm , \blacklozenge (50/100) μm_{x1} ,

\circ (50/100) μm_{x2} , \bullet (50/100) μm_{x4} ; (TiC/alumine, RH=50%, $f=5\text{Hz}$, $P=100\text{N}$);

— Modélisation de l'endurance du dépôt à partir du concept d'épaisseur effective.

$$(N_C = \frac{E_{dhe}}{E_{dh}}, E_{dhe} = 2.7 \cdot 10^{-3} \text{ J}/\mu\text{m}^2).$$

Tenant compte des aspects compétitifs entre l'usure progressive du dépôt activée par un processus énergétique et la décohésion de l'interface contrôlée par des mécanismes de fatigue, on formule la durée de vie du dépôt en prenant compte non pas l'épaisseur physique du dépôt initiale mais en considérant une épaisseur effective (t_e) éliminée par le processus d'usure :

$$E_{dhe} = \frac{t_e}{\beta} \quad \text{avec} \quad t_e = t - t_r \quad \text{et} \quad N_c = \frac{E_{dhe}}{E_{dh}} \quad (t_r \approx 0.3 \mu\text{m}).$$

La comparaison entre les résultats expérimentaux et le modèle montre une parfaite corrélation. Ainsi au travers d'une seule et unique variable, la capacité énergétique effective d'endurance du dépôt, il devient possible de prédire la durée de vie des dépôts quelques soient les cycles de chargement imposés et ceci pour une très large gamme de durée de vie. Il existe cependant des limites à cette formulation qui devra être étendue pour mieux intégrer les effets de l'environnement et les mécanismes de décohésion de l'interface. A partir de cette formalisation des processus d'usure, une démarche simplifiée a été développée de façon à comparer l'endurance de différents traitements de surface. Il devient possible d'extraire l'endurance des traitements de surface à partir d'un nombre restreint d'essais de fretting wear et de comparer leurs performances au travers de courbes maîtresses d'endurance en fretting wear (Fig. 16).

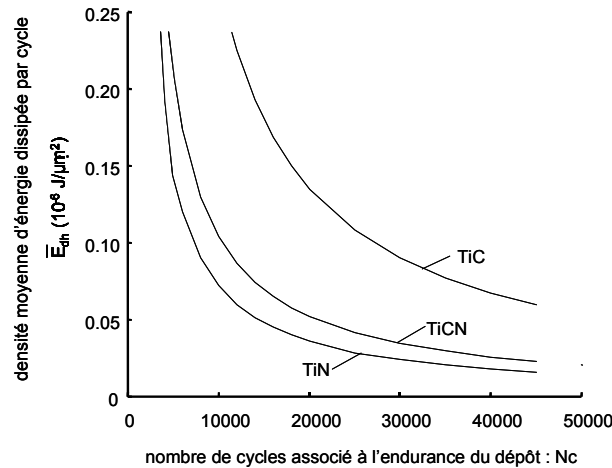


Figure 16. Développement de courbes maîtresses de tenue de traitements de surface : TiC, TiN et TiCN.

Une illustration de la capacité à prédire la durée de vie d'un traitement de surface, consiste à considérer une condition de chargement donnée, établir la densité moyenne d'énergie dissipée associée, considérant un coefficient de frottement représentatif et en appliquant la formulation proposée, prédire la durée de vie du dépôt. La Figure 13

illustre cette démarche et montre qu'il est possible de comparer différents traitements de surface et prédire la durée de vie du système.

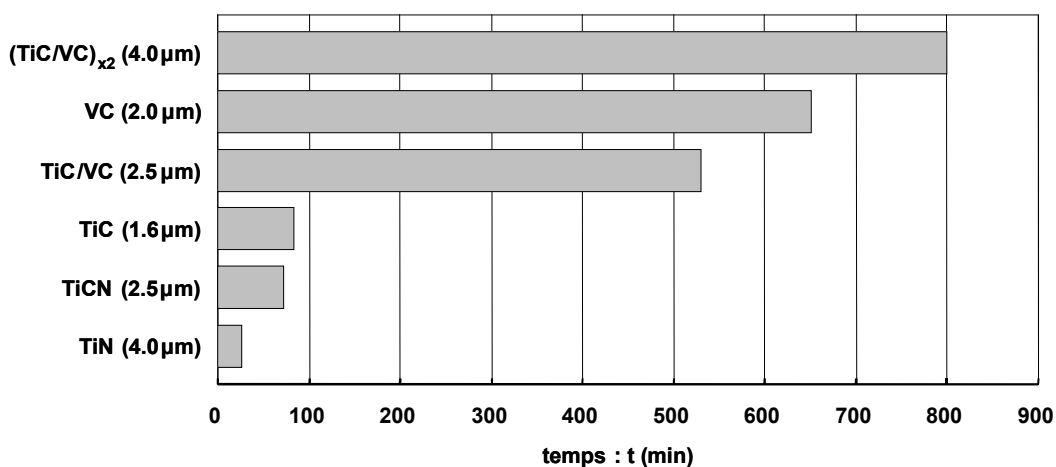


Figure 17. Endurance de différents traitements de surface établie à partir du concept de capacité énergétique (prédiction développée pour une condition fixée de chargement).

Un dernier résultat de cette recherche a été de démontrer comment et pourquoi on observe classiquement une différence de durée entre celle estimée et celle prévue d'un système tribologique. La Figure 18a illustre l'évolution de l'usure d'un système non revêtu. Si on suppose une relation directe entre la cinétique d'enlèvement de matière et l'endurance du système revêtu, on peut s'attendre à une évolution de l'usure faible jusqu'à l'interface du substrat puis à une cinétique équivalente à celle du matériau non traité. Ceci se traduit par une augmentation non négligeable de la durée de vie du système. L'analyse expérimentale montre systématiquement un comportement intermédiaire. Autrement dit, une durée de vie sensiblement inférieure à celle attendue. Les résultats de cette recherche permettent d'expliquer et de rationaliser cette différence. En effet, si on considère qu'une proportion et non toute l'épaisseur du dépôt est éliminée par le processus d'usure activé par l'énergie dissipée et que la partie rémanente du dépôt est enlevée par écaillage alors, on peut expliquer cet écart. La durée de vie résiduelle N_r observée peut être quantifiée au travers de la différence entre la densité d'énergie théorique et la densité d'énergie effective. Enfin, on confirme que plus l'adhérence et les propriétés de cohésion entre le dépôt et le substrat sont fortes, plus la composante résiduelle sera négligeable et plus la durée de vie observée se rapprochera de la valeur théorique. Cette analyse souligne tout l'intérêt de travailler sur le problème de la cohérence des dépôts sur le substrat de façon à optimiser le potentiel de résistance à l'usure des dépôts durs.

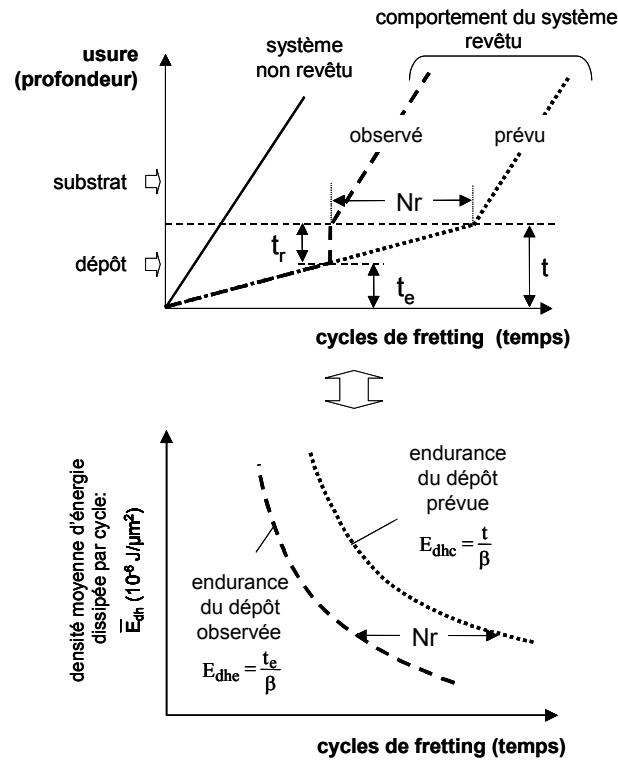


Figure 18. Illustration de la différence entre l'endurance prévue et l'endurance observée d'un dépôt dur à partir de la démarche énergétique mise en oeuvre. (N_r – nombre de cycles (ou temps) associé à la différence entre l'endurance prévue et observée).

6. Conclusion

Les conclusions suivantes peuvent être tirées de ce travail de recherche :

- On montre que la relation résistance à l'usure – dureté est vérifiée tant que l'impact du troisième corps reste négligeable. Ce comportement a été validé pour le système Ti-V-C. En revanche on montre que l'élément N favorise les phénomènes d'adhésion du troisième corps dans l'interface et que dans ce cas la relation *dureté usure* n'est plus validée.
- En introduisant pour la première fois une analyse en amplitudes variables de débattement de chargement de fretting wear, on démontre la stabilité de l'approche énergétique pour prédire la cinétique d'usure en volume d'usure des tribo-systèmes étudiés : $W_V = \alpha \cdot \Sigma E d$.
- On montre, que pour prédire la durée de vie d'un dépôt, l'approche volumique n'est pas pertinente et qu'il est préférable de considérer la condition telle que l'on atteint le substrat, ce qui suppose une analyse locale de l'usure.

- L'approche locale de l'énergie dissipée qui consiste à considérer la densité d'énergie cumulée maximale dissipée dans l'interface, permet de quantifier la cinétique de la profondeur d'usure. La propriété d'additivité de l'approche énergétique est confirmée et la cinétique de profondeur d'usure est formalisée à partir d'une expression linéaire :

$$h = \beta \cdot \Sigma E_{dh}$$
- On montre que l'endurance d'un traitement de surface peut être associée à une capacité énergétique spécifique (E_{dhc}) telle que si cette densité d'énergie est dissipée dans l'interface on atteint le substrat.
- Couplant l'approche énergétique locale avec la démarche endurance (nombre de cycles avant d'atteindre le substrat), on introduit une courbe maîtresse d'endurance d'un dépôt. Ainsi, à partir d'une seule variable regroupant l'ensemble des chargements tribologiques (densité moyenne maximale d'énergie dissipée dans l'interface (\bar{E}_{dh})) il devient possible de quantifier la durée de vie du traitement de surface.
- La comparaison entre les résultats expérimentaux d'endurance et le modèle d'endurance telle que : $N_c = \frac{E_{dhc}}{\bar{E}_{dh}}$ avec E_{dhc} établie à partir de la cinétique de profondeur d'usure, confirme une évolution hyperbolique mais montre un décalage significatif des courbes.
- L'expertise des endommagements montre qu'il existe deux processus d'endommagement du dépôt, une usure progressive activée par des processus énergétiques d'une part et une décohésion de l'interface activée par des processus de fatigue de l'interface d'autre part.
- En considérant une épaisseur effective de l'usure ($t_e = t - t_r$; t – épaisseur physique du dépôt, t_r – épaisseur rémanente au moment de la décohésion; t_e – épaisseur effectivement éliminée par des processus d'usure) et en réinjectant cette variable dans l'identification d'une capacité énergétique effective spécifique (E_{dhe}), il est possible de prédire la durée de vie du système.

- La démarche a été étendue pour différents traitements de surface ce qui permet de prédire la durée de vie des systèmes et surtout de prédire la durée de vie d'un dépôt pour un chargement énergétique donné. Ainsi, le classement obtenu, dans un ordre décroissant, des traitements de surface étudiés en terme d'endurance est le suivant : VC, TiC/VC, (TiC/VC)_{x2}, TiC, TiCN, TiN. Ce classement est différent de celui obtenu à partir de la valeur de dureté VC, (TiC/VC)_{x2}, TiN, TiCN, TiC/VC, TiC, dans un ordre décroissant. Cette différence pose la question d'une relation directe entre la dureté et la résistance à l'usure. Ainsi d'autres grandeurs comme la tenacité et surtout l'adhésion sur le substrat doivent être considérées. On notera que la démarche proposée permet d'isoler indirectement ces différents aspects et ainsi de mieux les étudier.

En conclusion, la démarche énergétique proposée, introduisant le concept de capacité énergétique, pour rationaliser l'endurance des traitements de surface permet non seulement de comparer les traitements de surface mais aussi et surtout de formaliser la durée de vie pour un très large spectre de chargements. Cette démarche permet aussi une analyse physique des endommagements et ainsi de développer une approche thermodynamique de l'usure. Elle permet aussi d'isoler respectivement les différents mécanismes d'endommagement activés. Enfin, tout en facilitant une analyse physique des endommagements, elle est compatible avec une démarche d'ingénieur et l'utilisation des moyens modernes de calcul tels que les éléments finis. La grandeur de densité d'énergie, est intrinsèque par elle-même c'est-à-dire transposable quelque soit le contact. Identifiée pour un contact elle peut directement être transposée à des contacts industriels plus complexes. Ainsi le calcul de l'énergie de frottement est souvent implémenté sur les codes actuels et par ailleurs très facile à programmer de sorte que la démarche proposée soit directement transposable au milieu industriel.

On retiendra cependant que l'analyse conduite dans ce travail, qui a pour objectif premier de développer un système modèle fait abstraction de différents aspects qui devront dans le futur être mieux formalisés. En particulier, l'aspect humidité et environnemental bien que traité doit être approfondi. Enfin et surtout, l'analyse doit être étendue à différents tribocouples et d'autres aspects comme les phénomènes d'adhésion. Cependant, par son caractère formalisé, cette démarche pourra servir de trame à de multiples développements futurs.

CONTENTS

INTRODUCTION	3
<u>CHAPTER 1: BIBLIOGRAPHY SYNTHESIS</u>	5
1.1. TRIBOLOGICAL PROCESSES IN MACHINES AT WORK	5
1.1.1. Friction in contact between solid surfaces	6
1.1.2. Surface layers of the interacting elements	9
1.1.3. Destruction mechanisms of the surface layer	11
1.2. FRETTING AS A SPECIFIC DESTRUCTION PROCESS	13
1.2.1. Introduction	13
1.2.2. Contact conditions	14
1.2.3. Sliding conditions	16
1.2.4. Transition criteria	19
1.2.5. Fretting maps	20
1.2.6. Fretting damage mechanisms	21
1.2.6.1. Fretting fatigue	22
1.2.6.2. Fretting wear	26
1.2.6.3. Fretting damage methodology	33
1.2.7. Protection against fretting	34
1.3. HARD COATINGS	35
1.3.1. Introduction	35
1.3.2. Hard coatings manufacturing	37
1.3.2.1. Deposition techniques	38
1.3.2.2. The role of process parameters	44
1.3.3. Hard coatings in current engineering practice	45
1.3.4. Hard coatings under fretting regime	47
1.4. OBJECTIVES AND FIELD OF THE WORK	49
1.4.1. Thesis of the work	50
<u>CHAPTER 2: ELABORATION AND PROPERTIES OF THE MATERIALS UNDER INVESTIGATION</u>	51
2.1. THE SUBSTRATE MATERIAL	51
2.2. THE COUNTER-BODY MATERIAL	53
2.3. HARD COATINGS INVESTIGATED IN THE WORK	54
2.3.1. Titanium and vanadium carbide coatings	54
2.3.1.1. Coatings manufacturing	54
2.3.1.2. Coatings characterization	56
2.3.2. Titanium nitride and carbonitride coatings	57
2.3.2.1. Coatings manufacturing	57
2.3.2.2. Coatings characterization	58
2.3.3. Multilayer titanium and vanadium carbide coatings	59
2.3.3.1. Coatings manufacturing	59
2.3.3.2. Coatings characterization	59

CONTENTS

CHAPTER 3: FRETTING WEAR EXPERIMENTS	61
3.1. TRIBOLOGICAL ANALYSIS OF THE INVESTIGATED SYSTEM	61
3.1.1. Fretting apparatus	61
3.1.1.1. Contact geometry	62
3.1.2. Experimental conditions	62
3.1.2.1. Applied loads and displacement amplitudes	62
3.1.2.2. Variable loading conditions	63
3.1.2.3. Environmental conditions	64
3.2. FRETTING WEAR OF HARD COATINGS UNDER INVESTIGATION	64
3.2.1. Titanium and vanadium carbide coatings	64
3.2.2. Titanium nitride and carbonitride coatings	66
3.2.2.1. Impact of Ti interlayer on tribological properties of the TiN coating	68
3.2.3. Multilayer titanium and vanadium carbide coatings	69
3.2.3.1. Introduction of the diffusion mixed layer	70
3.3. IMPACT OF HUMIDITY ON THE PROCESS OF FRETTING WEAR	73
3.3.1. Dry conditions	73
3.3.2. Medium conditions	75
3.3.3. Wet conditions	76
3.3.4. Synthesis	78
3.4. MORPHOLOGY OF DAMAGED SURFACES	80
 CHAPTER 4: HARD COATINGS TRIBOLOGICAL EVALUATION	 83
4.1. COMPARISON OF INVESTIGATED HARD COATINGS WITH USE OF THE ARCHARD'S WEAR COEFFICIENT	83
4.2. PREDICTION OF THE WEAR VOLUME EVOLUTION	86
4.2.1. Global dissipated energy analysis	87
4.2.2. Energy wear coefficient	88
4.2.3. Stability of the approach under variable loading conditions	89
4.2.4. Hard coatings comparison	90
4.3. HARD COATINGS DURABILITY APPROACH	91
4.3.1. Local dissipated energy analysis	91
4.3.2. Contact area evolution	92
4.3.3. Energy density wear coefficient	95
4.3.4. Application of the approach under variable loading conditions	96
4.3.5. Coatings endurance: 'Energy-Wöhler' wear chart	97
4.3.5.1. Determination of the critical number of fretting cycles	99
4.3.6. Introduction of the effective coating thickness concept	101
4.3.7. Cumulative damage approach	104
4.3.8. Durability assessment of hard coatings under investigation	106
4.3.8.1. Comparison of TiC, TiCN and TiN coatings	106
4.3.8.2. Confrontation of all the hard coatings under investigation	111
4.4. SYNTHESIS OF THE CHAPTER	113
 GENERAL CONCLUSIONS	 117
 NOTATIONS	 121
 REFERENCES	 125

INTRODUCTION

Degradation of surface layers due to wear is one of the principal industrial problems resulting in necessity of repairing or replacing mechanical components. Wear is a complex process and is considered as an interdisciplinary one in which different mechanical, physical, and chemical phenomena are involved. Fretting as a specific type of degradation is defined as an oscillatory motion at small amplitude between two nominally stationary solid bodies in mutual contact. This process, usually induced by vibrations, is considered as a plague in all fields of the transport sector and has been identified in e.g. rolling bearings, keys, riveted joints, screw joints, steel ropes or electric contacts.

The selection of a proper material for the particular engineering application is a complex problem, as different materials offer unique properties and it is not possible to gather all useful characteristics in one material. Hence, employment of different surface treatment processes is a widely used alternative solution. Some of the surface engineering techniques, like heat or mechanical treatment are known and applied for a long time. Nevertheless, the majority of surface treatments realised nowadays are physical or chemical vapour deposition techniques, as thin, hard coatings manufactured by these methods guarantee high hardness of the surface, low friction coefficient and improve the wear resistance. On the other hand, in many industrial applications, coating failure may be conducive to catastrophic consequences. Thus, to prevent the component damage it is essential to establish the coating endurance and indicate the safe running time.

In this work the durability criterion for hard coatings under fretting wear is developed. The coating lifetime is estimated through the local dissipated energy approach, where the maximum energy density dissipated in the center of the contact is related to the maximum wear depth. The proposed methodology introduces the critical value of the dissipated energy density, which is a characteristic variable for each surface treatment and durability of different coatings can be compared with use of this variable.

A series of coated specimens: TiN, TiCN, TiC, VC, TiC/VC, (TiC/VC)_{x2} has been prepared in the Institute of Materials Engineering at the Technical University of

INTRODUCTION

Lodz and then subjected to fretting experiments in Laboratoire de Tribologie et Dynamique des Systèmes at Ecole Centrale de Lyon.

The work is divided into four chapters. In Chapter 1 after a short discussion of surface layer composition and properties, the basic damage mechanisms are considered and followed by description of fretting phenomenon. Hard coatings engineering and deposition techniques are reviewed and different types of hard coatings are discussed. Finally, the objectives and thesis of the dissertation are presented.

In Chapter 2 the materials used in the experiments are presented. The substrate and the counter-body material and the applied hard coatings are described. The manufacturing processes of surface treatments are discussed and followed by analysis of mechanical properties and phase composition.

The third Chapter is divided into four parts. The first one presents the experimental equipment and test conditions. In the next part fretting wear mechanisms of the coatings under investigation are described, the impact of Ti interlayer on tribological properties of TiN coating is considered and the notion of the diffusion mixed layer in multilayer TiC/VC system is introduced. The third part of the chapter points out the influence of the relative humidity on fretting wear. The last part gives some examples of surface morphology analysis.

On the fourth Chapter the hard coatings under investigation are compared in terms of their resistance to fretting wear. The classical Archard's law is applied at the beginning. Then surface treatments are classified by means of a global dissipated energy analysis. Finally, hard coatings durability approach is introduced and its endurance is estimated. The thesis of the work is proved in this Chapter.

CHAPTER 1



BIBLIOGRAPHY SYNTHESIS

CHAPTER 1: BIBLIOGRAPHY SYNTHESIS

After a short discussion of surface layer composition and properties, the basic damage mechanisms are considered. In the second part of the Chapter fretting phenomenon is described, with a main focus on fretting wear. The third part is related to hard coatings engineering, where deposition techniques are reviewed and different types of hard coatings are discussed. Finally, according to the completed bibliography synthesis, the objectives and thesis of the dissertation are presented.

1.1. TRIBOLOGICAL PROCESSES IN MACHINES AT WORK

Tribology defined as:

“Science and technology of interacting
surfaces in relative motion and of related
subjects and particles”

is investigated from some hundreds of years. Tribology combines issues of lubrication, friction and wear into a complex framework for designing, maintaining and troubleshooting of mechanical systems. Due to greater requirements imposed upon the materials and general occurrence of tribological processes, it is continuously developing field of science which plays an important role for efficient operating of all kinds of machines. In the engineer practice the materials and loadings are carefully selected and wide range of simulations is completed to exclude the failure of constructions by cracking or plastic deformation. It is a general procedure leading to extension of warranty period and working time without breakdowns. Nevertheless, it happens sometimes that the catastrophic damage occurs due to hidden material defects. Incidents like this finish often in the courts, so the tribologists around the world work on the reliability of mechanical constructions. The research in tribology driven during last years has a complex character taking into account that friction is generally characterised as a branch of physics or mechanical engineering, wear is a part of the material science or

metallurgy, while lubrication is a branch of chemistry. The development of tribology brought along new fields of science like tribophysics or tribochemistry.

Tribology has an important economic impact, which strongly justifies its intensive exploration. It has been reported already by Jost P. (1966) that near 1% of the British gross national product could be saved by applying the fundamental principles of tribology. Maybe this first evaluation was a little bit overestimated however the potential savings related to tribology are significant which was pointed out in the recent books by Rabinowicz E. (1995) or Hutchings I.M. (1992).

Finally we should note the ecological meaning of tribology. It was very meaningful that the motto of Eurotrib'81 Conference was „Tribology Development – the Base of Materials and Energy Savings”. While the friction and wear of the machines parts is reduced, the technical systems are more reliable and less energy is consumed. As a result, the natural resources are saved as well as the pollution of the atmosphere is reduced. The both effects have got a great meaning during the last, pro-ecological decade.

1.1.1. Friction in contact between solid surfaces

When two solid surfaces are mated and the normal load is applied there will be always some deformation of each of them. It can be only elastic or may involve some plastic deformation. When the tangential force is added to such a contact, the friction expressed by the friction force will occur and the degradation process of both bodies will take place.

The most effective way to prevent wear of materials is introducing the lubricant between two bodies in contact. Then, the external dry friction is transformed into the internal friction of the lubricant. As a result, the only condition of the relative movement is to overcome the resistance of lubricant viscosity. Additionally, heat and the third-bodies as well as other impurities from the contact area are carried out by the lubricant. Most of the oils and greases can also protect the mechanical systems against the corrosion during its standstill.

However, in this dissertation only dry sliding friction is being studied, where the contact area of the moving bodies is a function of surface irregularity and physical properties of mated materials as well as of applied normal load. The irregularity results from roughness of the mechanically treated elements, waviness and the shape

inaccuracy. The real contact area is in fact much smaller than the nominal one and the contact between two solid bodies takes place only between peaks and asperities. The adequate contact area is a sum of all elementary contact areas. Taking into account the plastic character of the elementary surfaces the real contact area (A_r) can be expressed by:

$$A_r = \frac{P}{\sigma_{pl}} c \quad (1)$$

where:

P – normal force;

σ_{pl} – yield point of the softer material;

c – geometry-dependent coefficient.

Applying some simplification, the yield point can be replaced by the Brinell's or Vicker's hardness value. Then the real contact area is proportional to the applied normal load and inversely proportional to the material hardness.

Two possibilities of contact between the peaks from the interacting surfaces can be distinguished. When the asperities lock each other (Figure 1a) and when they only adhere (Figure 1b).

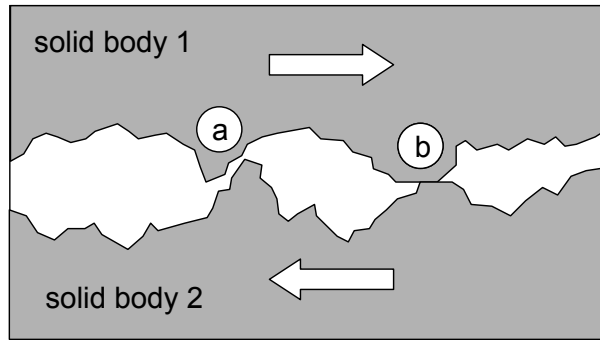


*Figure 1. Roughness of the interacting surfaces subjected to move:
(a) asperities lock each other; (b) asperities adhere to each other.*

The former case leads to the plastic or elastic deformations of the peaks or to cutting off, if the value of tangential force is high enough. In the latter, the adhesion forces between two peaks can extract the asperities. Both cases contribute to the formation of debris, which are the third-body in the contact and which change the tribological properties of the system. Debris formation process is significant for the friction [Rigney D.A. et al. (1984), Godet M. (1984)] and is different for different materials and loading conditions. According to Stachowiak G.W. (2000) it depends also

on the particles shape. The third-body can be ejected outside the wear scar or stay within and play the role of an abrasive particle. Its high hardness accelerates the wear process, particularly during last – catastrophic stage.

The great part of the energy resulting from sliding contact is transformed to heat. In close neighbourhood of the contact are the temperature gradient is present with the highest values of flash temperatures on the peaks. Under the extreme loading conditions and high sliding speeds the flash temperatures can reach value about 1000°C [Czichos H. (1978)], which strongly influences the physical properties of the mated materials. Accumulation of heat in the sliding contacts of the mechanical devices can again, like the presence of the third-body, promote wear and even cause the scuffing.

Although not in all cases, decrease of the friction force usually results in reduction of wear rate. Therefore, the engineers make an effort to decrease the coefficient of friction (COF: μ), taking into account the basic relations:

$$Q_s = \mu_s P \quad (2)$$

$$Q_k = \mu_k P \quad (3)$$

where:

μ_s – static coefficient of friction;

μ_k – kinetic coefficient of friction;

Q_s - force sufficient to prevent the relative motion between two bodies;

Q_k – force necessary to maintain relative motion between two bodies.

What is important in the coefficient of friction definition, is that its value is a function not only of one investigated material but of two interacting materials. What is more, the tabulated values of the coefficient are different for the same sliding materials [Blau P.J. (2001)]. Hence, to describe properly the studied tribo-system, the results of tests under controlled conditions should be rather considered than published values of coefficient of friction.

Fabrication of as smooth as possible surface layers was a natural purpose to obtain the low value of friction forces. However, it appeared that there exists a critical value of the roughness, below which the COF starts to increase.

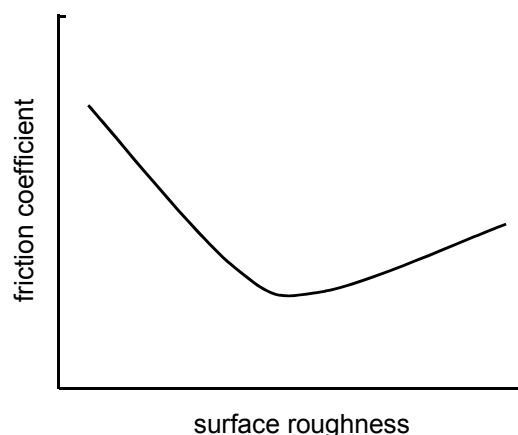


Figure 2. Relation between coefficient of friction and surface roughness.

That relation pointed out that there can be other nature of friction forces than the mechanical one and the molecular theories should be applied [Solski P. and Ziembra S. (1965), Deriagin B.V. (1952)].

1.1.2. Surface layers of the interacting elements

To discuss the field of surface engineering it is essential to define well the surface layers of mating elements which are subjected to friction and wear. According to Kula P. (2000) the *operational surface layer* is a part of the element limited – on the one hand – by its surface and – on the other hand – by the conventional border within the material which limits the set of reasons of the destruction. This general definition comprises the permanent and irreversible changes of the areas near the element surface as well as temporary and reversible efforts of the material. Independently, the *technological surface layer* can be explained as a zone of the material where the structure and the chemical composition was intentionally changed, in order to prevent the destructive processes at work.

The surface layer consists of several zones and can be modelled as depicted in Figure 3 [Bhushan B. (Ed.) (2000)]. Each zone is responsible for the particular processes that affect friction and wear. Deformed sub-layer follows the base material where two zones can be distinguished: heavily plastically deformed layer where crystals are preferentially oriented and lightly plastically deformed layer without preferential orientation. The subsequent Beilby's layer is characterised by an amorphous structure formed by degradation of crystallites during the machining or wear processes.

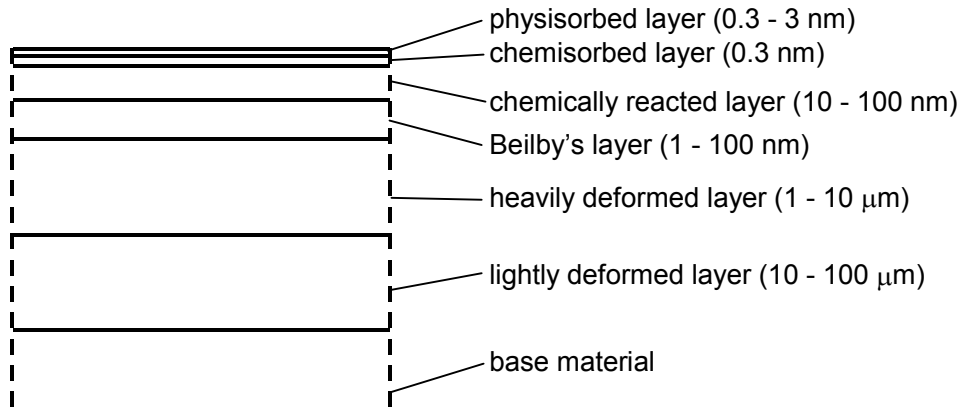


Figure 3. Model of solid surface layer [Bhushan B. (Ed.) (2000)].

The top of the model surface layer consists of chemically reacted layer as, with some exceptions, surface oxides in metals and alloys exposed to the air. There are also physisorbed and chemisorbed layers generated by adsorption of hydrocarbons, water or greasy particles from the environment.

As mentioned in the previous paragraph the surface roughness strongly affects the friction and wear. Even a visually smooth surface appears rough while subjected to the surface profilometry (Figure 4).

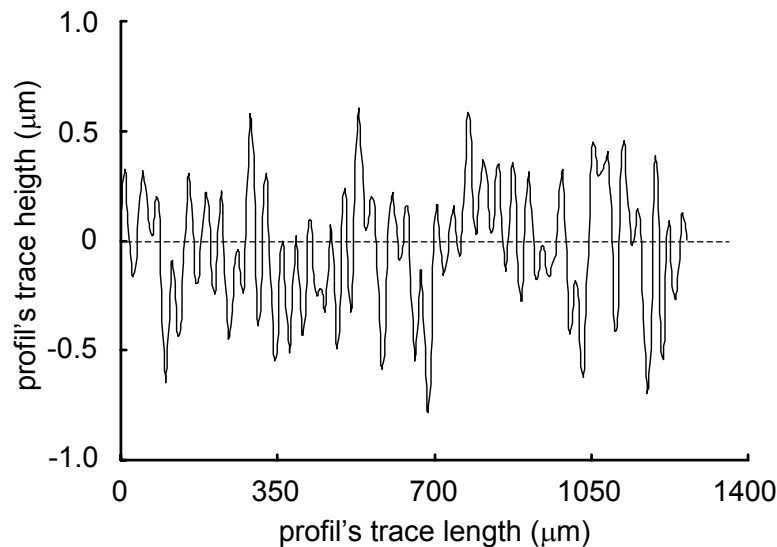


Figure 4. Schematic of surface profile ($R_a=0.2$).

The surface irregularity directly influences the load transmission in the contact area. It decreases the real contact area and promotes high local pressures which are much higher than the theoretically estimated ones. During the relative motion of two interacting bodies the interlocking of surface asperities can take place and friction force will increase.

When considering the surface layer in the contact area under the load the stress distribution plays the significant role. There are some zones situated under the surface layer where the risk of cracking is particularly great due to critical values of material effort: maximal compressive stress (p_{max}) and maximal tangential stresses (τ_{max}). The former can be established with use of the Hertzian equations [Hertz H.R. (1882)] while the latter are situated in the Belaev's point and are equal to $0.3p_{max}$, Figure 5. Therefore, the intentional surface treatment should take into account the depth where the critical value of material effort is situated and provide the thickness of the designed surface improvement process greater than this critical depth.

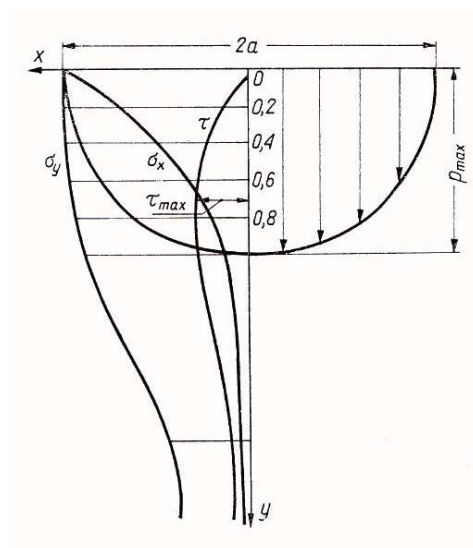


Figure 5. Stress distribution in the point contact [Hebda M. and Wachal A. (1980)].

When a ceramic, hard and brittle material is applied as the top layer of the element the areas around the point contact are subjected to failure as well. Brittle materials are usually much more resistant to compression but highly sensitive to the tensile stresses.

1.1.3. Destruction mechanisms of the surface layer

Tribological wear is a destruction process caused by the friction. The current engineering practice enhances the tribo-systems so that wear of mechanical components proceeds relatively slowly, what allows to extend the time of unfailing work. This period of wear called stabilised-normal wear is acceptable for most of tribological systems. As distinct from the above, during the period of catastrophic wear very fast devastation of the mating elements takes place. In the operation of machines the following general wear

processes can be distinguished: abrasive wear, adhesive wear, fatigue wear and wear by oxidation [Kosteckij B.I. (1970), Barwell J.T. (1980), Hebda M. and Wachal A. (1980), Bhushan B. (Ed.) (2000)].

Abrasive wear means the loss of the material in the contact area due to the ploughing effect of the softer material by the particles of the harder one. Some particles can also be detached and freely move within the contact area or be immobilized in one or both of the interacting surfaces. Abrasive wear usually proceeds very fast and is the most common kind of wear. Depending on the type of surface destruction the following abrasive wear mechanisms can be listed:

- grooving,
- micro-fatigue,
- micro-cutting,
- micro-cracking.

The classical abrasive ploughing takes place when the hardness of abrasive material is higher than the hardness of worn material. However, with significant difference between hardness of mated elements after some operating time, mainly the harder material can be subjected to wear. This is due to a great number of hard debris pushed in the surface of the softer material which forms a kind of abrasive brush.

Adhesive wear occurs in the micro-areas of surface layer plastic deformations, especially within the roughness peaks. This kind of wear takes place at the real contact areas if the atoms of both interacting surfaces are close enough to activate the inter-atomic forces, under low speed sliding friction and high unit pressure. The process progresses easier if bodies subjected to contact are characterised by high chemical affinity. The catastrophic form of adhesive wear is scuffing.

Oxidation wear is the most representative form of corrosive wear of metals. During this process the oxide film is removed by the normal and tangential forces and reproduced on the surface. In case when the oxide forming speed is equal or higher than the removal speed, intensity of process is low. In the opposite case the oxidation wear can be very intense. This kind of surface destruction is typical for friction between metals and their alloys, the chemical and mechanical properties of which considerably

vary. Process can be controlled by applying appropriate materials, surface treatment and selection of suitable lubricant or by decreasing contact temperature.

Fatigue wear is generated during friction under periodically changing loads. High-cycle fatigue or low-cycle fatigue mechanisms are distinguished. It leads to micro-cracks formation and propagation that evolves to macro-cracks and results in separating of material particles. This latter phenomenon is called spalling. The typical configuration where fatigue wear occurs is rolling friction and the surface of the worn element is covered with craters, pits and spalls.

1.2. FRETTING AS A SPECIFIC DESTRUCTION PROCESS

Fretting is considered as a specific type of reciprocating sliding. It is defined as a small displacement amplitude oscillatory motion (usually induced by vibrations) between two nominally stationary solid bodies in contact under normal load. Depending on the loading conditions (displacement amplitudes, normal loading) fretting causes damage by surface fatigue and wear induced by debris formation.

1.2.1. Introduction

Although, first mentions about fretting go back to the beginning of the 20th century, the definition and term *fretting* was established by Tomlinson G.A. (1927). The successive works were conducted among others by Godfrey D. and Bailey J.M. (1952) that pointed out the significant impact of oxide particles, Halliday J.S. and Hirst W. (1956) who reported the wear debris presence in the contact area, Vingsbo O. and Soderberg S. (1988) that were first who applied the fretting maps to describe the relationship between wear and displacement amplitude, later developed by Vincent L. et al. (1992b) by introducing the fretting regimes. For the last fifty years the significant contribution has been carried out by R.B. Waterhouse. The basic findings in the field of fretting are given in his fundamental work “*Fretting Corrosion*” [Waterhouse R.B. (1972)].

The most part of mechanical systems induce vibrations and work under variable loading conditions. This in turn provokes degradation by fretting which leads to the failure of the elements. Even though the process is treated as a plague in many industrial

fields, its meaning is often trivialized what can have disastrous effects. The devastation by fretting was identified for example in rolling bearings, keys, riveted or screw joints, steel ropes, electric contacts and medical implants. It is potentially dangerous for all kinds of transport vehicles beginning from rail-vehicles (where the contact between wheel and axis is concerned), through aircrafts (where e.g. the clampings of the turbine blades are submitted to fretting) and finally automotive vehicles (in which, e.g. the loaded elements of immovable gear-box are concerned). Fretting is indeed a complex process and not all the kinetics and mechanisms are well known. Collins J.A. (1981) defined more than 50 factors that influence fretting, however the list is not closed as it is still being completed by other aspects like, e.g. impact of the magnetic field [Sato K. et al. (2000)].

1.2.2. Contact conditions

In order to simplify the real complex tribo-systems occurring in mechanical devices and constructions, several basic geometries have been developed. The three main types of fretting contact geometries are:

- plane/plane,
- cylinder/plane,
- sphere/plane.

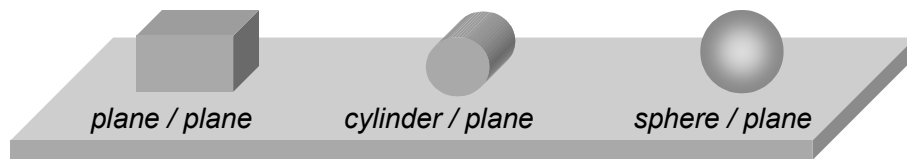


Figure 6. Three fretting contact geometries.

Even though the plane/plane contact configuration allows investigating the wear process on a large surface and is easy to perform, there is a discontinuity in the pressure distribution on the border of the contact. Such circumstances make difficult the mechanical analysis of the interacting bodies. To solve this problem the linear and point contact geometries were proposed where the border effect is eliminated and the maximum pressure values are present along the axis of the cylinder and in the centre of the contact with sphere. The stress distribution and elastic deformations for the contact configurations cylinder/plane and sphere/plane can be determined analytically in the

frame of Hertz's theory [Hertz H.R. (1882)]. More complex and profound investigations of contact mechanics were carried out by Johnson K.L. (1985) and Hills D.A. et al. (1993).

There are two different test configurations that have been developed (Figure 7):

- *fretting fatigue test* derived from a classical fatigue test where two pads are pressed on the fatigue specimen. Relative displacement (δ) and cyclic tangential load (Q) are induced by the strain generated through the fatigue part subjected to external loading. In this configuration crack nucleates and then propagates due to applied external loading.
- *fretting wear test* where contact load is generated by a relative motion between two bodies induced by electro-dynamic shaker or hydraulic system. This configuration is usually applied to analyse wear process due to micro-displacements in a classical reciprocating wear test.

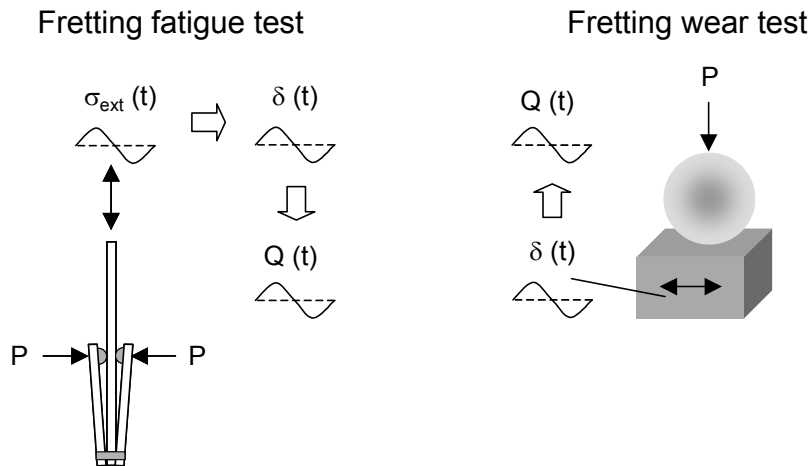


Figure 7. Fretting test configurations.

The most popular fretting test configuration widely used in the tribology of fretting wear is ball-on-flat one. In this case ball can be treated as a model of single surface roughness which makes possible to simplify the theoretical considerations. In such a contact the ball is subjected to normal load and rotation load (P_r), which leads to three fretting modes corresponding to the displacement between two solids can be distinguished [Mohrbacher H. et al. (1995b)]:

- linear displacements (mode I),
- radial displacements (mode II),
- circumferential displacements (mode III).

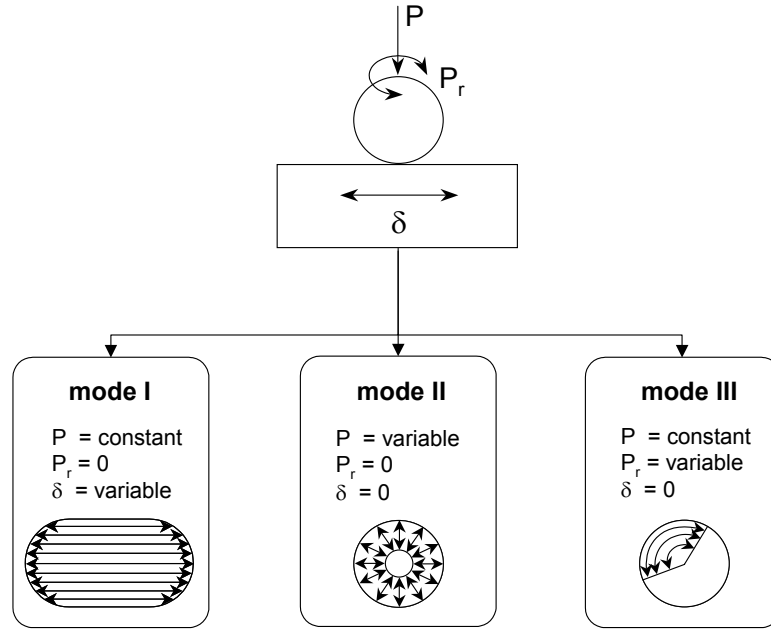


Figure 8. Three basic fretting modes with representative displacement tracks.

Most literature references is related to fretting *mode I* because the wear and friction mechanisms in that case are described by similar laws as sliding friction. However, other modes are being encountered also in the industrial applications and need to be investigated as well. The fretting *mode II* occurs in such a mechanical systems as ball bearings or electrical contacts while fretting *mode III* can be observed in the specific areas of heat exchangers or steam generators.

1.2.3. Sliding conditions

Bibliography sources quote different values of displacement amplitudes as a border between fretting process and reciprocating sliding motion. This value is variously interpreted and contained within a wide range of amplitudes between 50 and 300 μm [Halliday J.S. et al. (1956), Vaessen G.H.G. et al. (1968-1969), Ohmae N. et al. (1974), Gordelier S.C. et al. (1979)]. Although it is possible to limit the relative displacements between particular elements of mechanical systems by means of engineering measures, it is nearly not possible to eliminate fretting as this kind of degradation of friction nodes was reported even for displacement amplitudes δ less than 1 μm [Gordelieen S.C. et al. (1982), Kennedy P.J. et al. (1983)].

Even if we know the lower limit of the fretting displacement amplitudes, to establish the fretting regime the upper limit of displacement amplitudes should be

determined. This issue can be clarified by introducing the e coefficient [Fouvry S. et al. (1996)], which is defined as a sliding ratio:

$$e = \delta_g / a \quad (4)$$

where:

δ_g – sliding amplitude, which is different from the displacement amplitude due to the contact and testing device compliance;

a – contact radius.

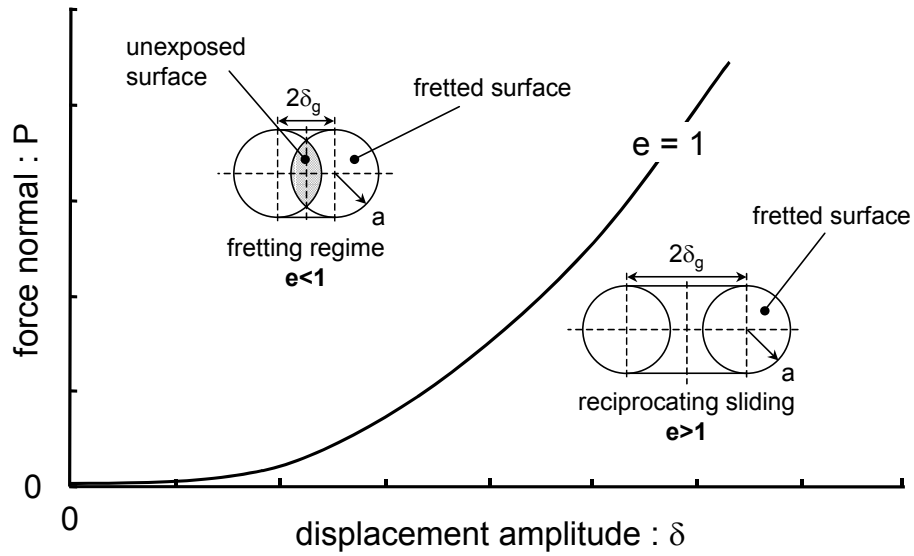


Figure 9. Definition of sliding ratio “ e ” and identification of transition between fretting regime and reciprocating sliding motion (contact sphere/plane).

The tribo-system remains in the fretting regime ($e < 1$) when the unexposed surface is maintained at the centre of the fretted surface. The system turns into reciprocating sliding regime ($e > 1$) when all the surface of mutual contact is exposed to the atmosphere.

It is evident that when investigating the fretting process, the state of stresses and elastic deformations as well as friction forces should be taken into account. For a small value of tangential force, the micro-displacements between two bodies are occurring. Nevertheless, when tangential stress is higher than the friction force corresponding to unit contact area, particular stick and slip zones can be distinguished in the Hertzian contact area [Mindlin R.D. (1949)].

To describe the ball-on-flat geometry the circular stick zone in the centre of the contact and surrounding annular slip zone should be separated (Figure 10).

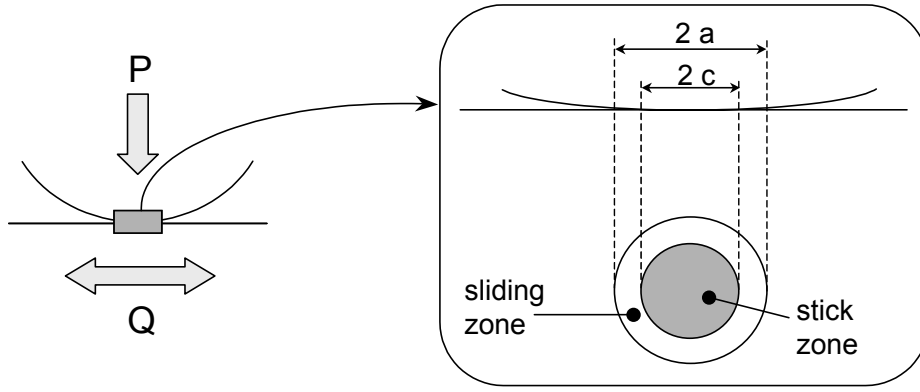


Figure 10. Sphere on plane contact with a constant normal force (P) and a variable tangential force (Q).

Increase of the relative tangential force induces change of the amplitude toward higher displacements and influences the fretting contact conditions. Dynamic recording of the tangential force and displacements amplitudes during the fretting tests as well as some wear scar observations allowed Vingsbo O. et al. (1988) to map the following fretting regimes:

- *stick regime*: the interfacial sliding between two bodies doesn't occur as displacement is accommodated by elastic deformations. Stick domain is maintained by locked asperities that can be plastically shared in the direction of micro-movement. Low fretting fatigue damage can originate mainly by crack nucleation and propagation. For this regime the evolution $Q=f(\delta)$, called fretting log, takes form of closed linear relation (Figure 11a).
- *stick-slip regime*: even though the sliding does occur, the stick zone is a dominating area in the contact. Surface degradation is characterised by cracking as a result of contact fatigue particularly close to the stick-slip boundary. If rough surfaces are subjected to contact the stick zone can be spread for a number of single contacts. The $Q - \delta$ curve takes a characteristic shape of elliptic hysteresis (Figure 11b). In the case of sphere/plane contact the ratio between stick zone radius and contact radius is

expressed by: $\frac{c}{a} = \left(1 - \frac{Q}{\mu P}\right)^{1/3}$ [Johnson K.L. (1985), Mindlin R.D. (1949)].

- *gross slip regime*: with still higher displacement amplitude, the stick zone no longer occurs and entire contact area is subjected to sliding. In this regime the wear mechanism takes place by debris formation (by creating and breaking the adhesive junctions). The debris can also remain within the contact area as abrasive particles. The maximal tangential force doesn't depend upon the sliding amplitude and can be

described by the classic Amonton's friction law: $Q=\mu P$. The evolution of the fretting log in this regime takes more quadratic shape (Figure 11c).

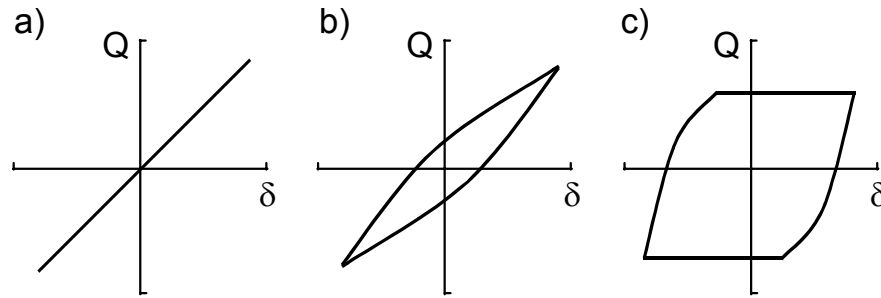


Figure 11. Fretting logs characteristic for different fretting regimes: (a) stick regime; (b) stick-slip regime; (c) gross slip regime.

With successive increase of sliding amplitude the surface degradation process moves toward reciprocating sliding regime in which the progress of wear is not so intensive.

1.2.4. Transition criteria

Depending on the fretting sliding regime different damage mechanisms are occurring. Therefore the determination of the transition criterion is an important issue. In order to identify the single fretting cycle and verify if it remains in the partial or gross slip regime Fouvry S. et al. [Fouvry S. et al. (1995, 1996)] have proposed three criteria (A_t , B_t and C_t , Figure 12) for the sphere/plane contact assuming Mindlin's hypotheses.

The transition values of coefficients A , B and C have been determined as $A_t=0.2$, $B_t=0.26$ and $C_t=0.77$, for sphere/plane contact geometry and are independent of the material properties. Nevertheless, computation of parameters A and B requires determination of the compliance of the system as they depend on the tangential accommodation of the fretting rig. Taking into account that the amount of dissipated energy for each cycle (E_d) is less dependent on the data scattering than the sliding aperture (δ_0), determination of an accurate value of A parameter is the easiest. As distinct from the latter, it is much more complicated to obtain the C parameter due to insignificant difference between E_d and E_0 values (Figure 12).

Transition between fretting and reciprocating sliding regime can also be associated with changes of wear coefficient, wear volume, friction coefficient, wear scar profile and wear debris characteristics before and after the transition point. Taking into account the findings above, some "maps" can be plotted for different pairs of materials.

For steel/steel friction node wear coefficient and wear volume were reported as the most appropriate parameters for identifying the transition criterion [Chen G.X. et al. (2001)].

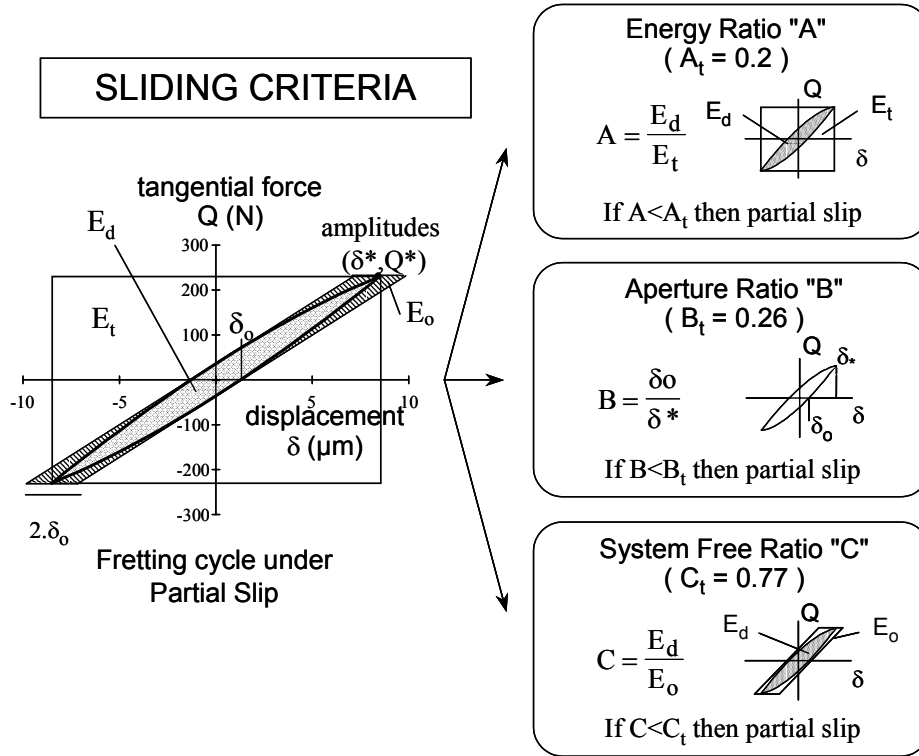


Figure 12. Fretting cycle analysis by quantitative parameters A , B , C to define the sliding transition [after Fouvry S. et al. (1996)].

1.2.5. Fretting maps

Fretting sliding domains were mapped by Vingsbo O. et al. (1988) for a sphere/plane configuration and it describes relation between three fretting parameters: normal force, displacement amplitude and frequency. This approach was then developed by Vincent L. et al. (1992) by defining three fretting regimes for the running conditions recorded during fretting test:

- *partial slip regime (PSR)* corresponding to the condition when stick-slip sliding regime is maintained during running test, observed for the smallest amplitudes;
- *gross slip regime (GSR)* corresponding to the condition when gross slip sliding regime is maintained during running test, observed for the largest amplitudes;
- *mixed fretting regime (MFR)* corresponding to the condition when gross slip and partial slip regimes are present in one fretting test, observed for intermediate amplitudes.

Taking into account the above classification the Running Condition Fretting Map (RCFM) was proposed [Vincent L. et al. (1992)], where fretting regimes are mapped in the function of normal force and displacement amplitude (Figure 13).

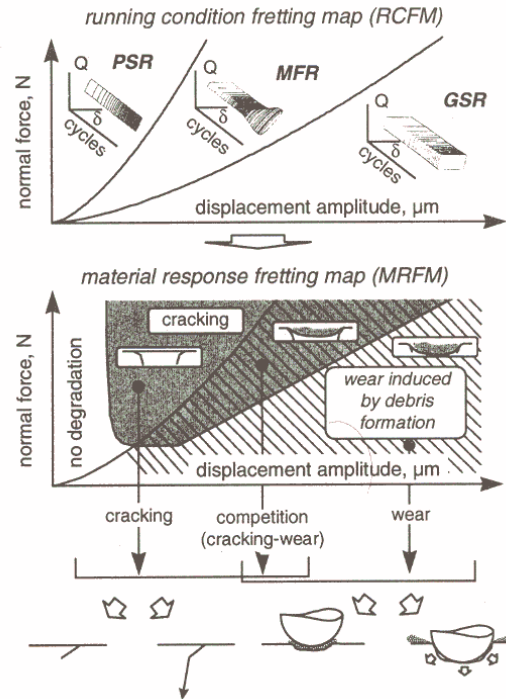


Figure 13. Fretting maps, (a) fretting regimes classification (RCFM); (b) material response analysis (MRFM); [after Fouvry S. et al. (2000)].

The fretting maps approach was completed by introducing by Blanchard P. et al. (1991) the Material Response Fretting Map (MRFM), depicted as well in Figure 13. For the same dependence on normal load and displacement amplitude two main degradation mechanisms – cracking and wear – are being mapped. This type of fretting map is an important tool for mechanical engineers and designers as it permits to define the relevant response of the bulk material and predict the course of such a dangerous process as the crack nucleation is. The RCFM maps are plotted from the direct analysis of the fretting logs while the MRFM maps require some more profound metallographic observations and analyses on carefully prepared specimens cross-sections.

1.2.6. Fretting damage mechanisms

It is well approved that *fretting wear* and *fretting fatigue* are two main mechanisms of damage that can lead to the catastrophic failure of contact areas.

Fretting fatigue is due to stresses resulting from the relative motion between interacting bodies, which are conducive to cracks nucleation and their propagation. Fretting fatigue can be comprehended as a response of the tribo-system to the local overstressing.

Fretting wear is due to the interfacial shear work resulting from the relative motion between interacting bodies and is related to the debris formation and loss of material of contacting bodies. Fretting wear can be comprehended as a response of the tribo-system to the global overstraining of the surface.

Even though these two mechanisms are usually considered separately, one should take into account that under certain operating conditions they can be identified as two competing processes. That situation has been depicted on the Material Response Fretting Map in Figure 13. That is the reason that cracking can be observed under fretting wear regime, while debris formation characteristic for fretting wear is reported also under fretting fatigue configurations [Waterhouse R.B. (1981), Zhou Z.R. et al. (1992)].

Apart from the two main mechanisms of fretting damage, the third one – fretting corrosion – can be distinguished as well. In fact, that latter has been previously considered as a synonym of fretting damage. Corrosion appears in case of oxidation, it can intensify the degradation mechanisms and is nowadays treated as a secondary process in relation to fretting wear or fretting fatigue. Fretting corrosion can be defined as a destruction process under fretting regime boosted by corrosive impact of the ambient atmosphere. Pure fretting, when the chemical reactions don't occur, is rather unusual process. In order to investigate the fretting phenomena without corrosion, a particular testing equipment has to be applied with neutral gases or vacuum as surrounding atmosphere. Wear products take usually form of metal oxides detached from the surface or oxidized debris. Fretting damage is additionally accelerated by stresses generated by interacting solids, which increase the chemical reactivity of surfaces.

1.2.6.1. Fretting fatigue

Fretting fatigue is due to cyclic stresses and initiates when cracks begin to nucleate. It takes place usually within or at the edge of the contact area. The affected part can be easily damaged if the crack propagates. Fretting fatigue is observed mainly in the areas of stress concentration, e.g. in splines, shaft keys or cables.

Two basic parameters are studied in this case: applied normal force and displacement amplitude. Cracking behaviour of material is considered as a function of contact pressure (i.e. tangential effort induced by contact pressure and relative displacement) and fatigue stresses. In fretting fatigue the relative displacement between two bodies is a function of normal force and amplitude of tangential stress. As reported by Waterhouse R.B. (1981) the critical relative displacement amplitude for cracking phenomena is contained within the limits from $10\mu\text{m}$ to $25\mu\text{m}$. With further increase of displacement, the degradation process moves toward debris formation. Particles detachment eliminates the micro-cracks before they begin to propagate.

There are two forms of cracks: short ones (of the length of some tens of micrometers) and the long ones that have propagated. For fretting fatigue investigations, the point of first crack initiation and its direction are of great importance due to their industrial relevance. It was pointed out by Nakasawa K. et al. (1992) for the plane/plane configuration, that the point of crack nucleation within the contact area is a function of sliding conditions (Figure 14). For higher normal loading and smaller displacement amplitudes crack is expected to nucleate on the contact border. With increase of slip zone in the contact some multi-cracks are observed.

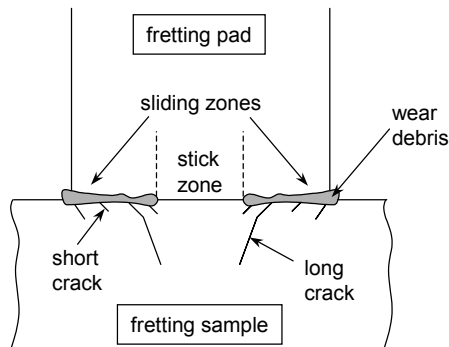


Figure 14. Fretting damage mechanism for the plane/plane configuration [Nakasawa K. et al. (1992)].

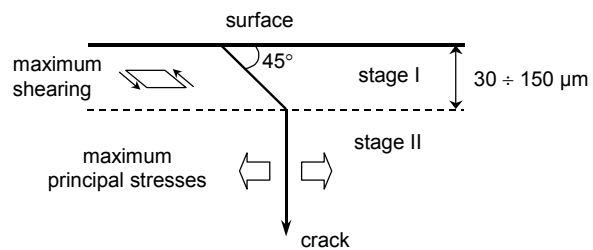


Figure 15. Two stages of crack propagation [Forsyth P.J.E. (1961)].

There are different conditions for generating the short and long cracks. Nucleation of short cracks takes place under lower loading conditions than propagation of long cracks. One can distinguish two stages of cracking originally proposed by Forsyth P.J.E. (1961) (Figure 15):

- *stage I*: crack initiates with the orientation of 45° to the surface, direction which corresponds to the maximum shearing plane. The length of the crack varies and

depends on the tribo-system, however the material properties have the most significant impact.

- *stage II*: the crack propagation is controlled by the principal tensile stresses and point of cracking. Crack initially oriented at 45deg to the surface propagates perpendicularly to it. This direction is the privileged one due to the material properties factors.

Under stable load crack nucleation can be predicted with use of the multiaxial fatigue criteria. The analysis allows to identify the nucleation of first very small cracks usually shorter than 30µm. The following four formulations seem to be the most frequently applied for prediction the crack initiation:

- *Dang Van fatigue approach [Dang Van K. (1993)]*: the crack nucleation process is a function of two macroscopic stresses: shear stress and hydrostatic pressure. If these two variables reach the limit value then there is a high risk of cracking on a critical grain;
- *Crossland fatigue description [Crossland B. (1956)]*: the macroscopic loading path is considered and crack nucleation risk is expressed as a combination of shear stress and hydrostatic pressure;
- *McDiarmid fatigue formulation [McDiarmid D.L. (1991)]*: identifies the maximal shear stress amplitude and indicates the critical plane where the crack is expected;
- *Smith-Watson-Topper fatigue criterion [Smith K.N. et al. (1970)]*: crack will initiate due to shear stress and will grow on a certain plane perpendicular to the direction of the principal stress.

Fretting fatigue process is controlled by cyclic stresses, which are conducive to surface degradation by cracking. In pure fatigue investigations the lifetime of the specimen under uniaxial tension stress is often described in terms of useful and widely applied Wöhler fatigue curves, which relate the number of cycles to failure with maximal amplitude of cyclic stresses. The relevant Wöhler's graphs allow to establish the endurance limit of materials, i.e. the maximal tension value at which the specimen failure will not occur even after great number of cycles (i.e. from the range of $10^8 \div 10^9$ cycles or greater). The approach can be applied with success to fretting fatigue studies by adding the lateral loading pads to the classical fatigue test configuration (Figure 7). This action takes immediate effect on the Wöhler curve position and the influence of fretting fatigue can be expressed by the decrease of the endurance limit (Figure 16). The latter has been reported by numerous research worker, e.g. McDowell O.J. (1953), Endo

K. (1976), Lindley T.C. et al. (1985), Hoepfner D.W. (1994), Del Puglia A. et al. (1994), Sato K. et al. (1994).

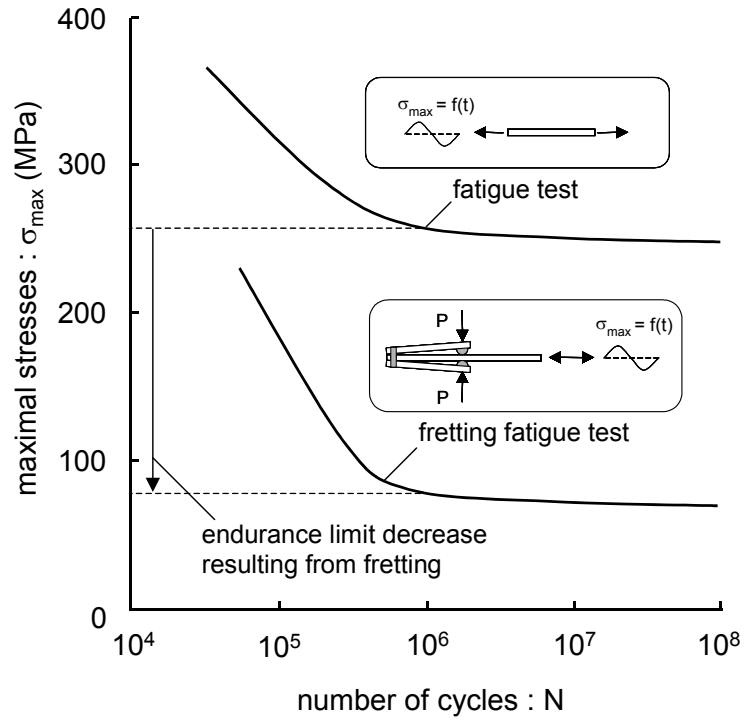


Figure 16. Wöhler curves for fatigue and fretting fatigue tests.

In case of mechanical elements subjected to variable fatigue stresses the Miner's rule [Miner M.A. (1945)] can be applied. It allows to determine the failure point of investigated solid body by cumulative fatigue damage approach:

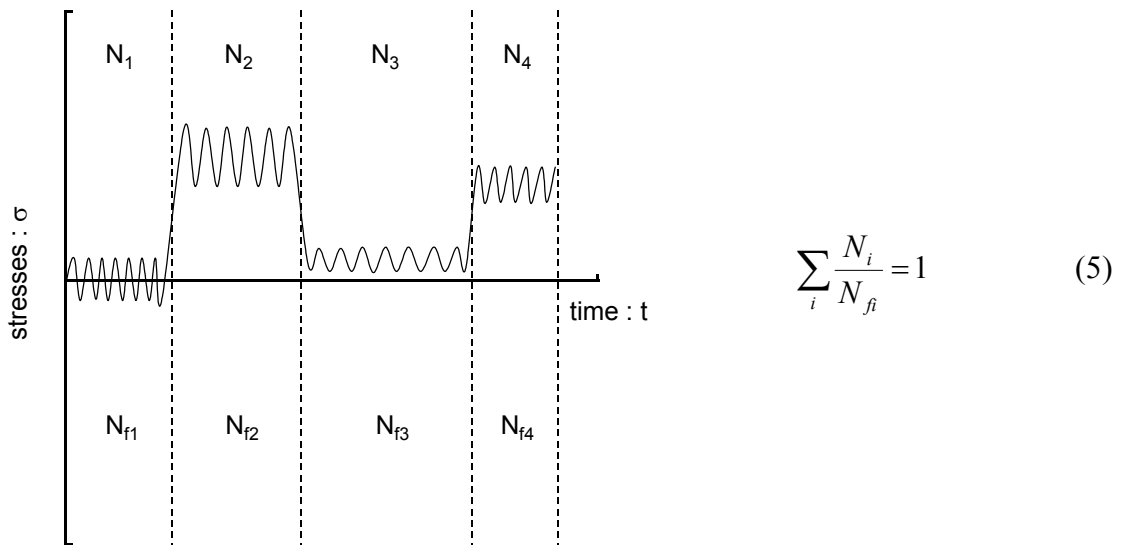


Figure 17. Cumulative fatigue damage approach.

In the above equation N_{fi} is the number of cycles to material failure under i^{th} stress value, whereas N_i/N_{fi} ratio is related to used lifetime of the material after N_f number of cycles. The investigated element will result in failure when the sum in the left term of equation (5) reaches value equal to 1.

1.2.6.2. Fretting wear

In the tribological wear processes the mass, structure and physical properties of the surface layers within the contact area are subjected to changes. The intensity of wear is a function of different interactions between contacting bodies and of the resistance to wear of a friction area. Fretting wear is a specific surface destruction process, where the reciprocating sliding motion with a relatively small amplitude is responsible for the debris formation and loss of material by interfacial shear work. In steel/steel contacts it is easy to identify the lost material – usually the characteristic “red powder” of oxides can be observed in the contact area [Berthier Y. et al. (1985)]. However, fretting wear is not only limited to steel and it is recognised in all friction nodes under fretting.

Wear modelling

Due to different wear mechanisms and numerous factors affecting the tribological processes a large number of theoretical models of wear has been proposed. As it was pointed out by Meng H.C. et al. (1995), 183 equations with more than 300 material and mechanical parameters describing the wear process can be listed. These models often have a theoretical-experimental character. Hence, in order to estimate the coefficients involved in a model the series of tests have to be completed. Moreover, their prediction potential is relatively low as wear models are usually related to specific tribo-systems and it is hardly possible to employ them to any other practical situation. Nevertheless, the tribologists make every effort to find a relatively universal approach to estimate the component duration by predicting the wear mechanisms and their intensity. It has been pointed out in the review of wear models by Meng H.C. et al. (1995) that between 1947 and 1992 one can distinguish three stages of wear modelling:

- *Years 1947-1970:* empirical equations are wide used and applied. They are developed directly with results of tests carried out under various experimental conditions.

Rhee S.K. (1970) during his investigations of the wear behaviour of polymers has observed the impact of applied load, sliding speed (V) and time (t) on the total wear of friction and proposed the following formulation:

$$\Delta m = K P^a V^b t^c \quad (6)$$

where:

Δm – weight loss;

K, a, b, c – empirical constants.

Even though the empirical models are applicable only within the limits for which they were defined, they are often more precise than the theoretical ones developed to describe the relations in the same conditions.

- *Years 1970-1980*: wear models are elaborated on the basis of mechanical contact. Many of them take into account the real contact area and mechanical properties of the materials under investigations as e.g.: Young's modulus or hardness.

The most representative wear model for this group, has been elaborated by Archard [Archard J.F. (1953)]. This model was proposed well in advance to other laws of contact mechanics:

$$W_V = KS \frac{P}{p_f} \quad (7)$$

where:

W_V – wear volume; S – sliding distance;

K – wear coefficient; p_f – flow pressure, approximately equivalent to hardness.

This formula was derived by Archard from an equation previously given by Holm R. (1946), in which a dimensionless coefficient K was introduced to provide the conformity of the formula with experimental results:

$$W_V = K \frac{P}{H} \quad (8)$$

where:

W_V – volumetric wear;

P – normal force;

H – hardness of the softer material.

The K coefficient was interpreted by Archard as a probability to form a wear particle by the asperities of the interacting solid bodies, however other authors propose different interpretations of this coefficient [Shaw M.C. (1977), Hutchings I.M. (1992), Johansson L. (1993)].

- *Years after 1980*: wear equations are based on the mechanisms of material failure. The resistance to wear is no longer considered as a material property and authors try to take into account fracture properties [Hornbogen E. (1975)] and fatigue [Evans A.G. et al. (1981)] or oxidation phenomena [Quinn T.F.J. (1971)].

Wear models developed over the last 25 years have a rather complex form as they comprise a considerable number of mechanical, physical or chemical factors that are taken into account. As an example the wear model for erosion process elaborated by Johansson S. et al. (1987) can be quoted:

$$\varepsilon = (1-f)K_1 \frac{\rho_t \rho_p^{2/9} E_r^{2/3} V_p^{22/9} d^{2/3}}{H_t^{5/9} K_c^{4/3}} + fK_2 \frac{\rho_t \rho_p^{1/3} E_r V_p^{8/3} d}{H_t^{1/3} K_c^2} \quad (9)$$

where:

ε – erosion rate;	E_r – erosion resistance;
f – fraction of volume loss due to spalling;	V_p – velocity of particle;
$K_{1,2}$ – proportionality constants;	d – particle diameter;
ρ_t – density of target;	H_t – hardness of target;
ρ_p – density of particle;	K_c – fracture toughness.

Prediction of wear rate and its mechanism in case of fretting is even more complicated than in case of sliding or erosive wear due to a great number of significant factors that influence this process and are difficult to model. These are, for example:

- modification of the interface and contact geometry during the wear process,
- occurrence of the third-body within the contact area,
- flow of debris,
- mechanisms of material transport between mated bodies,
- influence of the environment,
- impact and interaction of mechanical, thermo-dynamic and physico-chemical aspects.

To describe the fretting wear phenomenon, an attempt has been made by Klaffke D. (1994) by using similar wear coefficient to that in the classical Archard's model, to compare different surface treatments as a function of relative humidity (RH) under fretting regime. This problem has been raised also by the group of J.P. Celis, which has related the wear resistance of several hard coatings to the sliding distance, normal force and number of cycles [Blanpain B. et al. (1993)], (Figure 18).

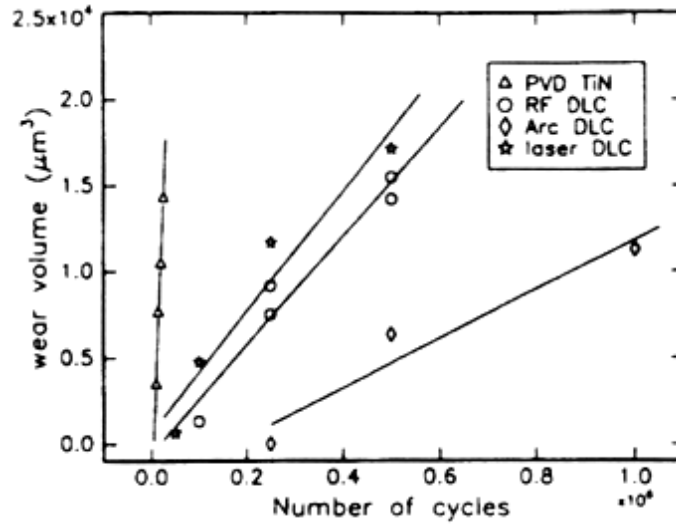


Figure 18. Wear volume of different hard coatings as a function of applied number of fretting cycles (counter-body: alumina ball $R=5\text{mm}$; test conditions: $P=1\text{N}$, $\delta = \pm 50\mu\text{m}$) [Blanpain B. et al. (1993)].

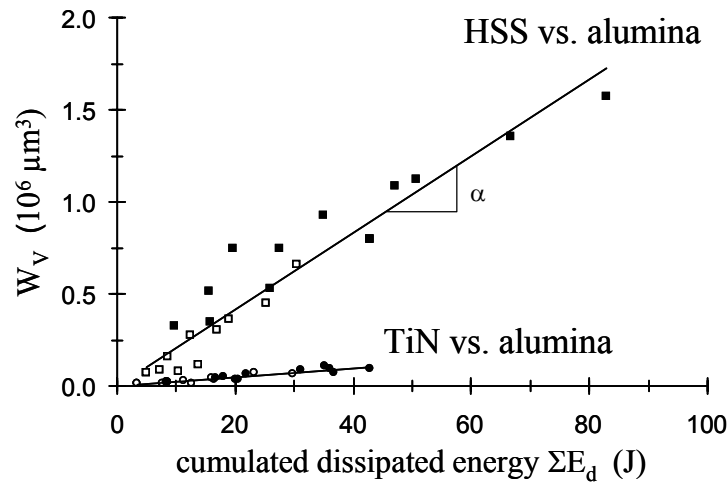


Figure 19. Correlation between wear volume and the cumulated dissipated energy (counter-body: alumina ball $R=12.7\text{mm}$; test conditions: $P=50\text{N}$, $\delta = \pm 25\mu\text{m}$) [after: Fouvry et al. (1996)].

One should consider first the fact that the wear volume is not a product of effort originating from normal load, like that it is comprised in the Archard's law, but from the tangential effort induced by friction force. This approach was completed by the energy factor [Mohrbacher H. et al. (1995a), Fouvry S. et al. (1996, 2001a, 2003)]. The wear volume is related to the quantity of cumulated dissipated energy in the contact area (Figure 19). This approach takes into account the normal load, evolution of coefficient of friction, displacement amplitude and the fretting test duration. It is also possible to determine the energy wear coefficient (α) to compare wear resistance of different bulk materials and coatings.

Recently the group of T.N. Farris has proposed to quantify the wear by local formulation of the Archard's law [Goryacheva I.G. et al. (2001)]. This study was carried out by fretting-fatigue in the partial slip regime, in which wear is not a principal mechanism of destruction. The evolution of wear is correlated with the modification of the contact geometry during the fretting test. This modification generates the redistribution of the stress field and deformation, which is connected with the wear volume by the integration of the local Archard's law within the whole contact area.

This global analysis permits to determine the scalar coefficients (wear coeff.) more or less apart from the test conditions and allows to compare the components in the studied contact. Nevertheless, a change toward another contact configuration changes the established test conditions, which is a great obstacle in the way of developing an universal model. The quantitative variables are defined globally while the volume of worn material related to the energy dissipated within the contact area does not consider the local aspects of degradation. Hence, local energy approach [Fouvry S. et al. (1997)] is a reliable formulation to relate the local wear to the energy dissipated in the interface of the contact area. The global and local aspects of energy approach are employed in this dissertation and are described wider in Chapter 4.

Debris formation and Tribologically Transformed Structure

The approach proposed by M. Godet and his research group [Godet M. (1984), Berthier Y. et al. (1988), Vincent L. et al. (1992a)] is based on the assumption that the degradation of the surface layer is rather associated with the quantity of debris ejected outside the contact area than with the total wear volume. Debris remaining in the contact participate in the process of loads transmission and protect indirectly the first-bodies against degradation. In this case, the following statement can be quoted: 'a good anti-wear material combination is one that sacrifices its surface to save its volume' [Berthier Y. et al. (1989)]. The third-body can be introduced to the interface voluntary (grease, oil...) or can results from wear process of the first-bodies – debris screen maintained within the contact area.

Successive observation of the friction interface [Berthier Y. et al. (1988)] allowed to introduce a capable formalism, which defines different sites and processes of the accommodation mechanism in the contact area (Figure 20). In fact the approach is based on five sites (S_i) and four accommodation modes (M_j). The five identified sites are

two rubbing solids, a “bulk” third-body and two screens separating first-bodies and bulk third-body, while four modes are the elastic, rupture, shear and rolling ones. The accommodation mechanism is defined by the couple of site and mode ($S_i M_j$) and 20 different combinations can be distinguished. It was observed [Vincent L. et al. (1992a)] that third-body screens S_2 - S_4 are also activated in fretting.

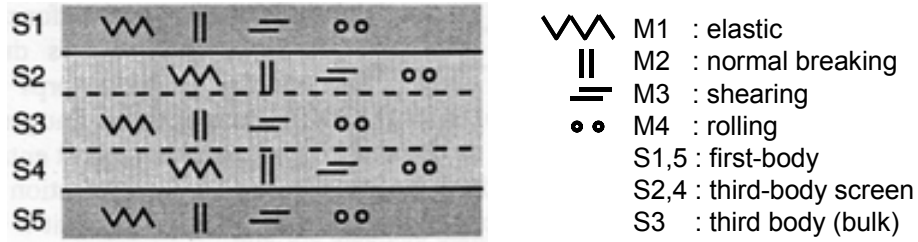


Figure 20. Accommodation mechanisms in the contact [Berthier Y. et al. (1988)].

Hence, wear of the studied material is defined by the quantity of particles ejected from the interface and can be calculated by determination of the flow of debris (w). For an unidirectional contact:

$$w = l \int_0^{h_d} u(y) dy \quad (10)$$

where:

l – length of contact;

h_d – thickness of the debris screen;

u – debris ejecting velocity gradient distribution.

This model well describes the reality of the physics of an accommodation and damage mechanisms, however it is quite complicated to formalize and not favourable to introduce some precise variables to compare different materials. This analysis allows rather to interpret the complex tribological mechanisms proceeding at the interface, like impact of the third-body on decrease of the coefficient of friction or its advantageous influence on wear kinetics. The third-body approach permits also to better distinguish tribo-contacts where debris are trapped within the contact area in contrast to the ones where wear particles are rapidly ejected outside the contact area and do not play a protective role any more. This can clarify why such a great differences of the wear kinetics are observed between results of fretting tests and other ones obtained for example in the experiments with rotative friction. Application of this guidelines in fretting investigations makes easier analysis of evolution of the tribo-contacts as

a function of test duration or sliding regimes. Modification of accommodation site or mechanism can influence friction coefficient and consequently transition from partial to gross slip fretting regime due to the alteration of friction behaviour on interface level.

This approach encouraged the researchers to further study the debris generation laws. It has been shown that metallic materials subjected to alternating sliding, tend to generate a specific transformed layer on the top surface [Blanchard P. (1991), Sauger E. (1997), Sauger E. et al. (2000)] (Figure 21). This layer, called tribologically transformed structure (TTS), has a particular nanocrystalline structure, corresponding to the chemical composition of the primary material.

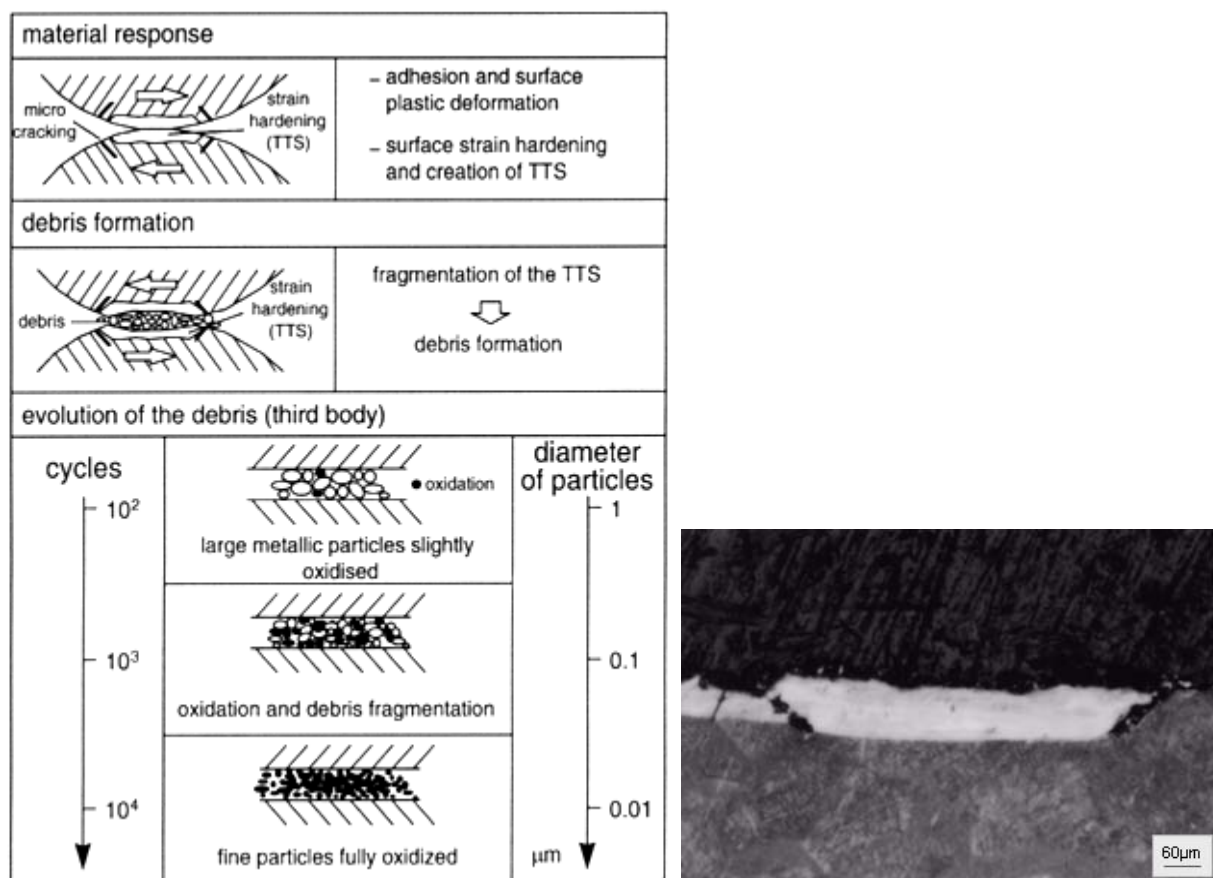


Figure 21. Tribologically transformed structure; (a) Creation and evolution of the third-body through the contact interface [Blanchard P. (1991)]; (b) cross-section of TTS (35NiCrMo) [Fouvry S. et al. (2003)].

Tribologically transformed structure forms as a result of plastics deformations induced by a relative motion of solid bodies under load and has the Young's modulus like that of the original metallic structure but its hardness is significant high. The transformed layer is formed during the very first fretting cycles and corresponds to the

intermediate stage between a material of the first-body and debris of the third-body. Within his thesis E. Sauger [Sauger E. (1997)] has studied different tribo-systems with titanium and has proposed the following two-stage wear mechanism (Figure 22): accumulation of plastic deformation (without wear and TTS) and then rapid formation of TTS leading to formation of wear debris. Thickness of the created TTS remains constant afterwards, while total thickness of worn surface increases in accordance with transformation $TTS \rightarrow$ wear debris.

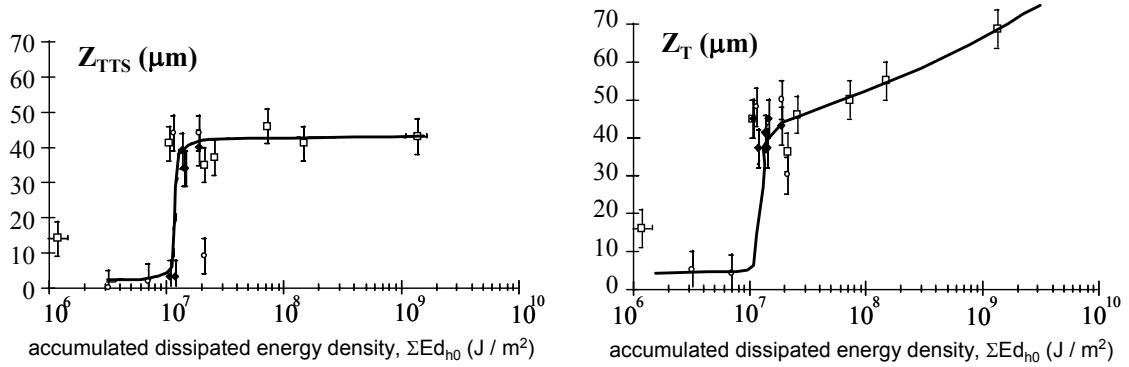


Figure 22. Thickness evolution in the function of cumulated local dissipated energy of: (a) TTS; (b) total worn surface [Sauger E. et al. (2000)].

Even though the existence of the TTS layer has been proved, some of the mechanisms are still not clear and need to be solved. Importance of the parameters like adhesion and roughness or a mode of the first transfers are not comprehensible yet. Nevertheless, these transformations of the superficial layer modify the initial properties and behaviour of the materials subjected fretting contact, and in consequence, have to be taken into account in all analyses of debris formation. Impact of the surface processes induced by the plastic deformations plays a key-role in comprehension of the third-body approach, but it is difficult to integrate this parameter into a quantitative model.

1.2.6.3. Fretting damage methodology

An interesting holistic methodology to investigate the fretting damage was proposed by Fouvry S. et al. (1996) (Figure 23). It begins by identification of sliding condition through the quantitative parameters A , B , C indicating the transition between partial and gross slip conditions. Having defined the fretting regime we are able to point out the main mechanism responsible for surface process degradation. If it is the partial slip, the cracking phenomenon is expected and nucleation condition can be precisely

quantified by one of the fatigue approaches, e.g. by means of Dang Van multiaxial fatigue analysis. Under gross slip, material removal and debris formation are mainly encountered and material surface degradation can be identified by referring the loss of material to the energy dissipated in the contact area.

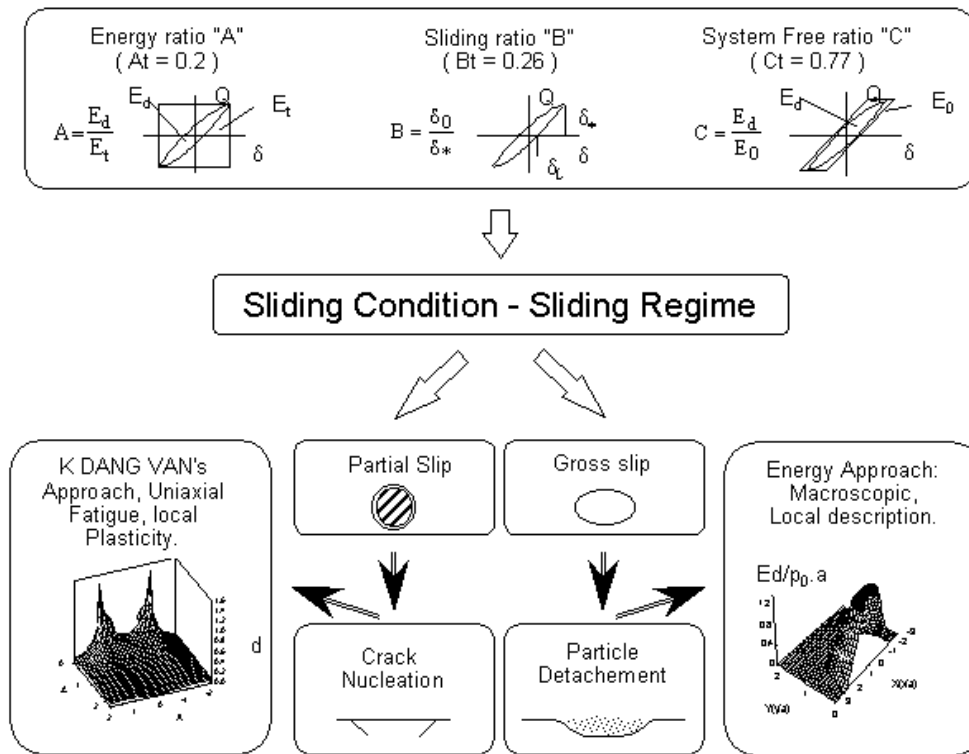


Figure 23. Fretting damage methodology [after Fouvry S. et al (1996)].

1.2.7. Protection against fretting

In view of potential failure of responsible mechanical systems, fretting can lead to catastrophic consequences. Therefore, considering the economical and social factors, some due steps should be taken in order to exclude or to limit the adverse effects of fretting.

Protection against fretting has to be taken into account even at design stage of the fretting couple. By designing the appropriate contact geometry of nominally immovable junction, the concentration of stresses and consequently fatigue cracking can be avoided. Construction treatment can also contribute to decrease of reciprocal displacement amplitude [Guzowski S. (1998)]. Nevertheless, destruction by fretting can not be completely excluded as this kind of damage was reported even under amplitude $\delta < 1\mu\text{m}$ [Kennedy P.J. et al. (1983)].

Taking this into account, the designer should make an adequate choice of materials. Tribo-systems with polymers are characterised by higher fretting resistance than e.g. steel/steel ones, while hard steel has higher resistance than the soft one. There are also some exceptions like high chromium steel, in which hard and brittle oxides formed on the surface lead to increase of wear rate [Varenberg M. et al. (2002)].

Appropriate surface engineering techniques can provide an effective protection against fretting wear. To obtain this goal the following methods with adequate processes increasing fretting resistance should be followed [Harris S.J. et al. (1985), Labedz J. (1988), Waterhouse R.B. (1988), Fu Y. et al. (2000)]:

- *induce a residual compressive stress*: one of the most effective measure in order to decrease the fretting fatigue (e.g. by shot-peening, nitriding, carburizing, ion implantation, etc.);
- *decrease the coefficient of friction*: higher value of friction forces leads to higher shear stresses which can promote fatigue failure and delamination (e.g. by physical vapour deposition (PVD) and chemical vapour deposition (CVD) techniques, solid lubricated coatings, nitriding, carburizing);
- *increase the surface hardness*: increase in surface hardness prevents the adhesive and abrasive wear in fretting (e.g. by nitriding, carburizing, shot-peening, PVD and CVD techniques, ion implantation, laser cladding);
- *control of surface chemistry*: the surface chemistry can generate a lubricant effect and improve fretting resistance (e.g. by formation of an oxide, nitride or carbide layer).

An obvious way to decrease the fretting wear rate is to employ the lubricants wherever it is possible [Shima M. et al. (1997), Zhou Z.R. et al. (1999)]. However, taking into account low sliding speeds and high pressures, lubricating not always delivers desirable effects. An effective lubricating in case of fretting consists in constant inflow of grease or oil to the contact area.

1.3. HARD COATINGS

1.3.1. Introduction

One of the most important materials properties that influence significantly the tribological wear is hardness. Hard materials first of all have higher abrasive wear

resistance (e.g. against micro-cutting or ridging). According to Kragielskij I.V. et al. (1977), the resistance of carbon and alloy steels after hardening and tempering against abrasive wear increases linearly with increase of hardness:

$$Wr_H = Wr_{H_0} + c(H - H_0) \quad (11)$$

where:

Wr_H – wear resistance of steel after heat treatment;

Wr_{H_0} – wear resistance of steel after annealing;

H – hardness of steel after heat treatment;

H_0 – hardness of steel after annealing;

c – chemical composition dependent proportionality coefficient .

This increase of wear resistance for harder materials is also proved by the classical Archard's law [Eq. (8)] previously presented in sub-chapter 1.2.6.2.

More effectively than by means of conventional heat treatment processes, wear resistance of a material can be enhanced by different thermo-chemical treatments, like carburising, nitriding or boriding [Burakowski T. and Wierzchoń T. (1995), Haś Z. and Kula P. (1995), Pełczyński T. (1991)]. Due to these processes hard anti-wear carbides, nitrides or borides of transition metals are build into the surface layer of steel. Simultaneously the steel matrix (martensitic, ferritic or austenitic) is being enriched by diffusion in an adequate interstitial element (B, C, or N) up to a depth depending on diffusing species, steel grade, process temperature and dwelling time. Due to higher hardness of the matrix with fine-dispersed hard carbides, borides or nitrides the abrasive wear resistance of steel increases. Simultaneously the surface of the treated steel is more resistant to the adhesive wear as the creation of adhesive junctions between mated materials is much more difficult due to different structure, chemical composition and type of interatomic bonds [Łunarski J. (1989)].

The most effective way to increase durability of tools and machine components is related to hard coatings deposition technologies. A large variety of functional properties, like wear resistance, mechanical response, corrosion resistance or biocompatibility can be optimized separately for bulk material and its surface by adequate surface treatment. The performance of coated components is usually superior in comparison to uncoated elements. Definition of hard coatings (sometimes called also ceramic coatings) is attributed to the material of surface layer with a hardness of above 1100HV, which makes them harder than the hardest tool materials like high speed steel or sintered carbides [Halling J. (1986), Burakowski T. and Wierzchoń T. (1995), Holmberg K. and

Matthews A. (2000)]. It has been demonstrated by Nordin M. et al. (1998) on the ground of experiments with a number of hard coatings that their resistance to wear increases linearly with their hardness. Nitrides, carbides, borides and oxides in Table 1 are especially attractive for anti-wear applications and the first ones are mostly employed in the engineering practice while the last ones rather seldom. These compounds are created by transition metals from groups IVb, Vb and VIb of the periodic table (usually: Ti, Cr, V, Zr, Ta, Mo, W, Nb, Hf) with nitrogen, carbon, boron and oxygen (acquired from reactive gases, vapours or by means of chemical reactions).

The coated tools have usually several times higher durability than the ones without coating and are conducive to lower friction coefficients. Due to hard coatings the direct costs (new tools, energy) as well as the indirect ones (service, standstills) can be reduced.

Table 1. The most often employed anti-wear hard coatings [Burakowski T. et al. (2000)].

Group	Coating	Hardness (HV)
Nitrides	TiN, ZrN, HfN, VN, NbN, TaN, CrN, MoN, WN, BN, AlN, Si ₃ N ₄	1100-5000
Carbides	TiC, ZrC, HfC, VC, NbC, TaC, Cr ₃ C ₂ , MoC, Mo ₂ C, WC, W ₂ C, B ₄ C, SiC	1500-4100
Borides	TiB ₂ , VB ₂ , NbB ₂ , TaB ₂ , CrB ₂ , Mo ₂ B ₅ , AlB ₂ , W ₂ B ₅ , LaB ₆ , TiB ₆	2100-3000
Oxides	TiO ₂ , Al ₂ O ₃ , Y ₂ O ₃ , VO ₂ , BeO, SiO ₂ , In ₂ O ₃ , ZrO ₂ , Be ₂ O ₂ , BeO ₂	1200-2500

1.3.2. Hard coatings manufacturing

Depending on the phenomena employed in the manufacturing process, the following surface engineering methods can be distinguished [Burakowski T. and Wierzchoń T. (1995)]:

- *mechanical*: the pressure induced by a tool or a moving particle is used to strengthen the surface layer of treated material;
- *thermo-mechanical*: coatings are obtained by action of heat and pressure (spraying, plating, detonation-strengthening, plastic working);
- *thermal*: the influence of heat is utilised to change state of aggregation or structure of materials subjected to treatment;
- *thermo-chemical*: the effects of heat and chemically active factors are employed. The process can be carried out in: powders, pastes, baths, gases;

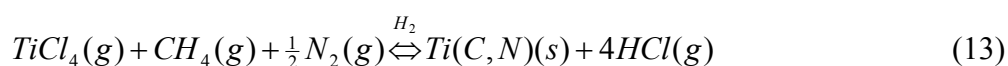
- *electro-chemical and chemical*: galvanic or chemical methods or electrochemical reduction are exploited for manufacturing metallic coatings;
- *physical*: under atmospheric or reduced pressure physical phenomena are realised, in most cases with use of ions of metallic or non-metallic elements.

1.3.2.1. Deposition techniques

As current industrial practice indicates, two techniques from the aforementioned ones with numerous of variations are most popular and deliver the largest number of coated components. These are *chemical vapour deposition* related to thermo-chemical techniques and *physical vapour deposition* attributed to physical techniques. In this section the *indirect deposition method* developed in the Institute of Materials Engineering at the Technical University of Lodz is also presented, as a significant number of specimens investigated in this work has been prepared by this novel method.

Chemical vapour deposition

The chemical reactions used for coatings manufacturing by means of chemical deposition from a gas phase are usually endothermic ones and to spark them off some additional energy is required. In conventional CVD processes initially developed by Arkel van A.E., Boer de J.H. (1925) and Münster A., Ruppert W. (1952, 1953) (*not supported* as it was proposed by Burakowski T. and Wierzchoń T. (1995)) thermal energy was employed for necessary activation. According to Hinterman H.E. (1979) the reactions conducive to creation of TiC or Ti(C,N) coatings using TiCl₄ vapour and methane or methane nitrogen and hydrogen (respectively) as the substrates are as follows:



where symbols *g* and *s* are related to gaseous and solid states.

Stock H. et al. (1986) estimated that under the 273K temperature and 1000 hPa pressure the difference of the thermodynamic potentials of products and substrates in the reactions (12) and (13) is equal to 210 kJ·mol⁻¹ and 160 kJ·mol⁻¹ respectively (Figure 24). Hence at this temperature both reactions proceed from the right side to the left one.

With increase of temperature, this difference of the thermodynamic potentials decreases and the reactions (12) and (13) proceed spontaneously from the left side to the right one above the temperature of 1131K or 1074K respectively.

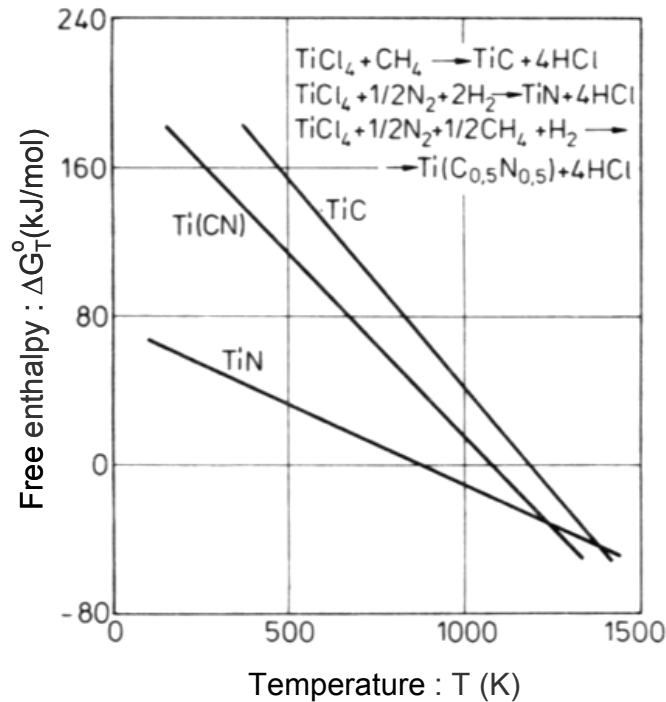


Figure 24. Evolution of free enthalpy of synthesis reactions of TiC, TiN and Ti(C,N) by means of CVD processes [Stock H. et al. (1986)].

Application of not supported CVD techniques is rather limited as the high temperature processes bring about supplementary heat treatment after completion the CVD operation, which can be detrimental to geometrical accuracy of treated elements. That was the reason that development of the chemical vapour deposition techniques aimed at more or less significant decrease of applied temperatures. In this way a number of *supported methods* has been introduced. Some of them are:

- *plasma assisted CVD (PACVD)*: with electrical activation or plasma excitation of gas environment, the temperature during deposition process can be reduced to 720-820K [Arai T. et al. (1987), Tyrkiel E. et al. (1995)];
- *low pressure CVD (LPCVD)*: under the pressure 1hPa – 1Pa the coatings are more homogenous, compact and the coatings thickness is more uniform as well [Chin J. (1993), Hitchman M.L. et al. (1993)];
- *metal-organic CVD (MOCVD)*: with use of metal-organic precursors and appropriate gas-atmospheres [Rie K.T. et al. (1991), Hitchman M.L. et al. (1993)];

- *laser CVD (LCVD)*: stimulation of laser is used to melt thin surface layer of treated element without interference into the bulk material structure [Hitchman M.L. et al. (1993)].

Physical vapour deposition

According to Bunshah R.F. (1982) all coatings deposition techniques under reduced pressure in which the phenomena like thermal evaporation, sublimation or spraying are employed, can be classified to PVD methods. Currently dozens of variations and modifications of PVD techniques are recognised [Burakowski T. and Wierzchoń T. (1995)], which have the following common attributes: (a) are based on physical processes proceeding under reduced pressure in the range of 10^{-10} to 10^{-5} Pa; (b) are conducted on cold substrates or heated ones below 773K. Coatings deposited by PVD methods are usually formed by beams of atoms and/or ions. For evaporation or sublimation electron beam or arc discharge is used, while for spraying usually Ar^+ ions accelerated in electric field. Incident upon substrate surface Ar^+ ions transfer their energy and momentum, which significantly influence coatings structure and properties [Mattox D.M. (1973)]. PVD techniques where electrical polarization of substrate is applied on purpose to control the structure and properties of coatings during deposition are called ion plating. Four variations of this method are employed in industrial applications [Sproul W.D. (1996)]:

- magnetron sputtering [Münz W.D. (1991)],
- cathode-arc evaporation under low pressure [Snaper A.A. (1971)],
- electron beam evaporation from low-voltage source [Moll E. et al. (1980)],
- triode-evaporating by means of electron gun with high-voltage cathode [Matthews A. et al. (1981)].

The above techniques are reactive ones, in which atoms of metals are moved into vapour state through sublimation, metal evaporating from the surface of the molten pool or by spraying the solid magnetron target. Simultaneously the appropriate reactive and/or transport gases are being dispensed into the chamber which they undergo the reactions with transition metals vapours and create the advisable phase, e.g. M_xC_y or $\text{M}_x\text{C}_y\text{N}_z$.

Magnetron sputtering [Miernik K. (1996a,b,c)] is one of the most widely used deposition methods as it is characterised by sufficiently high target sputtering rate and

by reduced range of applied pressure. Non-uniform target current density is characteristic for magnetron sputtering technique. Due to that particular erosion areas are being created on the target surface, where the ion current has the highest density. Different modifications of this method are related to variety of equipment constructions (Figure 25). Thickness of deposited coatings depends on spatial distribution of sputtered material, on target material, substrate geometry, deposition time and target/substrate distance. Atoms ejected from target are deposited on the nearby situated surface, which can be substrate or chamber walls or inside-chamber equipment. To make the most of the target material it is crucial to deposit most of this material on the substrate surface and to minimize the coating thickness dispersion [Westwood W.D. (1990)]. Coating thickness (t) deposited by means of magnetron sputtering on a flat substrate is a function of lateral dimensions of the substrate and of target emission field [Miernik K. et al. (1994)] and is defined by:

$$t = \frac{M_r}{\rho} f(x, y) F \left(\frac{f(\gamma) \cos \delta}{R_v^2} \right) t_d \quad (14)$$

where:

M_r – atomic weight of sprayed metal; t_d – deposition time;
 ρ – density of material; R_v – radius-vector;
 γ, δ – emission and deposition angles.

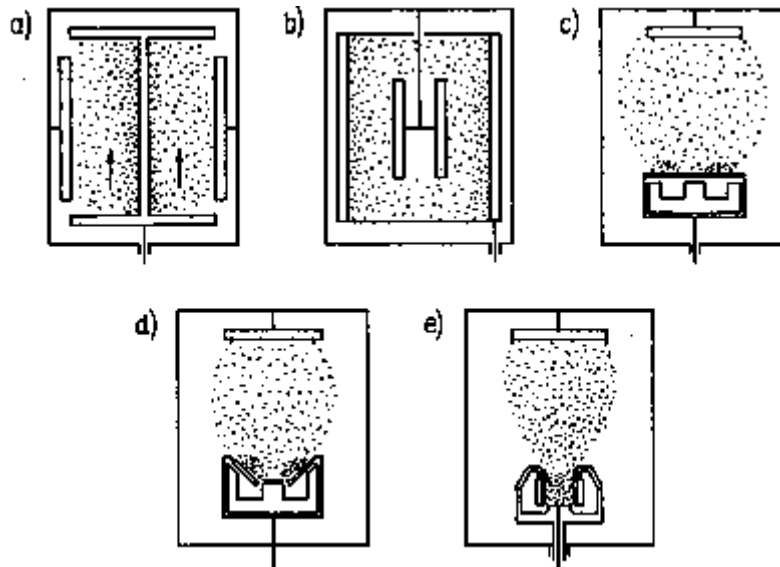


Figure 25. Magnetron sputtering realised by means of different magnetron constructions: (a) cylindrical; (b) cavity-cylindrical; (c) flat; (d) angle-conical; (e) spraying gun [after Burakowski T. and Wierzchoń T. (1995)].

Great variety of developed PVD methods results from the following [Dobrzański L.A. (1999)]:

- intensification of the deposition rate by means of reactive, activated, reactive-activated processes,
- variety of deposition processes (evaporation, spraying, sputtering),
- location of the generating and ionisation areas of material vapours,
- vapour generation of deposited material or compound: evaporation, sublimation, sputtering.

By means of PVD techniques compact carbide, nitride and carbonitride coatings of transition metals can be manufactured under much higher growth rate than in case of CVD methods. Taking into account relatively low substrate temperatures (below austenite/ferrite transition temperature), carbon from the steel-substrate do not take part in coating synthesis. Completely different situation takes place in the novel indirect deposition method.

Indirect deposition method

To form a CVD or PVD hard coating a number of parameters has to be controlled as it is necessary to deliver simultaneously atoms of carbon (or nitrogen or oxygen or boron) and those of a transition metal. These parameters have to be controlled and adjusted to create coatings with an expected chemical composition in a repeatable way, which leads to high costs of deposition equipment as numerous sensors, controllers and microprocessors needs to be installed. This in turn is a reason of lower reliability of the equipment. As distinct from the one-step CVD and PVD processes, an indirect, two-step method has been developed [Wendler B. et al. (1995)], especially suitable and effective for creation of transition metals carbides or carbonitrides on high speed steels (HSS) [Wendler B. (1998)]. The number of deposition parameters to be controlled in the same time is significantly lower in this method, which is a great advantage contributing to manufacturing high quality hard coatings on HSS steels.

In the first step of the process on the cleaned surface of steel with high carbon activity, thin metallic layer of carbide-forming transition metal from IVb or Vb group is deposited by means of any well known method, e.g.: thermal evaporation, electron beam evaporation, cathode sputtering or magnetron sputtering. The second step is to hold the substrate with deposited transition metal layer at an elevated temperature to create

a carbide coating or – in case of heating in pure nitrogen atmosphere – to create carbonitride coating. While heating, the thermally activated outward diffusion of carbon atoms from the steel substrate to transition metal coating (and/or eventually an inward diffusion of nitrogen atoms from the gas atmosphere) takes place and in result the pure transition metal coating undergoes structural and phase transformations conducive to forming the adequate carbides or carbonitrides (Figure 26).

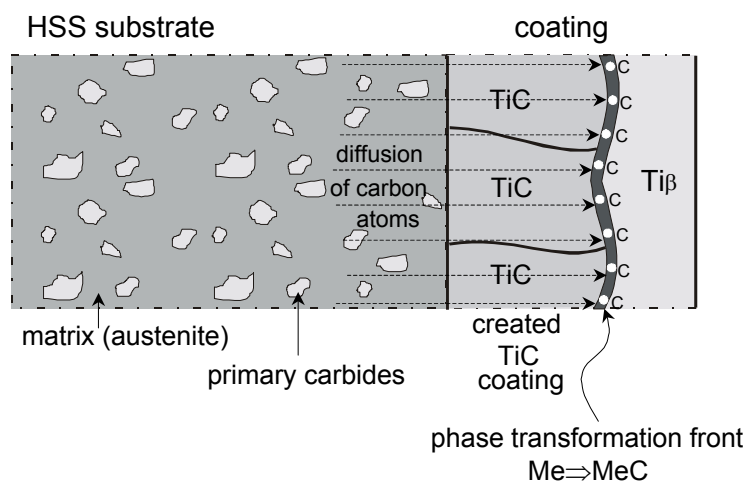


Figure 26. Structural modification $Me \Rightarrow MeC$ within a Ti coating deposited on HSS surface during vacuum heating above $Ti_{\alpha} \Rightarrow Ti_{\beta}$ transformation temperature [Wendler B. (2001)].

Substantial advantages of the indirect method arise from its two-step character. Deposition of thin carbide-forming transition metal layer as a first step is a very easy and simple operation and can be realised with use of numerous well known and relatively cheap techniques with high precision and repeatability. The second step also does not generate any technological difficulties as vacuum or inert-gas heating is a typical action widely applied in numerous manufacturing processes. The aim of this operation is also to increase the adhesion of the coating to the steel substrate. This second stage is finished by oil or water quenching and can be considered as a simultaneous heat treatment of the steel substrate material in the bulk, which decreases the time of processing cycle of a single component. Hard coatings deposited by the indirect method significantly increase the durability of treated components (Figure 27). There is also an important ecological aspect of this technique because its application do not induce any health or safety hazards and do not generate environment pollution. As distinct from other deposition methods there is no need to create special reactive carbon-carrying gas atmospheres as the steel substrate is a sufficiently rich carbon atoms source.

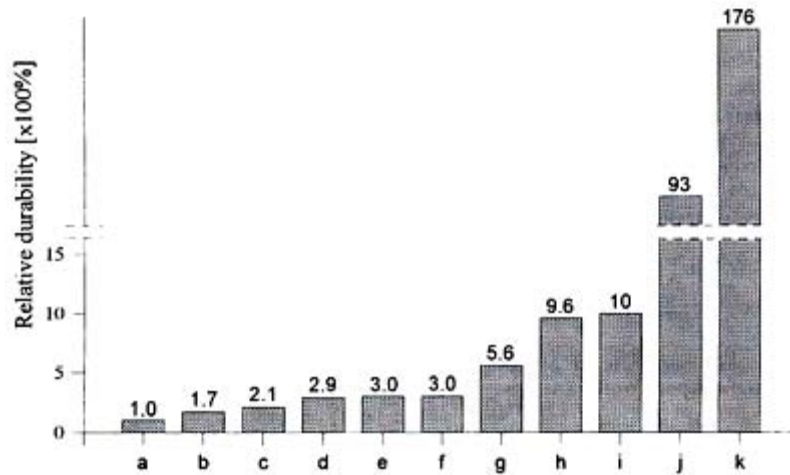


Figure 27. The effect of TiC coating of 6-5-2 HSS tools and machine parts on their relative durability at the working conditions: (a) uncoated tools; (b) machine tap M6; (c) piercing punch $\varnothing 3.0$; (d) piercing punch $\varnothing 2.56$; (e) elements of a reeler; (f) tenoning cutter; (g) piercing punch $\varnothing 3.6$; (h) piercing punch $\varnothing 1.56$; (i) bending punch; (j) plug die $\varnothing 33.0$; (k) plug die $\varnothing 27.0$ [after Wendler B. et al. (1997)].

1.3.2.2. The role of process parameters

Technological properties of hard coatings are in general related to their chemical composition, structure and adhesion to substrate, which in turn depend on deposition parameters. It is well known (however not beneficial) that the same kind of coating manufactured with use of different equipment usually has different technological properties [Hollahan J.L. and Bell A.T (1974), Fleischer W. et al (1979)]. Complexity of CVD and PVD techniques as well as that of the relevant equipment sometimes brings about different results of processes carried out with use of the same equipment. According to Keles O. et al. (2003) a fishbone diagram has been proposed to indicate a large number of parameters for the Sn-SnO deposition process (Figure 28). In this case large variety of uncontrollable and controllable, independent and dependent parameters can be identified, which help researchers to choose adequate parameters for designing relevant deposition process on purpose. The problem of coated surface properties (like porosity, stage of oxidation, microhardness, fracture toughness) as a function of process parameters has been also raised by Li J.F. et al. (2003) for the case of plasma sprayed TiN coating. It has been shown that the controlled parameters, i.e. arc current, Ar and H₂ flow, spraying distance and powder feed rate significantly influence the coating properties. That was the reason that a trial of finding the relationship between inputs (process parameters) and output (coating quality) has been undertaken.

Hence, it is clear that the final coatings properties are influenced by factors related to the deposition equipment, employed materials, deposition process course and process operator as well. Hard coatings manufacturing is very complex and usually we are not able to control exactly all the parameters, nevertheless a great effort is put towards mastering this field of surface engineering.

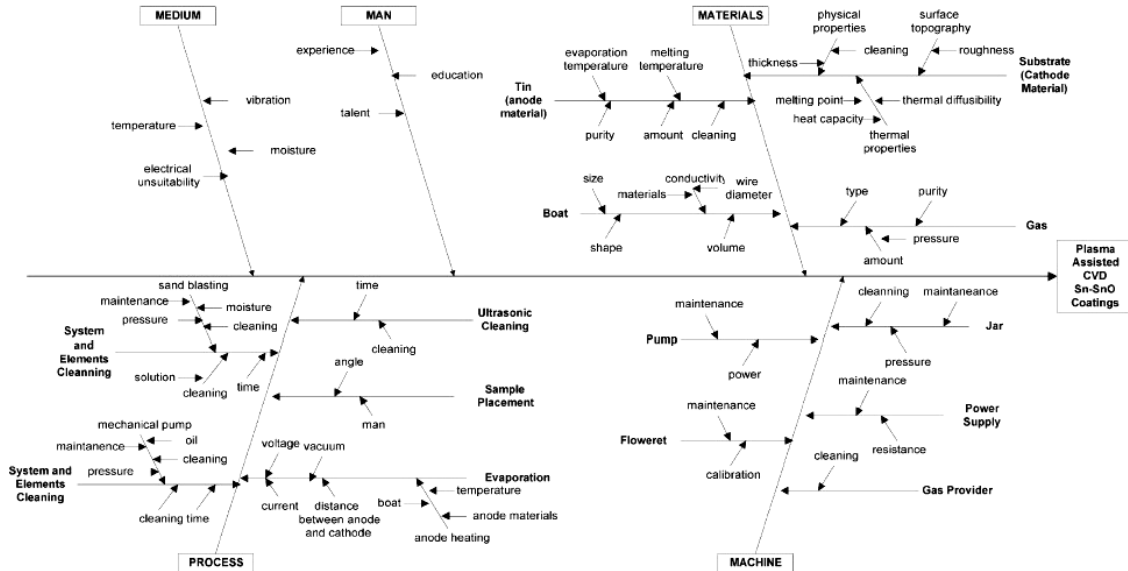


Figure 28. Cause and Effect diagram for Sn-SnO plasma assisted vapour deposited coatings [after Keles O. et al. (2003)].

1.3.3. Hard coatings in current engineering practice

At the present moment a large diversity of hard coatings is commercially available, for which the most widely applied ones are TiN, TiC, TiCN, TiAlN, CrN, Al₂O₃ with its combinations and some coatings with lubricating properties like DLC or MoS₂ [Hauert R. et al. (2000)]. Independently of the structural character of a coating, three main zones should occur [Burakowski T. and Wierzchoń T. (1995)]:

- *surface layer*: responsible for interacting within a contact area and with the environment;
- *core of a coating*: assures the properties like hardness, strength, cracking resistance or heat conductivity;
- *transient layer*: joins the coating with a substrate material and is responsible for interaction on coating/substrate interface.

Hard coatings can be classified taking into account: (a) number of components or phases, (b) composition uniformity of components or phases, (c) number of single

layers. The last division is the widest one as it can be broadened for several sub-groups [Burakowski T. et al. (1995)]:

1. MONOLAYERS

- *simple*: consists of one constituent or phase. Crystallographic structure contains atoms of metal with interstitially situated atoms of metalloid (Figure 29).

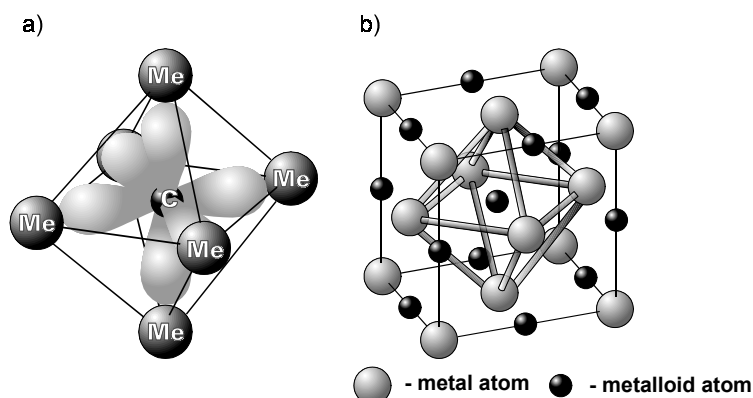


Figure 29. (a) Diagram of spatial configuration of carbon atom bonding orbitals sp^3 and corresponding regular octahedron MeC; (b) Elementary cell B1 (regular wall-centered) characteristic for carbides and nitrides of transition metals from IVb and Vb groups [Wendler B. (2001)].

- *alloyed*: sublattice of one metallic or non-metallic element is partially occupied by another one. Taking advantage of good mutual solubility of two compounds specific properties can be achieved (e.g. Ti(C,N), (Ti,Al)N, (Ti,W)C);
- *multi-phase*: mixture of two separable phases (e.g. TiN/Ti₂N);
- *composite*: variation of multi-phase coatings. Difference results from the distribution of phases and in case of composite coatings it is systematic distribution (e.g. TiC/Al₂O₃);
- *functionally graded*: in these coatings a gradient of particular material property is realised by continuous change of: chemical composition, grain size or atoms order in the function of location within a coating [Hodor K. et al. (1999)] (e.g. TiN/Ti(C,N)/TiC).

2. MULTILAYERS

- *common*: a few (usually 3 or 4) simple monolayers hierarchically deposited on each other. In designed multilayer each sub-layer assures different properties, from top surface: external layer-low friction, anti-corrosion; one or more intermediate layers: hardness, strength; internal layer: adhesion (e.g. TiC/TiN/Al₂O₃);

- *modulated*: composed of large number of thin layers [Bull S.J. et al. (1996)]. Coatings can be manufactured of materials of different structure (incoherent grain boundaries) or materials of same chemical bonds (coherent grain boundaries). In the latter case the hardness synergism can take place leading to 20% hardness increase in relation to harder phase (e.g. TiC/TiB₂, TiC/VC).

Necessity of novel materials subjected to thermal, mechanical or chemical loadings force engineers to search for new efficient solutions. Hence, in the nearest perspective, functionally graded and multilayer coatings seem to have the highest potential to meet multifarious needs. Wear mechanism of multilayer coatings is specific due to its unique structure (Figure 30). Generated micro-cracks on the coated component surface, change their direction of propagation if only the interface between different sub-layers has been reached. This phenomenon significantly increases the wear resistance of multilayer coating in comparison with simple or alloyed one.

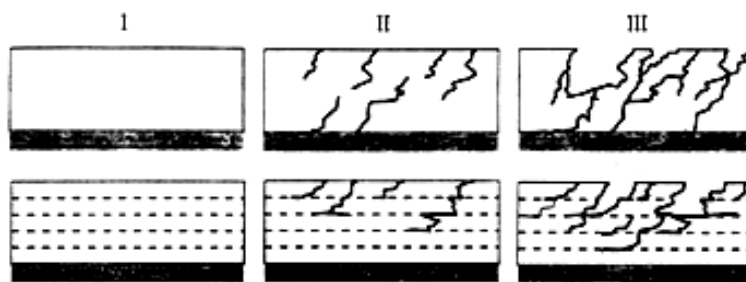


Figure 30. Successive stages of mechanical destruction of monolayer and multilayer coatings [after Burakowski T. and Wierzchoń T. (1995)].

1.3.4. Hard coatings under fretting regime

Among different surface engineering techniques, PVD and CVD ones are the most widely used to reduce destruction of coated components and to mitigate the fretting wear rather than to improve the fretting fatigue strength. To enhance fretting fatigue resistance surface treatments which are conducive to compressive residual stresses in the surface layer are recommended [Fu Y. et al. (2000)], e.g. shoot-peening, ion implantation, carburizing, nitriding or ion beam enhanced deposition. Nevertheless some preliminary results [Sato K. et al. (1994)] show that hard PVD and CVD coatings can also improve the fretting fatigue strength of steel (Figure 31a).

Currently, a PVD TiN hard coating is the most frequently applied one and degradation mechanisms of this coating have been extensively investigated, among the

others by research groups of S. Hogmark in Sweden [Bromark M. et al. (1997)], D. Klaffke in Germany [Klaffke D. et al. (1998)], J.-P. Celis in Belgium [Wu P.Q. et al. (2000)] or I.L. Singer in USA [Singer I.L. et al. (1991)]. Complex damage mechanism of PVD TiN coating under fretting regime is controlled by debris formation and oxidation wear, due to which a characteristic W-shape fretting scar is being formed [Wei J. et al. (1997a)] (Figure 31b). This damage manner is greatly dangerous for a coating as with a relatively small wear volume, significant wear depth occurs which leads to rubbing through the coating and reaching the substrate. It was proved [Mohrbacher H. et al. (1995a)] that relative humidity has a great effect on friction behaviour of TiN coating and it can be concluded that fretting at high RH is characterised by low friction and small wear volume in opposite to low RH with high COF values and bigger wear rates.

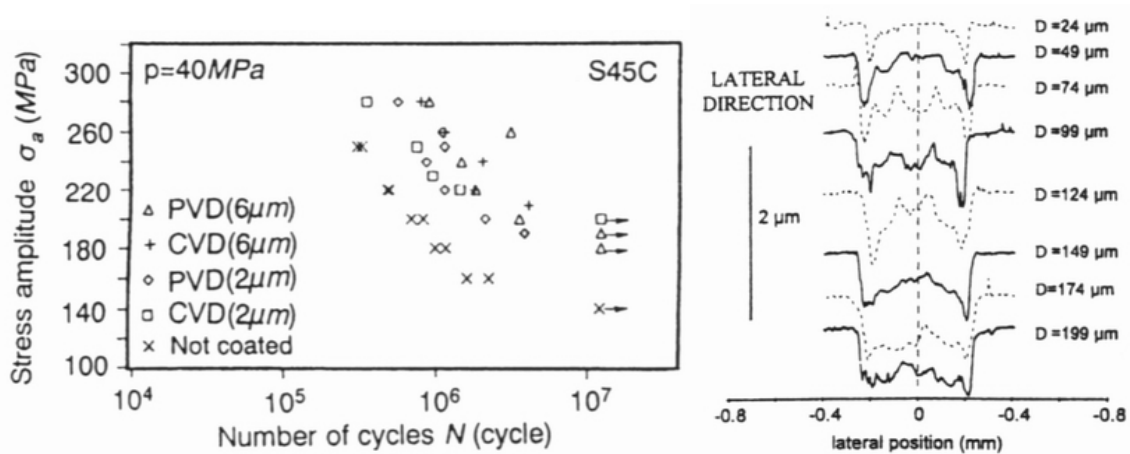


Figure 31. (a) Fretting fatigue characteristics of different TiN coatings on a S45C steel [Sato K. et al. (1994)]; (b) Effect of the slip amplitude on the shape of the fretting wear scar shape of a PVD TiN coating [Fouvry S. et al. (1996)].

Another potential PVD coating for fretting applications is DLC coating with good fretting wear resistance and low friction. Wear debris of DLC play a lubricant role within a contact as they consist of graphite forms of carbon [Schouterden K. et al. (1995)]. Here again relative humidity is an important factor that influence the wear process: according to Wei J. et al. (1997b) there is a threshold value of RH (near 25%), which marks a borderline between two damage mechanisms of the coating: abrasive wear with transfer under 25%RH and combination of mechanical and tribo-chemical wear for higher RH values.

PVD coatings have an advantage over the CVD ones because usually the latter technique leads to decrease of the substrate hardness due to elevated process temperatures during coatings manufacturing. On the other hand there is a disadvantage

of PVD coatings as they have relatively lower adhesion to the substrate, while coatings manufactured by CVD techniques usually exhibit significantly better adhesion.

1.4. OBJECTIVES AND FIELD OF THE WORK

It has been shown in the bibliographic survey that the domain of surface engineering has a prime importance for tribological applications. The crucial role of surface layer of mated elements has been pointed out. Fretting as a specific destruction process has been described and related to hard coatings as well. It is clear in view of the above mentioned factors that durability of employed hard coating has to be estimated in order to benefit in full from its high mechanical properties. In this work coating durability definition is referred to situation in which the technologically improved hard surface is worn through and the substrate material is reached.

Hence, the main research objective of this dissertation is to introduce the *hard coatings durability criterion* to predict the coating endurance but also to compare different coatings wear resistance. To achieve that, local variety of dissipated energy approach will be applied which will allow to model the wear depth evolution within a studied coating as a function of duration of the fretting test. The conditions of the tribological test programme realised within the framework of this thesis have been maintained in the gross slip fretting regime (Figure 32), where the energy delivered to the interface is mainly consumed for interfacial shear work resulting from the relative motion between interacting bodies.

To fulfill the objective of hard coatings criterion determination, the following questions have to be answered:

- How to estimate clearly the substrate reaching condition during execution of a fretting test?
- Do the stresses in the coating/substrate interface play a significant role in coating destruction and should they be taken into account in the formulation of the coatings durability criterion?
- What is a fretting scar and wear debris morphology for different hard coatings?
- Is it possible to predict hard coating durability independently of applied displacement amplitude?
- How to compare different surface treatments in case of wear depth evolution?
- Environmental conditions: should they be taken into account?

- What is the frictional behaviour and wear resistance of multilayer hard coating in comparison with that of monolayer hard coatings of the same type?

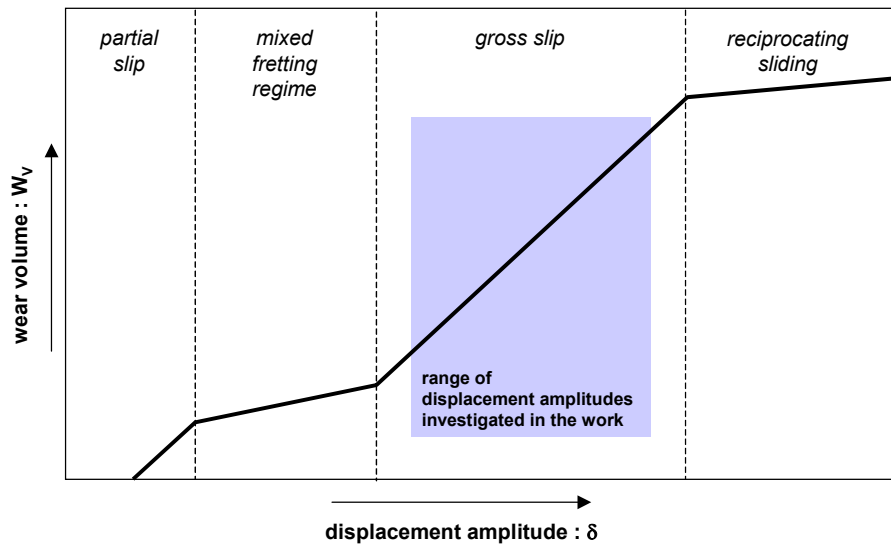


Figure 32. Evolution of wear volume as a function of fretting test displacement amplitude [Neyman A. (1992)].

1.4.1. Thesis of the work

Considering the engineering contents put forward above, the following thesis can be drawn:

It is possible to establish the durability criterion for hard coatings and predict the coated component endurance under fretting wear regime. The coating lifetime can be estimated through the local dissipated energy approach, where the maximum energy density dissipated in the centre of the contact is related to the maximum wear depth. The criterion will allow as well to compare the efficacy of different surface treatments as regards the resistance to wear of respective technological surface layers.

CHAPTER 2



ELABORATION AND PROPERTIES OF THE MATERIALS UNDER INVESTIGATION

CHAPTER 2: ELABORATION AND PROPERTIES OF THE MATERIALS UNDER INVESTIGATION

In Chapter 2 the materials used in the experiments are presented. The substrate material, counter-body material and the applied hard coatings are described. At first the manufacturing processes of surface treatments are discussed and next the analysis of mechanical properties and phase composition are given.

2.1. THE SUBSTRATE MATERIAL

High speed steel Vanadis23 has been selected as a substrate material for hard coatings deposition processes. This grade of steel is widely used in PVD and CVD practice due to high hardness of heat treated specimens. The chemical composition of the steel reported by the manufacturer is listed in Table 2. The received steel composition was verified and proved by means of energy-dispersive spectrometry (EDS) analysis (Figure 33).

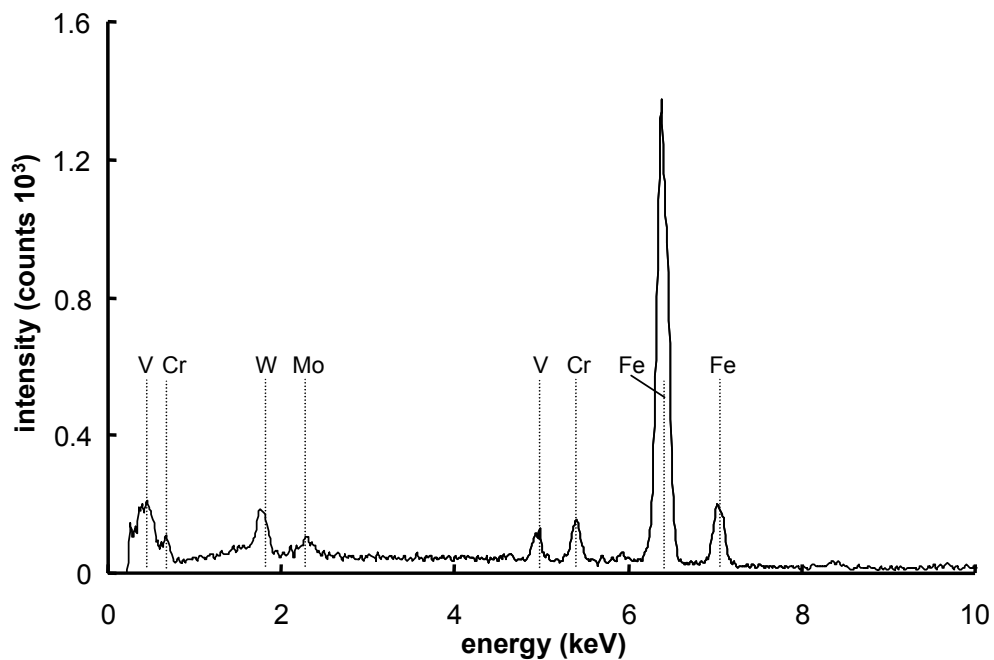


Figure 33. EDS analysis of Vanadis23 high speed steel.

Table 2. Chemical composition of Vanadis23 high speed steel (wt.%).

C	Cr	Mo	W	V
1,28	4,2	5,0	6,4	3,1

A series of 10x10x10mm specimens has been cut from the bulk steel. Next the surfaces have been mechanically ground and finally subjected to polishing with use of 3 μ m diamond paste, to ensure the proper surface roughness parameter. The surface properties identified by means of 3D surface analysis and scanning electron microscopy (SEM) are depicted in Figure 34. The adequate mechanical properties of the employed high speed steel are given in Table 3.

Table 3. Mechanical and surface properties of the substrate material.

	Young's modulus E (GPa)	Poisson's ratio ν	Hardness (HRC)	Surface roughness Ra (μ m)
Vanadis23	230	0.3	64	0.2

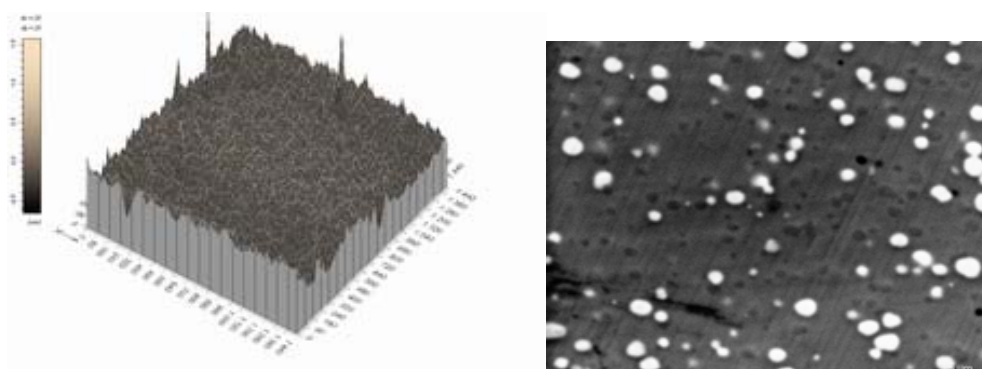


Figure 34. Surface morphology of a substrate material: (a) 3D isometric plot; (b) SEM image.

The vacuum sintered from uniform HSS powders Vanadis23 steel is especially predestined to be deposited by titanium carbide or nitride layers as the steel grade with a very homogenous carbides distribution (Figure 34b) and increased amount of VC-type carbides in the matrix (see Table 2). Due to the same regular MC-type elementary cells of TiC and VC carbides, the TiC phase nucleates epitaxially on the VC carbides of the substrate and provide a very good adhesion between the coating and the substrate. Simultaneously the very homogenous carbides distribution in the matrix due to powder metallurgy technology reduces the geometrical changes after heat treatment process.



Figure 35. Structure morphology of Vanadis23 high speed steel after heat treatment: 1 hour holding at the temperature 1423K followed by double 1 hour tempering at 823K (magnification x800). Structural constituents: tempered martensite with dispersive carbides.

2.2. THE COUNTER-BODY MATERIAL

As the counter-body during the fretting tests a polycrystalline alumina ball with a $R=12,7\text{mm}$ radius was used (Figure 36 and Table 4). The ceramic material was selected to reduce the material transfer from the tested coating surface onto the ball surface. As distinct from the ceramic ball in case of e.g. a steel ball, the adhesive wear plays a significant role in the surface degradation, which would disturb the elaboration of hard coating durability approach. It was the aim of this work to introduce a methodology for surface treatment durability criterion by choosing the counter-body material as neutral as possible. The probable future task will encompass the development of the proposed approach to other more complex tribo-systems.

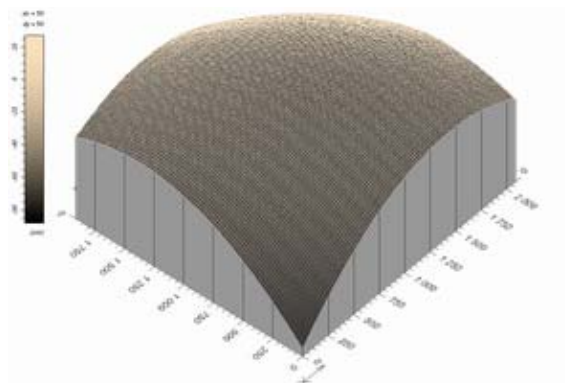


Figure 36. Surface morphology of the alumina ball: 3D isometric plot of summit.

Table 4. Mechanical and surface properties of the counter-body material.

	Young's modulus E (GPa)	Poisson's ratio ν	Hardness (HV _{0.1})	Surface roughness Ra (μm)
Alumina	370	0.27	2300	0.01

2.3. HARD COATINGS INVESTIGATED IN THE WORK

This sub-chapter is divided in three groups of materials related to: titanium and vanadium carbide coatings, titanium nitride and carbonitride coatings and multilayer titanium and vanadium carbide coatings. Two first parts differ in manufacturing technology and the third one refers to multilayer systems.

2.3.1. Titanium and vanadium carbide coatings

2.3.1.1. Coatings manufacturing

Titanium and vanadium carbide coatings have been manufactured with use of the indirect method described previously in Chapter 1 (§ 1.3.2.1. *Indirect method*). Deposition of metallic titanium and vanadium layers has been realised by magnetron sputtering technique with use of the equipment depicted in Figure 37. Prior to the coatings deposition the specimens have been ultrasonically cleaned with acetone and suspended under the rotary table in the centre of the chamber, in equal distance from all the four sputtering sources. The main deposition activity, carried out under parameters given in Table 5, has been preceded by glow discharge cleaning of the specimens surface.

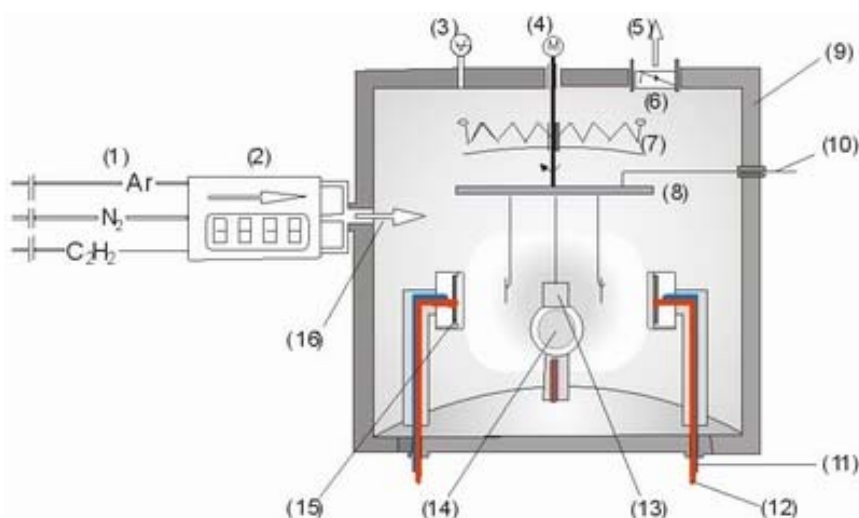


Figure 37. Equipment for deposition Ti and V metallic layers: 1–supply of inert and reactive gases; 2–gas flow mass controller; 3–vacuum meter; 4–motor drive; 5–connection to pumping stand; 6–throttle valve; 7–IR radiator; 8–rotary table; 9–high vacuum chamber; 10–table bias; 11–water cooling; 12–magnetron power feed; 13–specimen suspended under the table; 14 and 15–magnetrons; 16–gas inlet (inert and reactive) [Wendler B. et al. (2003)].

Table 5. Deposition parameters of Ti and V metallic layers.

Metallic layer	Atmosphere	Pressure (Pa)	Polarization (V)	Sputtering time (min)	Magnetron current
Ti	Ar	$5 \cdot 10^{-2}$	-50	42	600 V, 3 kW
V				90	350 V, 3 kW

After deposition, the specimens coated with metallic Ti or V layer have been held in vacuum furnace in order to induce the diffusion of carbon atoms. The heating has been performed at the temperature 1423K and residual pressure $1 \cdot 10^{-3}$ Pa during 1 hour. The temperature 1423K has been reached under mean heating rate 0.2K/s and with two mid-stops at 273K and 1073K. The substrate hardening was due to quenching in oil from the elevated temperature, which has been followed by double tempering at 823K during 1 hour.

The proceeding reactive diffusion process enriches the metallic (Ti, V) layers in carbon and generates carbide layers (TiC, VC) as high temperature increases the outward diffusion coefficient of carbon atoms dissolved in the austenite of the steel substrate to the coating. The X-ray diffraction patterns of metallic Ti and V as well as carbide layers TiC and VC (respectively) are given in Figures 38 and 39.

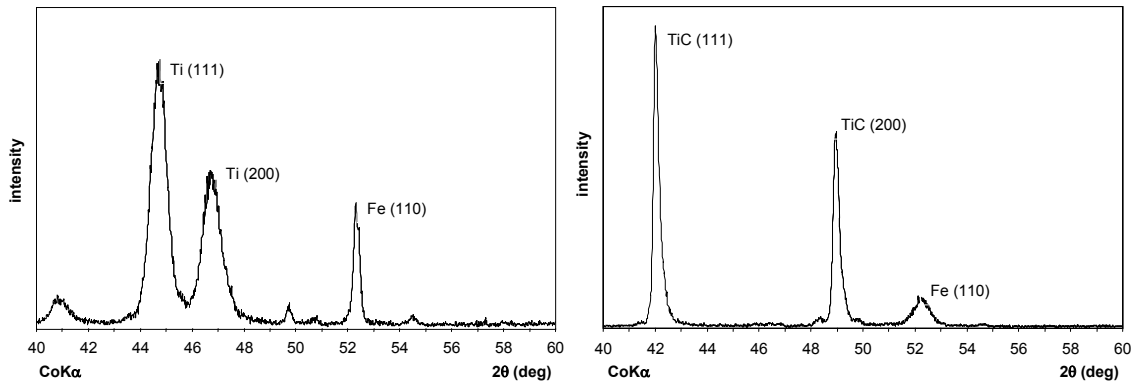


Figure 38. X-ray diffraction patterns of specimens after: (a) deposition of metallic Ti layer; (b) diffusion process of carbon atoms activated by vacuum heating and followed by quenching in oil.

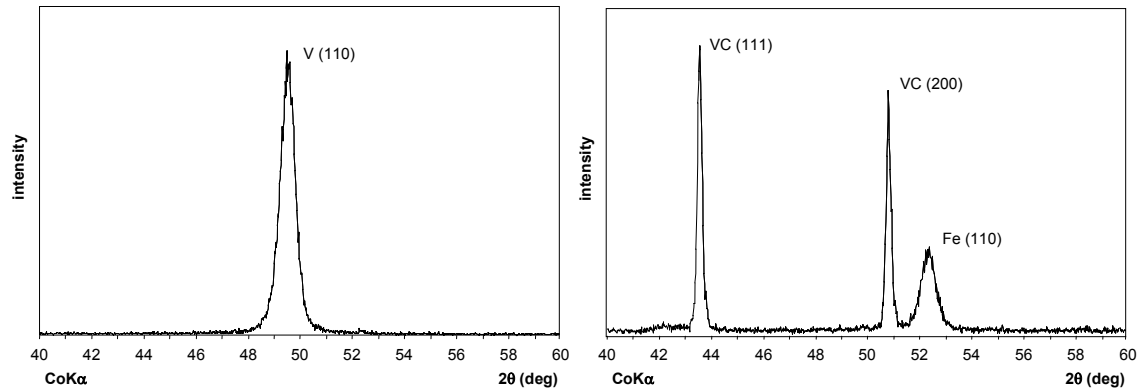


Figure 39. X-ray diffraction patterns of specimens after: (a) deposition of metallic V layer; (b) diffusion process of carbon atoms activated by vacuum heating and followed by quenching in oil.

2.3.1.2. Coatings characterization

All the manufactured hard coatings have been subjected to the following investigations of mechanical properties:

- *hardness*; with use of microhardness tester under the load of 0,05N;
- *thickness*; by means of surface morphology analysis of fretting wear scars and optical microscopy;
- *adhesion*; by means of a scratch tester under progressively changing load from 5N to 60N every 5N.

The coating surface morphology has been also analysed with tactile topometer *Surfascan S-M2 Somicronic-Hommel* (France) and observed on scanning microscopy (Figure 40). The properties of titanium and vanadium carbide coatings are listed in Table 6.

The VC coating is characterised by higher hardness in comparison to TiC coating, however the adhesion appeared to be lower. In case of VC coating the surface porosity has been observed.

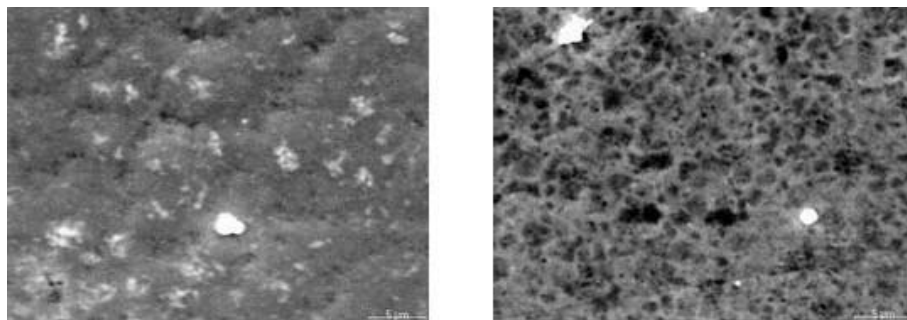


Figure 40. SEM image of coating surface: (a) TiC; (b) VC.

Table 6. Mechanical and surface properties of the TiC and VC coatings.

Coating	Young's modulus E (GPa)	Poisson's ratio ν	Hardness (HV _{0.05})	Thickness (μm)	Adhesion (N)	Surface roughness Ra (μm)
TiC	510	0.2	1300	1.6	45	0.2
VC	460		2500	2.0	35	

2.3.2. Titanium nitride and carbonitride coatings

2.3.2.1. Coatings manufacturing

The titanium nitride and titanium carbonitride hard coatings have been deposited by means of arc PVD method with use of a single source device (Figure 41). Substrates underwent typical preparation as follows:

- heat treatment (oil quenching and double tempering),
- mechanical grinding and polishing with diamond paste,
- immersing in acetone and cleaning in ultrasonic bath,
- glow discharge cleaning in working chamber (first process stage),
- high energy cleaning and heating by titanium ions (second process stage),
- deposition of the titanium nitride or titanium carbonitride coating (third process stage).

Parameters of three deposition stages are summarised in Table 7.

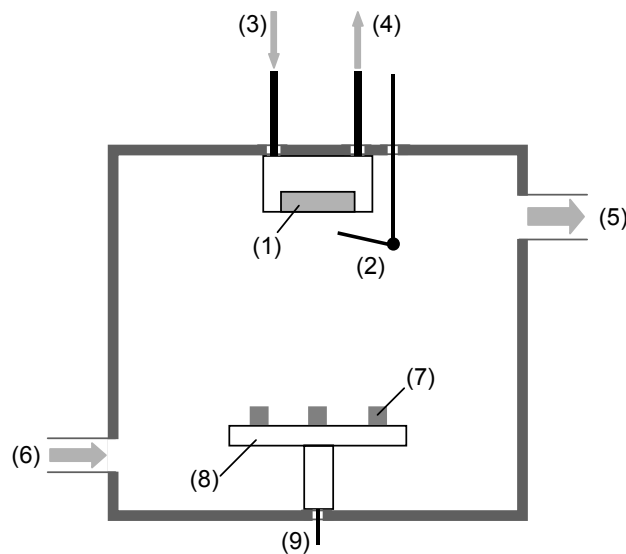


Figure 41. TiN and TiCN coatings deposition equipment: 1 – cathode; 2 – arc lighter; 3, 4 – cathode cooling; 5 – connection to pumping stand; 6 – gas inlet; 7 – specimens; 8 – rotary table; 9 – table bias.

Table 7. Deposition parameters of TiN and TiCN coatings.

Coating	Glow discharge cleaning			Titanium ions heating			Coating deposition			
	Time (min)	Bias (kV)	Pressure (Pa)	Time (min)	Bias (kV)	Pressure (Pa)	Time (min)	Bias (V)	Pressure (Pa)	Gas
TiN	15	1.2	2	2	1.2	10^{-1}	40	200	$4 \cdot 10^{-1}$	N ₂
TiCN	15	1.2	2	1	1.2	10^{-1}	40	200	$4 \cdot 10^{-1}$	C ₂ H ₂ +N ₂

2.3.2.2. Coatings characterization

The adequate material properties have been analysed as it was realised in case of TiC and VC coatings and the obtained values are given in Table 8. The titanium nitride coating has been identified to be a little bit harder but is characterised by lower adhesion. Low coating surface porosity has been observed for both materials, nevertheless for TiN coating the micro-craters have larger dimensions (Figures 42a and 43a). The phase composition of the coatings has been identified by means of X-ray diffraction analysis (Figures 42b and 43b).

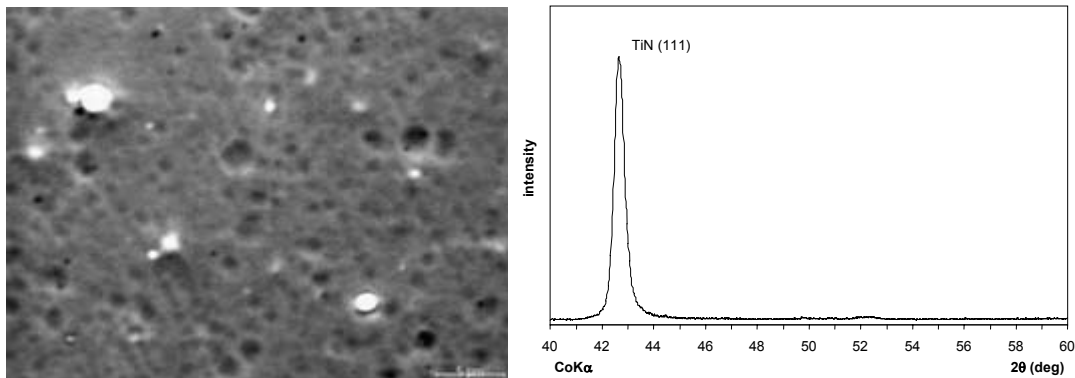


Figure 42. (a) SEM image of TiN coating surface; (b) X-ray diffraction pattern of TiN coating.

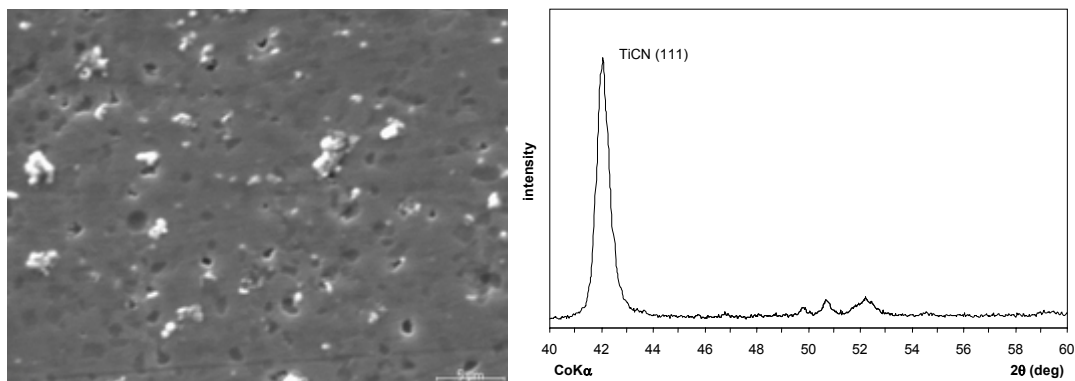


Figure 43. (a) SEM image of TiCN coating surface; (b) X-ray diffraction pattern of TiCN coating.

Table 8. Mechanical and surface properties of the TiN and TiCN coatings.

Coating	Young's modulus E (GPa)	Poisson's ratio ν	Hardness (HV _{0.05})	Thickness (μm)	Adhesion (N)	Surface roughness Ra (μm)
TiN	600	0.25	2000	4.0	35	0.2
TiCN	550		1700	2.5	40	

2.3.3. Multilayer titanium and vanadium carbide coatings

2.3.3.1. Coatings manufacturing

Multilayer coatings have been prepared by means of an indirect method and deposition equipment previously employed for TiC and VC monolayers (Figure 37). Two kinds of multilayer systems have been manufactured:

- *TiC/VC*; one bilayer, two single-layers;
- *(TiC/VC)x2*; two bilayers, four single-layers.

The same deposition and heat treatment parameters have been used as before. The sputtering time of metallic layers previously applied for TiC and VC monolayers has been appropriately divided in this case for 2 and 4 respectively.

2.3.3.2. Coatings characterization

Successively the mechanical characteristics and surface properties of the coatings have been studied in this case as well (Table 9). Hardness of both multilayer systems is positioned between values received before for TiC and VC monolayers. With increasing number of sub-layers the hardness of the multilayer coating increases as well. Such a tendency was previously confirmed on TiN/NbN superlattices by Yashar P.C. et al. (1999) or by other authors [Helmersson U. et al. (1987), Chu X. et al. (1995)] and could be explained with the theory of dislocations and the carbide grain size generated during the heat treatment process.

Similar surface morphology has been observed for TiC/VC and (TiC/VC)x2 coatings (Figure 44a). The occurrence of the carbide phases has been identified by the X-ray diffraction analysis (Figures 44b). Although, an additional glow discharge optical spectroscopy (GDOS) analysis has been undertaken to clearly indicate the multilayer coating composition and prove the reactive diffusion process (Figure 45). This semi-

quantitative chemical analysis, based on continuous ion sputtering, allows us to measure the relative concentration of chemical elements like C, V, Ti and Fe through the coating and near the coating substrate interface.

Table 9. Mechanical and surface properties of the multilayer TiC/VC coatings.

Coating	Young's modulus E (GPa)	Poisson's ratio ν	Hardness (HV _{0.05})	Thickness (μm)	Adhesion (N)	Surface roughness Ra (μm)
TiC/VC	580	0.2	1450	2.5	35	0.2
(TiC/VC)x2			2300	4.0	40	

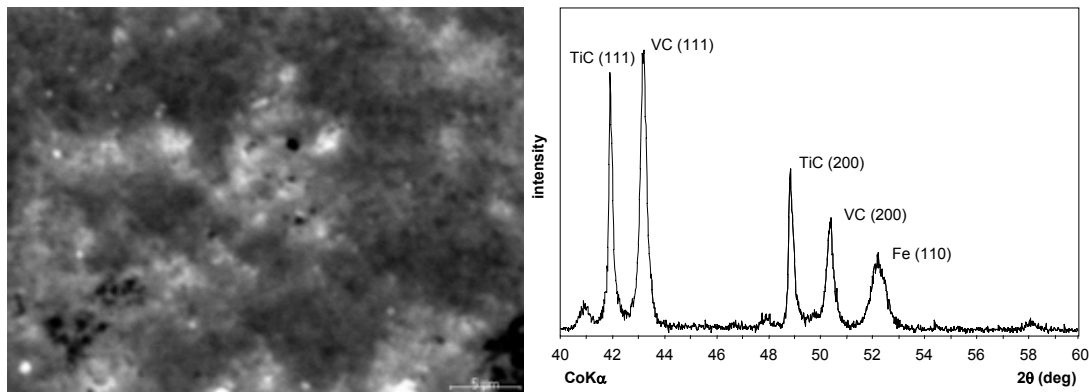


Figure 44. (a) SEM image of TiC/VC coating surface; (b) X-ray diffraction pattern of the TiC/VC coating.

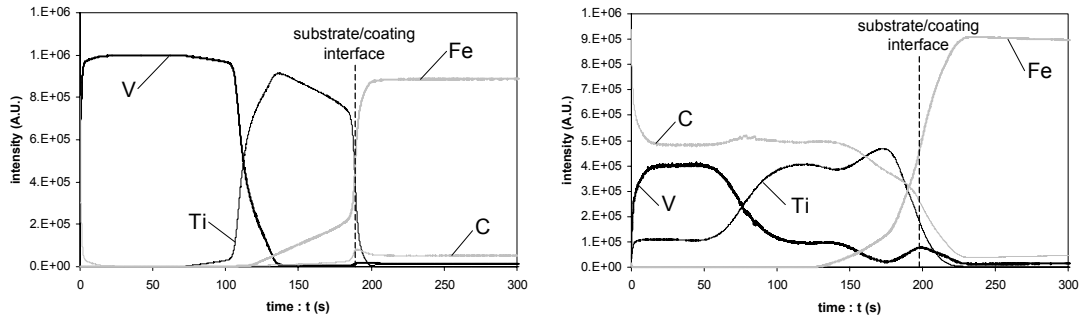


Figure 45. GDOS profiles of the TiC/VC coating as a function of the sputtering time: (a) pure metallic layer; (b) after holding at the elevated temperature.

CHAPTER 3



FRETTING WEAR EXPERIMENTS

CHAPTER 3: FRETTING WEAR EXPERIMENTS

The Chapter is divided into four main parts. The first one presents the experimental equipment and test conditions. In the next part fretting wear mechanisms of the hard coatings under investigation are described, impact of Ti interlayer on tribological properties of TiN coating are considered and diffusion mixed layer in multilayer TiC/VC system is introduced. The third part of the Chapter points out the influence of the relative humidity on fretting wear. Finally the last part gives some examples of surface morphology analysis.

3.1. TRIBOLOGICAL ANALYSIS OF THE INVESTIGATED SYSTEM

3.1.1. Fretting apparatus

Fretting tests were carried out using an electrodynamic shaker activating a specific fretting rig manufactured by *DeltaLab* (United Kingdom) illustrated in Figure 46. Tests were carried out in a closed chamber where both ambient and relative humidity were controlled. The normal force is kept constant, while the tangential force and displacement are recorded. The relative displacement is determined for each fretting cycle by an optical sensor. A reciprocating movement with a constant speed has been imposed.

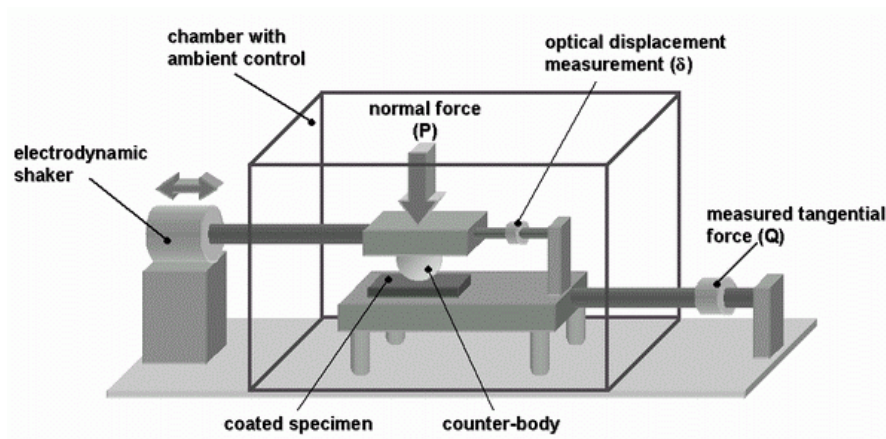


Figure 46. Schematic of the fretting rig.

3.1.1.1. Contact geometry

The ball-on-flat surface contact geometry has been applied (Figure 47). The coated specimen has been fixed rigidly on a mounting plate. Fixing system allowed to realise up to 25 fretting tests on a 10x10mm specimen surface. Before each test a new, not previously worn place on an alumina ball has been selected and positioned against the flat surface.

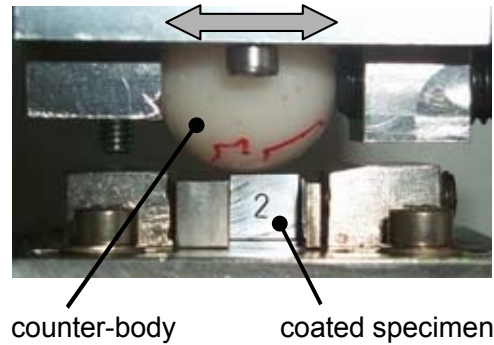


Figure 47. Fretting contact geometry used in the experiments.

3.1.2. Experimental conditions

All fretting wear experiments have been carried out under reciprocating sliding motion at the frequency (f) 5Hz. Dry conditions without external lubrication have been investigated within a framework of this dissertation. Tests have been realised with duration starting from 1000 cycles and usually lasted no longer than 20000. However, for some coatings with significantly higher tribological properties, the tests had to be extended up to 200000 cycles to describe well the fretting wear kinetics.

3.1.2.1. Applied loads and displacement amplitudes

A wide range of displacement amplitudes and normal loads has been applied (Table 10) in order to verify the new hard coatings durability approach under different loading conditions. The most part of the fretting tests has been carried out for medium-loads and medium displacement amplitudes: $\delta=100\mu\text{m}$ and $P=100\text{N}$. For the investigated contact geometry and materials of the friction node the maximum Hertzian pressure is equal to 1075MPa, 1350MPa and 1550MPa for the normal load 50N, 100N and 150N respectively. The relative displacement amplitude has not exceeded the value $200\mu\text{m}$ as

the sliding ratio e previously described in Chapter 1 (§ 1.2.3. *Sliding conditions*) is < 1 in this case and gross slip fretting regime is no longer maintained.

Table 10. Applied loading conditions for coatings:

◆ TiC, ◇ VC, ■ TiC/VC, □ (TiC/VC) $\times 2$, ▲ TiCN, △ TiN.

δ P	50	75	100	125	150	200
50	▲	▲	▲	▲	▲	▲
100	◆ △	▲ △	◆ ◇ ■ ▲ △	▲ △	◆ △ ▲	◆
150	▲	▲	▲	▲	▲	▲

3.1.2.2. Variable loading conditions

To evaluate the range of applicability of the hard coatings durability model, constant and variable sliding amplitudes have been applied. As it is illustrated in Figure 48, sets of different displacement amplitudes have been superimposed. The test duration, characterized by a total number of cycles, was divided into one, two and four sets of $\pm 50\mu\text{m}$ and $\pm 100\mu\text{m}$ displacement amplitude defining the studied $(50/100)\mu\text{m}_{\times 1}$, $(50/100)\mu\text{m}_{\times 2}$ and $(50/100)\mu\text{m}_{\times 4}$ sequences respectively.

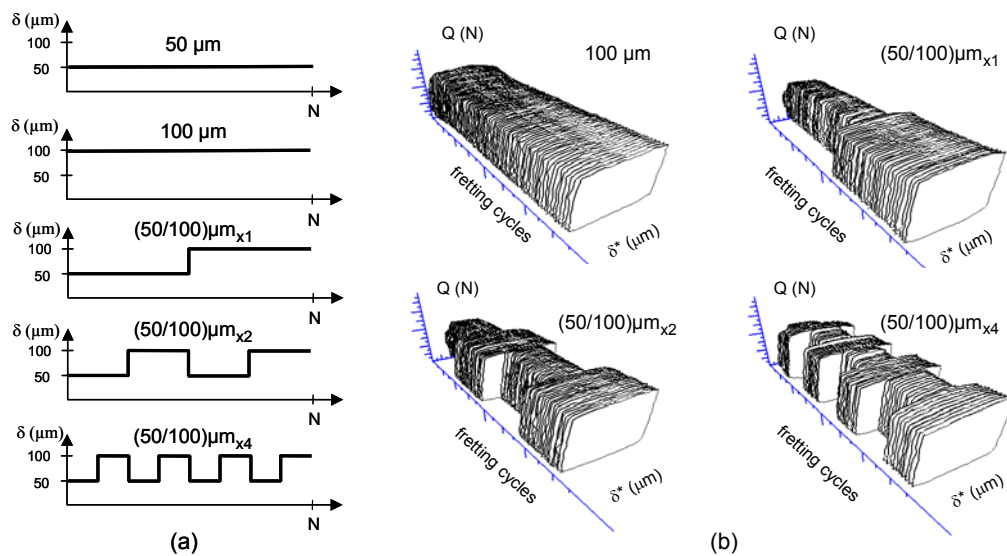


Figure 48. Illustration of the variable sliding amplitude approach (TiC/alumina, $RH=50\%$, $f=5\text{Hz}$, $P=100\text{N}$): (a) definition of constant and variable sliding amplitude conditions; (b) associated fretting logs.

3.1.2.3. Environmental conditions

The fretting test environmental conditions have been controlled during each experiment by simultaneous digital measurements of temperature and relative humidity. The particular PC-controlled system has been designed and elaborated in order to maintain the required humidity level by exhausting an adequate portion of wet or dry air. Three levels of relative humidity have been considered in this work:

- 5%: dry conditions;
- 50%: comfort air conditions;
- 90%: wet conditions.

Low relative humidity level has been reached by employing the granulated silica gel to absorb wet air in closed test chamber, while high RH by filling the bottom of the chamber with water.

3.2. FRETTING WEAR OF HARD COATINGS UNDER INVESTIGATION

3.2.1. Titanium and vanadium carbide coatings

After each fretting test the wear scar has been treated by surface profilometry to determine the wear volume of the removed material and to measure the wear depth as well. For each wear scar the longitudinal profiles (along the sliding direction) as well as the cross profiles have been obtained. Some of the scars have been also subjected to 3D surface morphology analysis, which is widely described in part 4 of this Chapter (§ 3.4. *Morphology of Damaged Surfaces*). To determine the total wear volume, a simplified integration has been used [Fouvry S. et al. (1997)]. An optical observation of each scar has been performed to identify the substrate reaching condition and the respective scar morphology. Figures 49 and 50 presents fretting scar and corresponding worn surface of counter-body for TiC and VC coatings. Some transfer of matter onto a ball surface has been observed in case of titanium carbide coating, while for vanadium coating the ball surface is smooth.

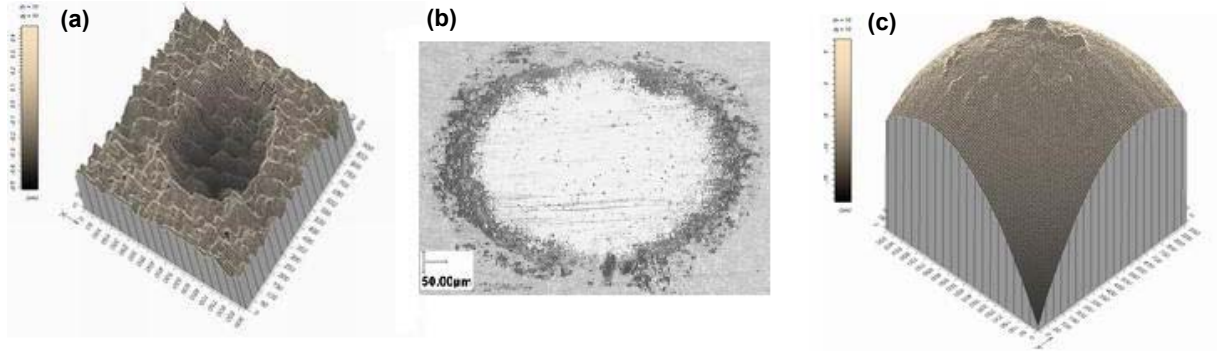


Figure 49. TiC coated specimen and alumina counter-body after fretting test: (a) 3D image of fretting scar in the surface of TiC coating; (b) optical image of the fretting scar; (c) 3D image of the surface of the alumina ball counter-body. Fretting test conditions: $P=100\text{N}$, $\delta=100\mu\text{m}$, $N=10\text{k}$, $f=5\text{Hz}$, $RH=50\%$. Remark: 1k denote the number of 1000 cycles.

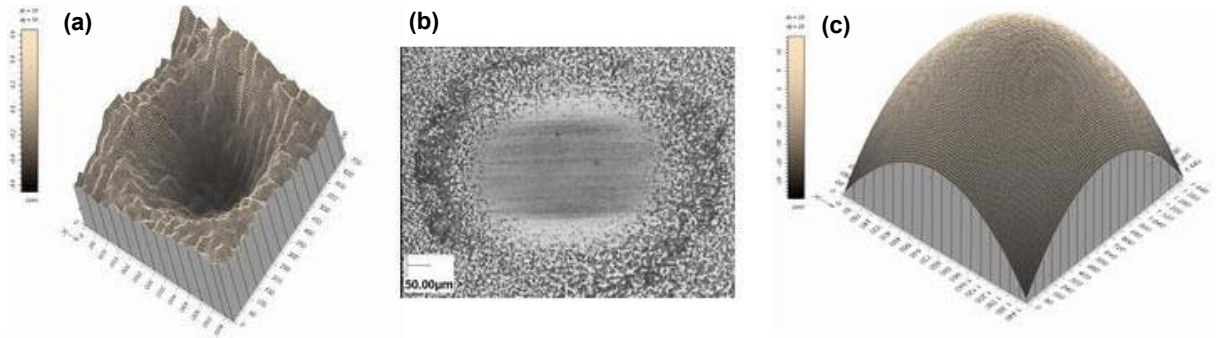


Figure 50. VC coated specimen and alumina counter-body after fretting test: (a) 3D image of fretting scar in the surface of VC coating; (b) optical image of the fretting scar; (c) 3D image of the surface of the alumina ball counter-body. Fretting test conditions: $P=100\text{N}$, $\delta=100\mu\text{m}$, $N=60\text{k}$, $f=5\text{Hz}$, $RH=50\%$.

The mean value of friction coefficient characteristic for each coating is given in Figure 51. This mean value is equal to 0.5 for TiC and 0.55 for VC coating. The running-in period up to 2000 cycles can be observed for the both coatings (TiC and VC). This transition period can be explained by the third-body theory (Chapter 1: § 1.2.6.2. *Fretting wear*). At the beginning of the fretting test there are no debris in the contact area. The debris are generated during first few hundreds cycles, which makes the friction coefficient to increase due to some adhesive junctions. Afterwards, the wear process is controlled by simultaneous generation and ejection of third-body particles with some debris permanently present at the interface, which corresponds to stabilised friction behaviour.

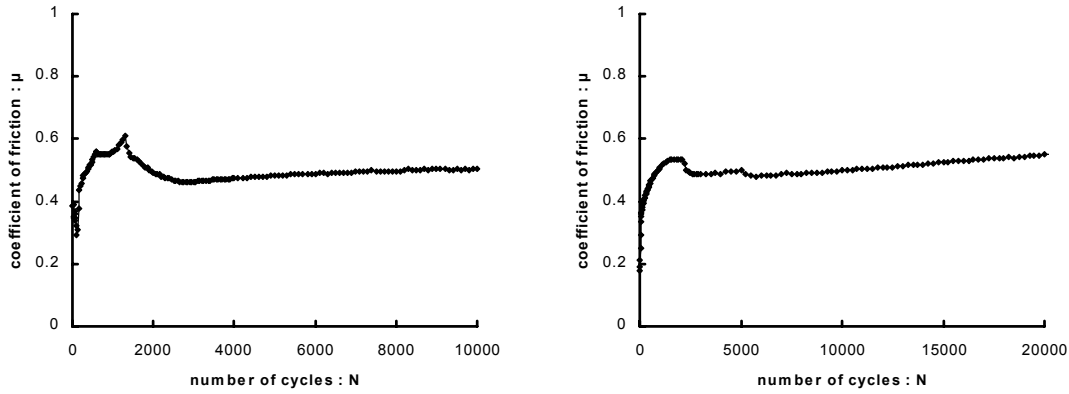


Figure 51. Evolution of coefficient of friction as a function of the number of fretting cycles: (a) TiC coating ($P=100\text{N}$, $\delta=100\mu\text{m}$, $f=5\text{Hz}$, $RH=50\%$); (b) VC coating ($P=100\text{N}$, $\delta=100\mu\text{m}$, $f=5\text{Hz}$, $RH=50\%$).

3.2.2. Titanium nitride and carbonitride coatings

It has been observed, that the maximum wear depth of the TiN wear scar is situated at the border of the contact area and a minimum at its centre. Therefore the longitudinal of the wear scar has a typical W-shape (Figure 52a, b). It has been proved earlier by Fouvry S. et al. (1997) that this characteristic scar shape is related to a modification of the surface geometry by the generation and distribution of third-body within the contact area. With increasing number of fretting cycles an annular spatial structure is being formed on the surface of the counter-body (Figure 52c) due to the material transfer onto the surface of alumina ball. Projection of the 3D structure on the surface of the alumina ball strictly correlates to the W-shape of the longitudinal section of the wear scar. The evolution of the contact geometry leads to the shear and pressure fields modification. The maximum stress values are observed in the centre of the contact at the beginning of the test and are being translocated towards the borders of the contact during test duration. This type of damage is very dangerous for a coating as with a relatively small wear volume, significant wear depth occurs and, in consequence, rubbing through the coating and reaching the substrate.

Similar W-shape fretting wear scar has been observed for TiCN coating, however in this case the geometrical tendency is not so deep (Figure 53).

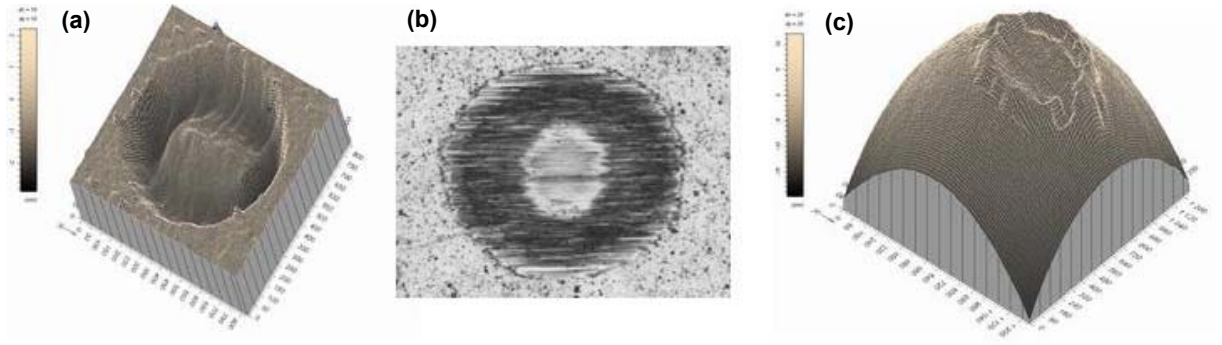


Figure 52. TiN coated specimen and alumina counter-body after fretting test: (a) 3D image of fretting scar; (b) optical image of the fretting scar; (c) 3D image of alumina ball counter-body. Fretting test conditions: $P=100\text{N}$, $\delta=100\mu\text{m}$, $N=10\text{k}$, $f=5\text{Hz}$, $RH=50\%$.

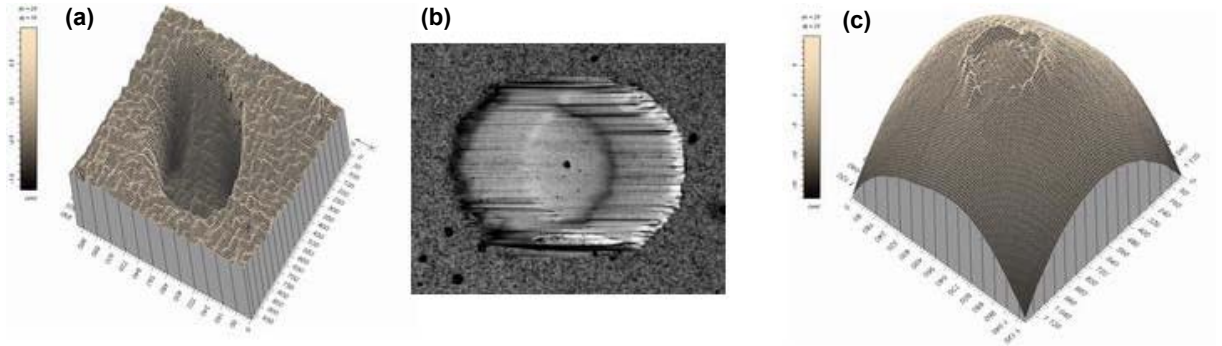


Figure 53. TiCN coated specimen and alumina counter-body after fretting test: (a) 3D image of fretting scar; (b) optical image of the fretting scar; (c) 3D image of alumina ball counter-body. Fretting test conditions: $P=150\text{N}$, $\delta=100\mu\text{m}$, $N=20\text{k}$, $f=5\text{Hz}$, $RH=50\%$.

Titanium nitride coating is characterised by relatively high coefficient of friction: 0.6, while it is significantly lower for the titanium carbonitride (0.2).

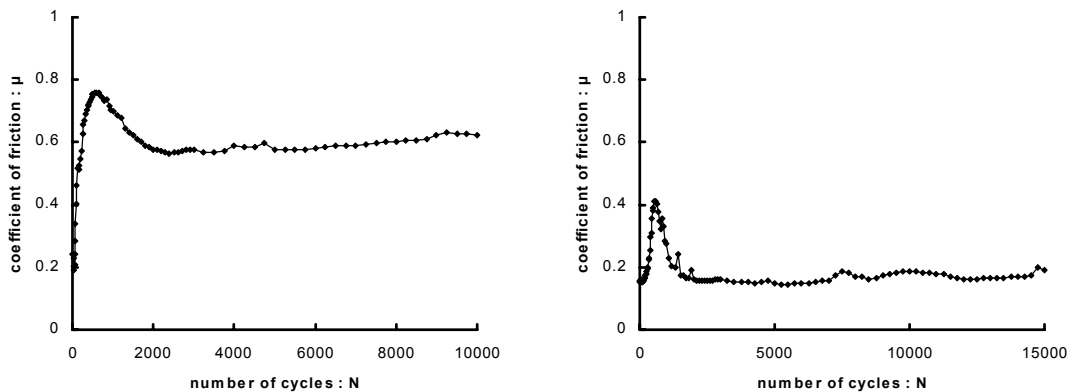


Figure 54. Evolution of friction coefficient as a function of the number of fretting cycles: (a) TiN coating ($P=100\text{N}$, $\delta=100\mu\text{m}$, $f=5\text{Hz}$, $RH=50\%$); (b) TiCN coating ($P=100\text{N}$, $\delta=100\mu\text{m}$, $f=5\text{Hz}$, $RH=50\%$).

3.2.2.1. Impact of Ti interlayer on tribological properties of the TiN coating

An attempt has been undertaken to determine the impact of thin Ti interlayer on wear resistance of TiN coating (Figure 55). This layer has been deposited directly onto a substrate surface and followed TiN coating as it was described in Chapter 2 (§ 2.3.2. *Titanium nitride and carbonitride coatings*). Four different thicknesses of Ti layer have been applied corresponding to four different deposition times of titanium: 60, 120, 180 and 240 seconds respectively. These systems have been compared with classical TiN coating without the interlayer (Figure 56).

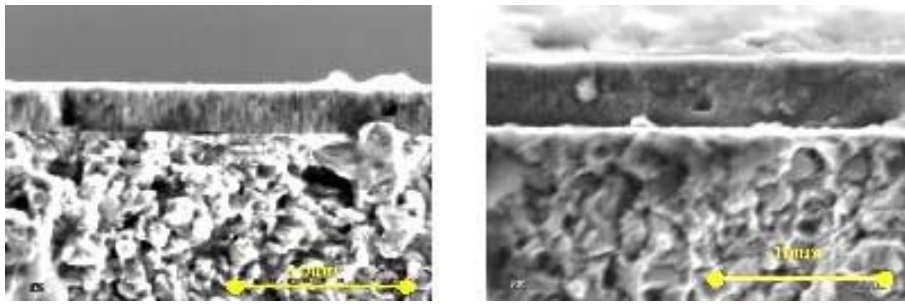


Figure 55. SEM images of coatings fractures: (a) TiN; (b) TiN with Ti interlayer (240s).

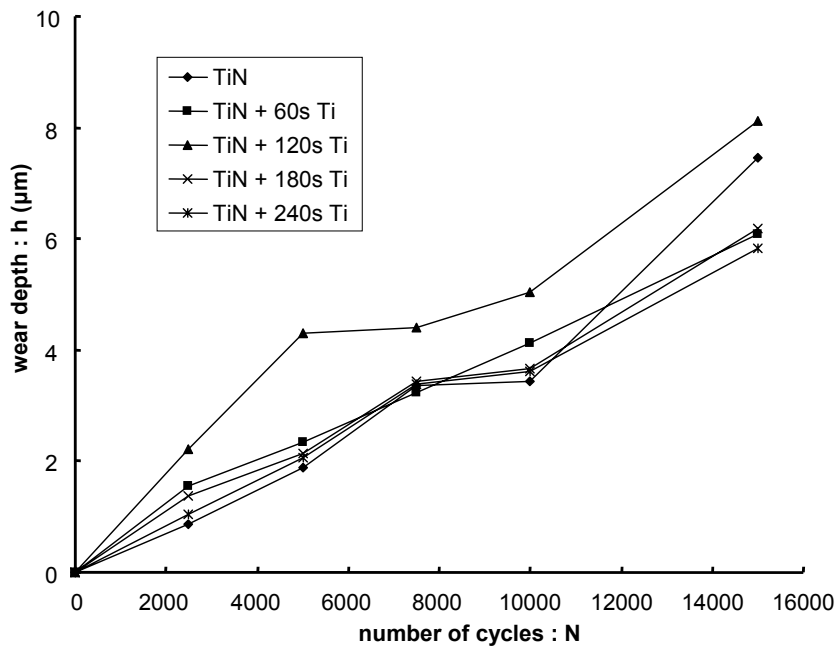


Figure 56. Results of the investigations of fretting wear for TiN coatings with and without a Ti interlayer.

Fretting experiments show that there is no significant difference between double layer coatings except for the specimen with 120s Ti layer, which can be due to extremely

disadvantageous distribution of residual stresses and should be analysed in terms of the interface effort. Nevertheless, it has been observed that the titanium interlayer thickness significantly influences the crystallization process of TiN coatings – TiN becomes more dense, the typical columnar structure disappears.

3.2.3. Multilayer titanium and vanadium carbide coatings

The morphology of fretting scars observed for TiC/VC multilayer coatings (Figures 57 and 58) is a function of properties of TiC and VC monolayers. However, the scar shape and ball surface morphologies are rather close to those in case of VC coating and are similar for both multilayer systems.

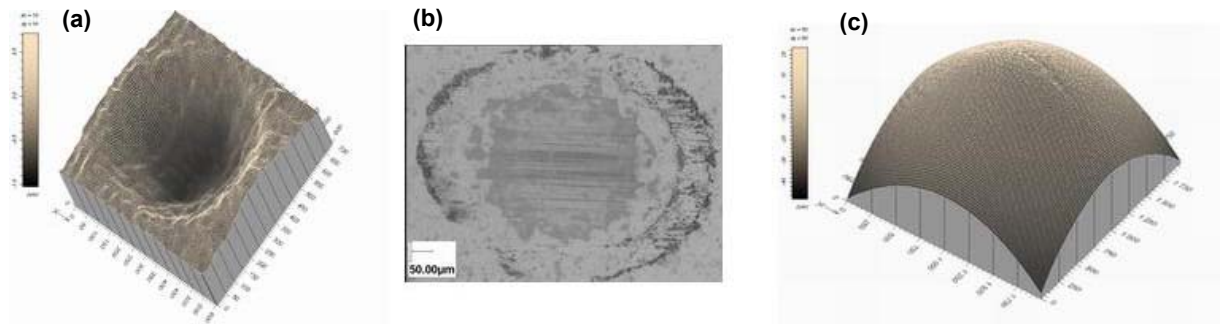


Figure 57. TiC/VC coated specimen and alumina counter-body after fretting test: (a) 3D image of fretting scar; (b) optical image of the fretting scar; (c) 3D image of the surface of the alumina ball counter-body in the respective contact area. Fretting test conditions: $P=100N$, $\delta=100\mu m$, $N=40k$, $f=5Hz$, $RH=50\%$.

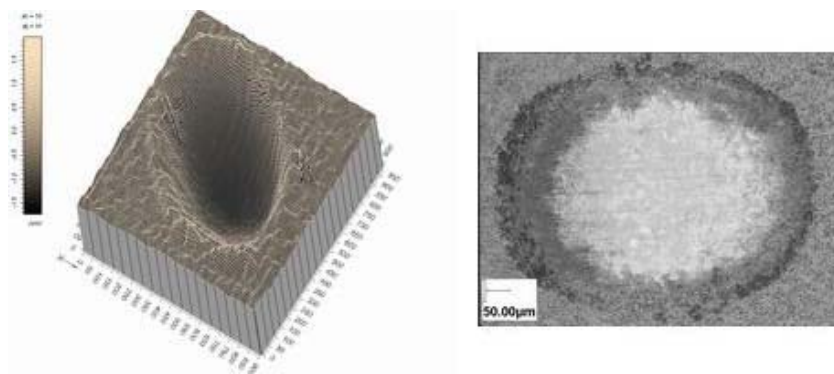


Figure 58. (TiC/VC)x2 coated specimen and alumina counter-body after fretting test: (a) 3D image of fretting scar; (b) optical image of the fretting scar. Fretting test conditions: $P=100N$, $\delta=100\mu m$, $N=30k$, $f=5Hz$, $RH=50\%$.

Observation of friction coefficient evolution for multilayer coatings delivers an interesting information about friction behaviour of this system. As it can be seen in

Figure 59, the value of the COF for (TiC/VC)x2 coating is changing with test duration in a manner corresponding with the particular material which takes part in the friction process.

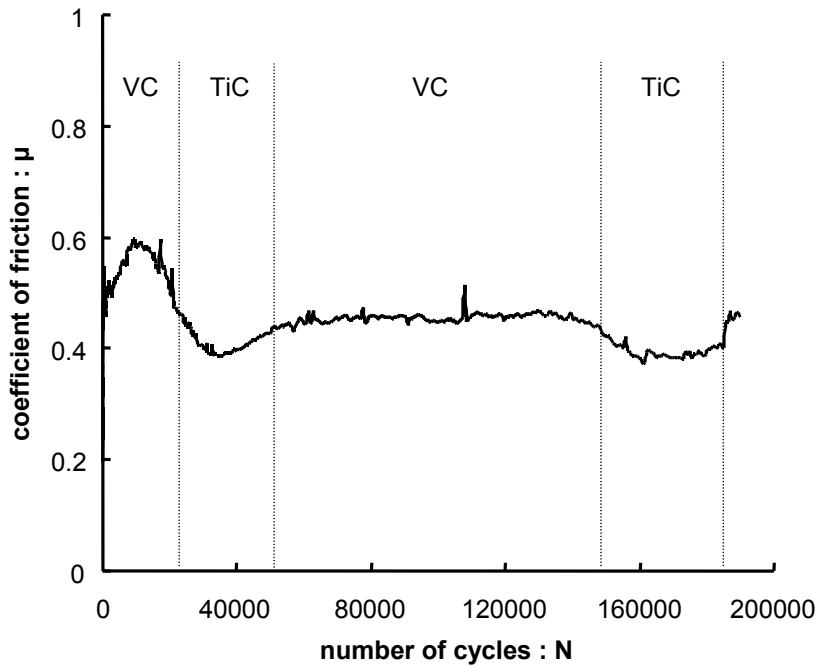


Figure 59. Evolution of friction coefficient as a function of fretting cycles for (TiC/VC)x2 coating ($P=100\text{N}$, $\delta=100\mu\text{m}$, $f=5\text{Hz}$, $RH=50\%$).

3.2.3.1. Introduction of the diffusion mixed layer

This sub-chapter is a short summary of a wider work, in which the author of this thesis took an active part as well [Fouvry S. et al. (2004)]. The background of the former is related with the resistance of the multilayer TiC/VC coatings to the fretting wear in comparison with that of monolayer TiC and VC coatings. It has been observed that vanadium carbide coating has the best resistance to the fretting wear as distinct to the titanium carbide one which has the worst resistance. Within the framework of this work the following multilayer systems have been investigated: TiC/VC, (TiC/VC)x2, (TiC/VC)x5, (TiC/VC)x20, (TiC/VC)x60 and (TiC/VC)x250. It has been found that wear resistance, characterised by α wear energy coefficient, of all multilayer coatings is comprised between α values for VC and TiC monolayer coatings (Figure 60). Hence, the main question was: why the resistance to wear of the multilayer TiC/VC coatings is changing with the number of bilayers, if the ratio of TiC and VC phases is constant in all the coatings under investigation?

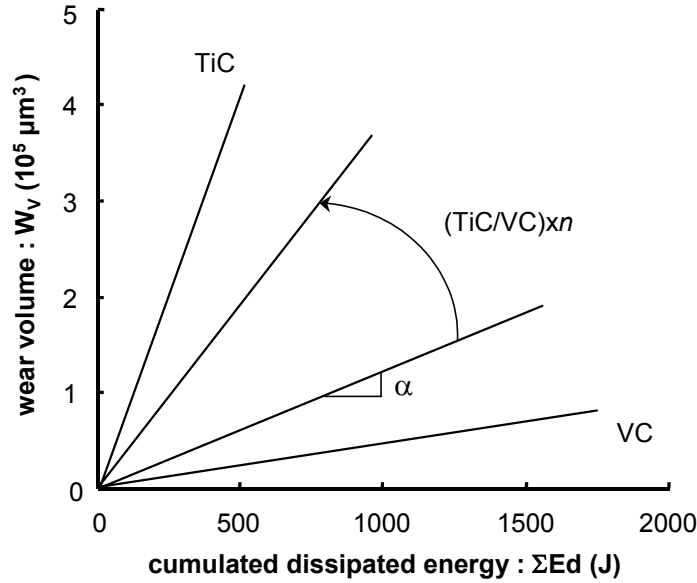


Figure 60. Evolution of energy wear coefficient α as a function of coated system under investigation. TiC and VC – monolayers, (TiC/VC) xn – multilayer ($n=1\div 250$).

To explain these changes, the mixed carbide layer concept has been proposed based on the inter-diffusion phenomena between the adjacent sublayers (Figure 61). Inspired by M. Berger and his co-workers analysis [Berger M. et al. (1999)], the concept of perfectly layered structure has been deepened by considering a mixed interlayer (MIL) which is assumed to have a constant thickness independent of the number of sublayers. Increasing the number of TiC and VC sublayers in the multilayer (TiC/VC) coating the volume fraction of this MIL layer increases, while the ratio of pure (not mixed) TiC and VC coatings remains constant: 1/1. Taking into account that the energy wear coefficient α of the mixed layer has a lower value than α_{VC} and higher than α_{TiC} , the wear resistance of the multilayer system decreases.

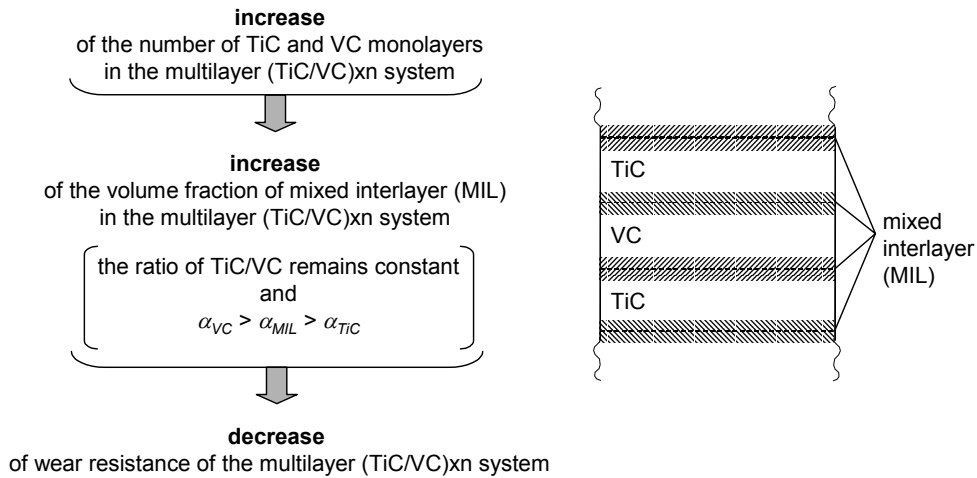


Figure 61. Impact of the increased number of mixed diffusion interlayers on the resistance to wear of the multilayer (TiC/VC) xn .

In order to understand better the layered structure of the investigated multilayer (TiC/VC)_{xn} carbide coatings, GDOS profiles of the chemical composition of the coatings have been performed before and after the vacuum heating (Figure 62). The deeper the GDOS analysis, the greater is the effect of intermixing of the adjacent layers, and the grater is the dispersion of the profiles of the chemical composition of individual sublayers. This limitation is clearly illustrated in Figure 62a where a well-defined square profile is observed for the first layer in contrast to interfered profiles for deeper layers. Another disadvantage of this technique is the non-direct correlation between sputtering time and the crater depth.

Comparing the GDOS profiles of the metallic and carbide layers, one can see that the mutual diffusion must have been activated near the sublayer interfaces during the heating process. A completely mixed TiC/VC layer is observed for a number of bilayers higher than 20. However, this limit must be considered with caution due to the scattering effect of the applied technique. One cannot rule out that a fully mixed carbide structure is obtained for a number of bilayers around 10.

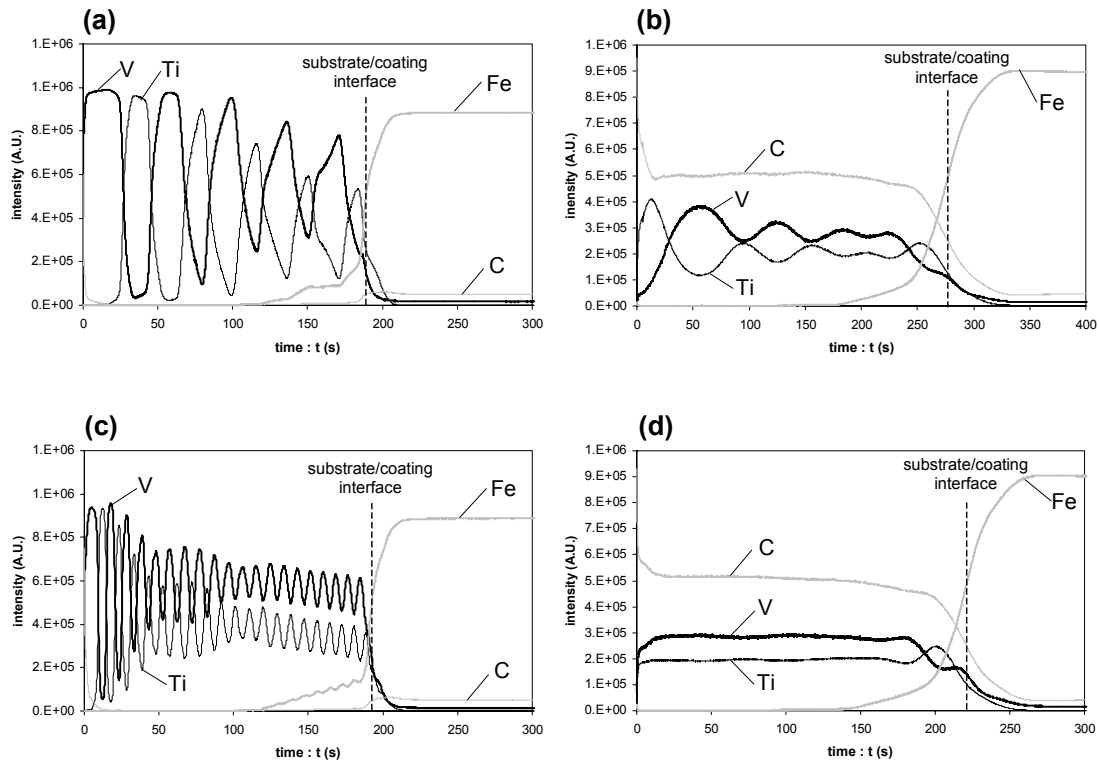


Figure 62. GDOS profiles of multilayer systems as a function of the sputtering time. (TiC/VC)_{x5} coating: (a) metallic layer, (b) after vacuum heating; (TiC/VC)_{x20} coating: (c) metallic layer, (d) after vacuum heating.

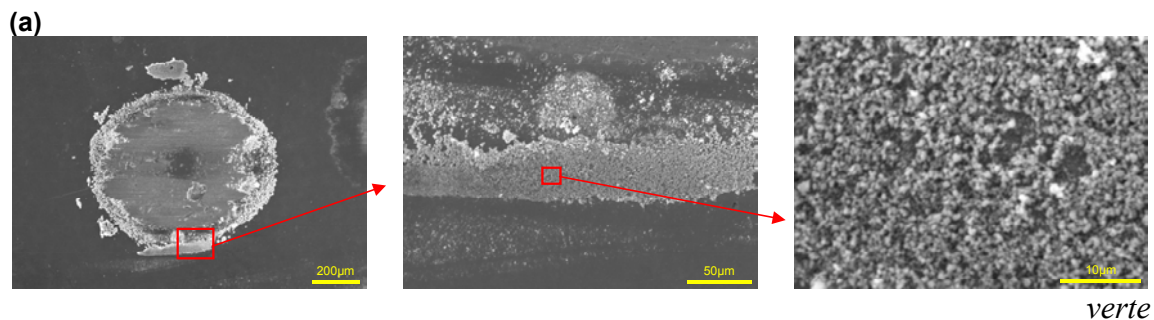
According to the mixed layer approach mentioned above, Fouvry S. et al. (2004) has characterized the wear and friction of multilayered coatings under gross slip fretting conditions. Taking into account the inter-diffusion in the mixed carbide structure, a “composite” approach has been developed. On the ground of the characteristics of the TiC and VC monolayers and the ones of the mixed carbide structure, a reliable wear rate as a function the number of bilayers can be predicted. It has been found also that the friction evolution is less predictable due to the smoothing effect of the third-body.

3.3. IMPACT OF HUMIDITY ON THE PROCESS OF FRETTING WEAR

According to the environmental test conditions (§ 3.1.2.3. *Environmental conditions*), three levels of relative humidity have been studied: 5%, 50% and 90%. In order to depict the impact of the third-body and to elucidate the wear mechanisms, the worn surfaces and the debris have been analysed by means of SEM and EDX methods. Four coatings have been selected to this study: TiC, VC, TiN, TiCN and the uniform test conditions have been applied for each test: $P=100\text{N}$, $\delta=100\mu\text{m}$, $f=5\text{Hz}$, $N=10000\text{cycles}$.

3.3.1. Dry conditions

A large amount of debris has been observed to be generated during a fretting test and coatings are damaged by material transfer due to adhesion and abrasion. It can be noticed that small amount of debris rests within a contact area, while large amount of debris is ejected outside and located near to the border of the fretting scar (Figure 63). The debris from all the coatings are not loose and their size can be estimated to be around $0.5\mu\text{m}$.



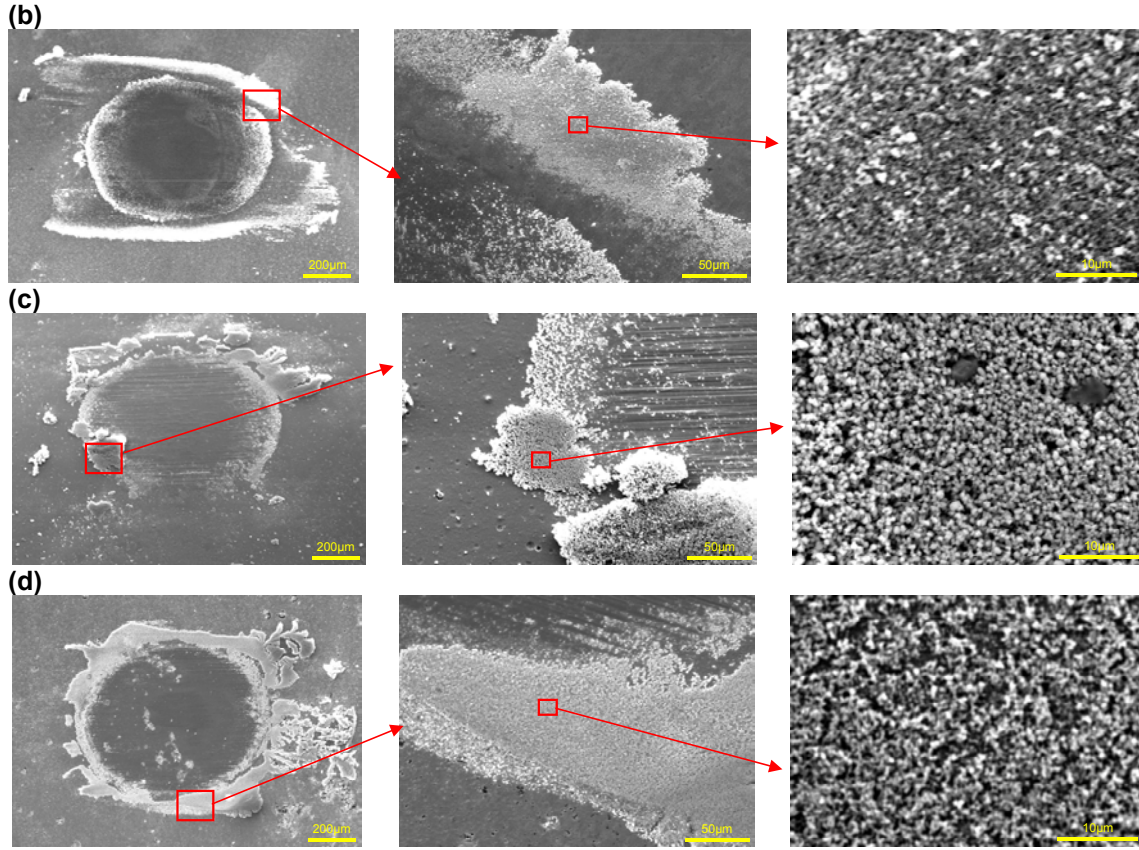


Figure 63. Fretting wear debris analysis, RH=5%: (a) TiC; (b) VC; (c) TiN; (d) TiCN.

The friction coefficient (Figure 64) is greater than 0.6 for all the coatings under investigation and is the greatest (near 0.9) for the TiC coating.

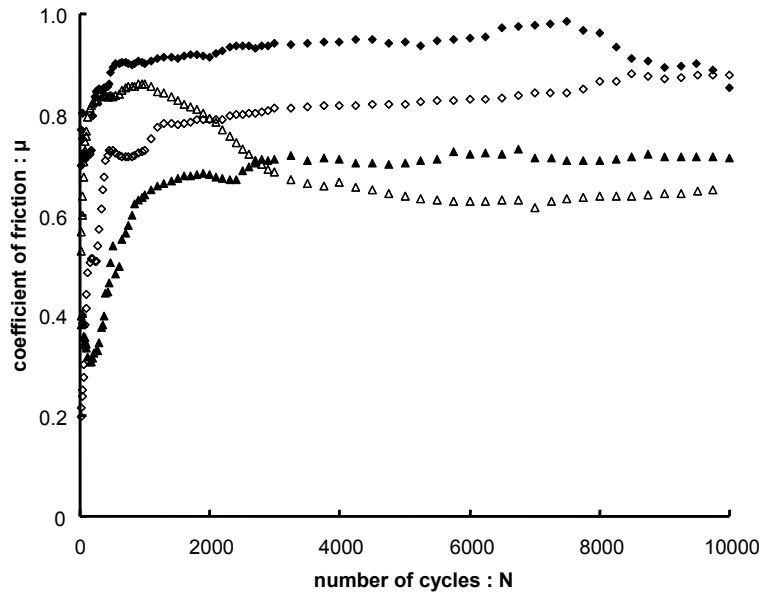


Figure 64. Evolution of friction coefficient as a function of the number of fretting cycles for different coatings: \blacklozenge TiC, \diamond VC, \blacktriangle TiCN, \triangle TiN. The relative humidity during the experiments had a value RH=5%.

3.3.2. Medium conditions

Fretting scars have three characteristic regions, which is clearly visible for TiN coating (Figure 65c): central convex region with slight abrasion traces, outer annular region covered with debris and transition region where the abrasion traces parallel to the sliding direction are easily identified. Such a morphology corresponds to the fretting scar profiles from § 3.2 *Fretting Wear of Hard Coatings under Investigation*.

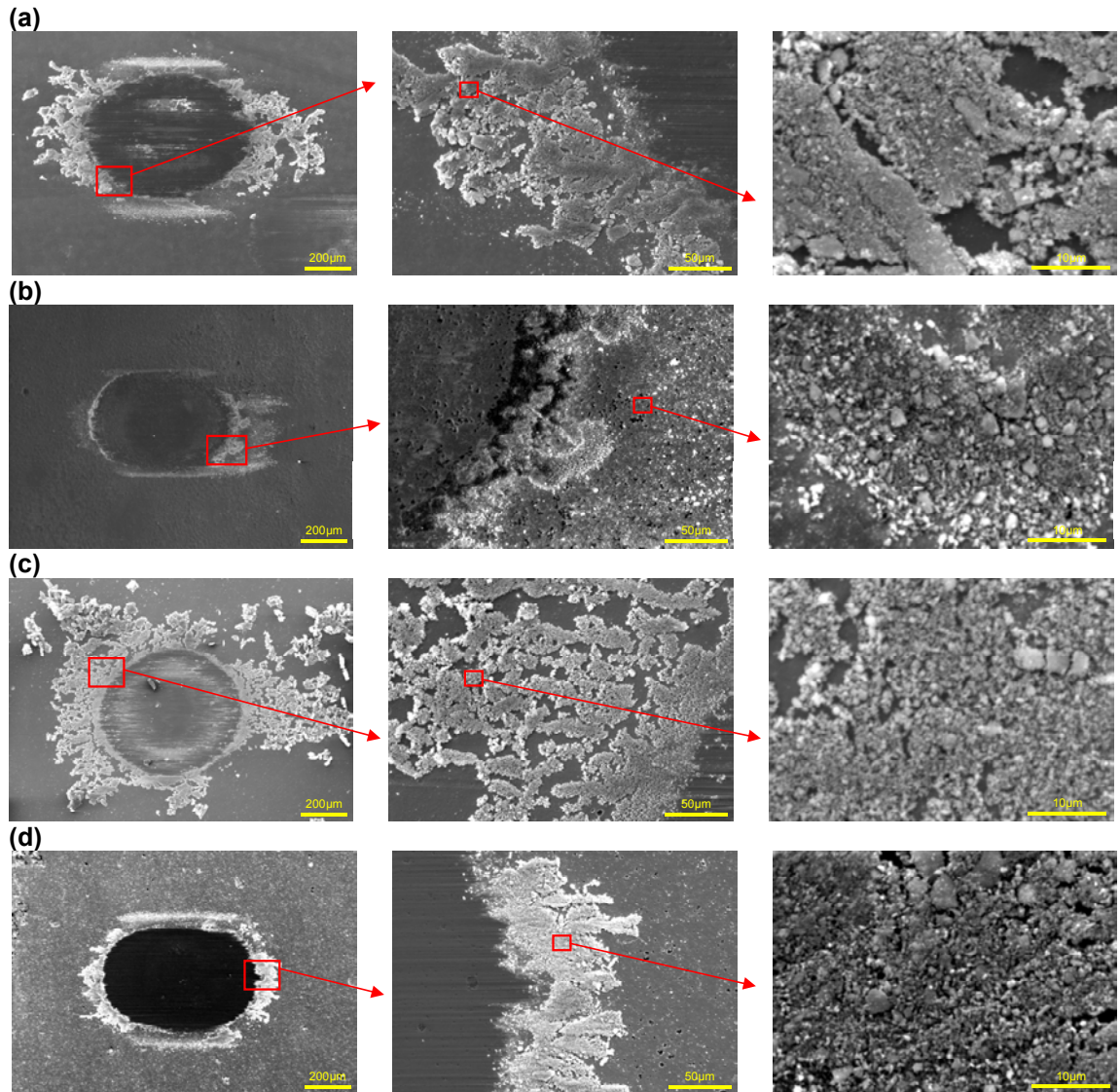


Figure 65. Debris created during fretting wear at medium humidity (RH=50%): (a) TiC; (b) VC; (c) TiN; (d) TiCN.

In the case of medium humidity environmental conditions (RH=50%) a significantly different evolution of friction coefficient has been observed in comparison with the previous dry conditions. COF values for all the coatings are lower

than 0.6 and the minimum value below 0.2 has been recorded for TiCN coating (Figure 66).

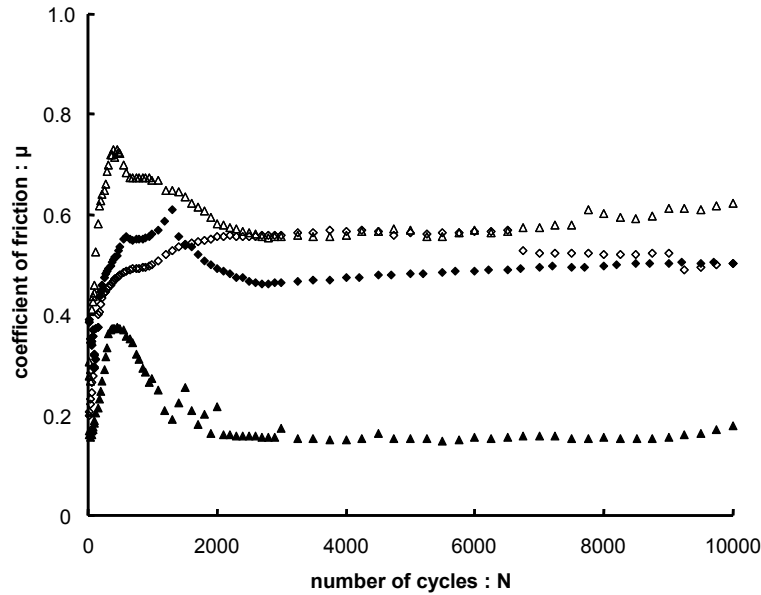
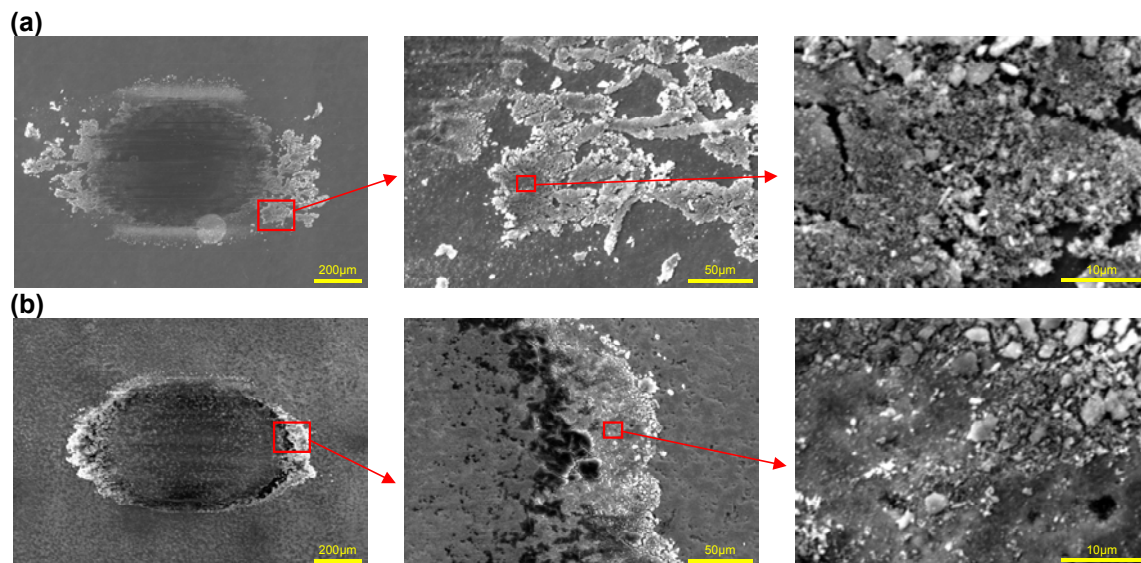


Figure 66. Evolution of friction coefficient as a function of the number of fretting cycles for different coatings during fretting wear at a medium relative humidity ($RH=50\%$):
 ♦ TiC; ◇ VC; ▲ TiCN; △ TiN.

3.3.3. Wet conditions

At the highest value of the relative humidity ($RH=90\%$) the conditions debris tend to agglomerate and the mean particle size can be evaluated to be greater than $1\mu m$ (Figure 67). It can be also noticed that the area of the fretting scar decreases with increasing relative humidity, which is closely related to smaller wear rates in wet conditions.



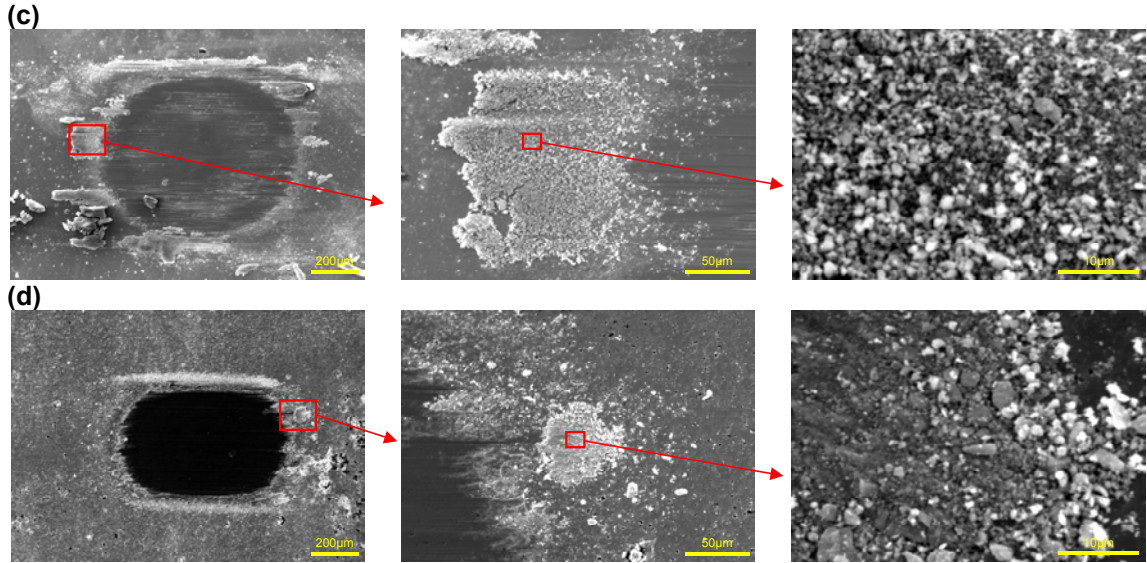


Figure 67. Wear debris produced during fretting in wet environmental conditions (RH=90%): (a) TiC; (b) VC; (c) TiN; (d) TiCN.

The friction force at the condition of high relative humidity is similar to the one observed for medium conditions. Only slight decrease has been identified, however the highest value of the friction coefficient for TiN and the lowest one for TiCN coating (Figure 68) have been observed as it was for the case of fretting wear at medium value of the humidity.

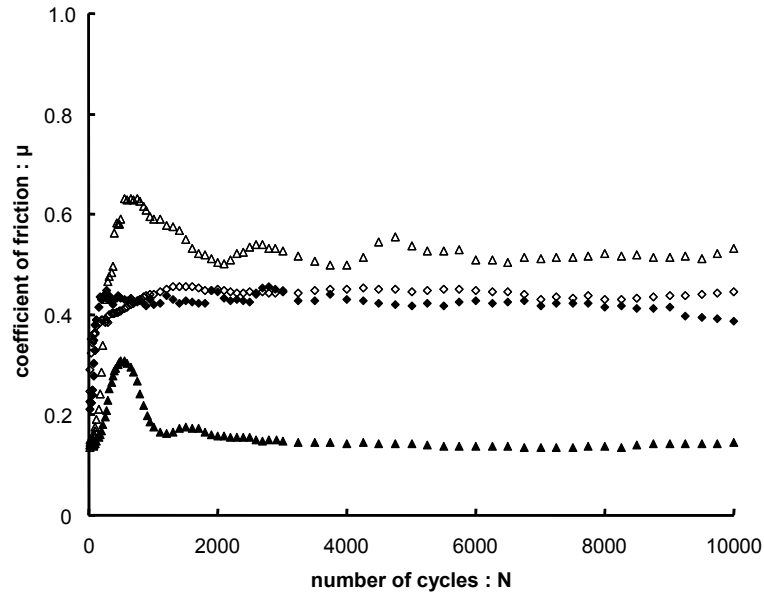


Figure 68. Evolution of coefficient of friction as a function of fretting cycles for different coatings in RH=90%: \blacklozenge TiC; \diamond VC; \blacktriangle TiCN; \triangle TiN.

3.3.4. Synthesis

The results mentioned above indicate the significant impact of the relative humidity on the third-body morphology. Now the evolution of friction coefficient as a function of the relative humidity can be explained. For each studied coating the value of the COF was decreasing with increase of the relative humidity. One should note however, that the difference for TiC and TiCN coatings at RH 50% and 90% is very small. The greatest change of the COF value has been noticed for TiCN: the COF value was equal to 0.7 at RH=5% and it was less than 0.2 at RH=90% (Figure 69). The measurements of the wear volume and the wear depth have been conducted as well to examine the impact of the relative humidity on the respective wear rates and results are listed in Table 11.

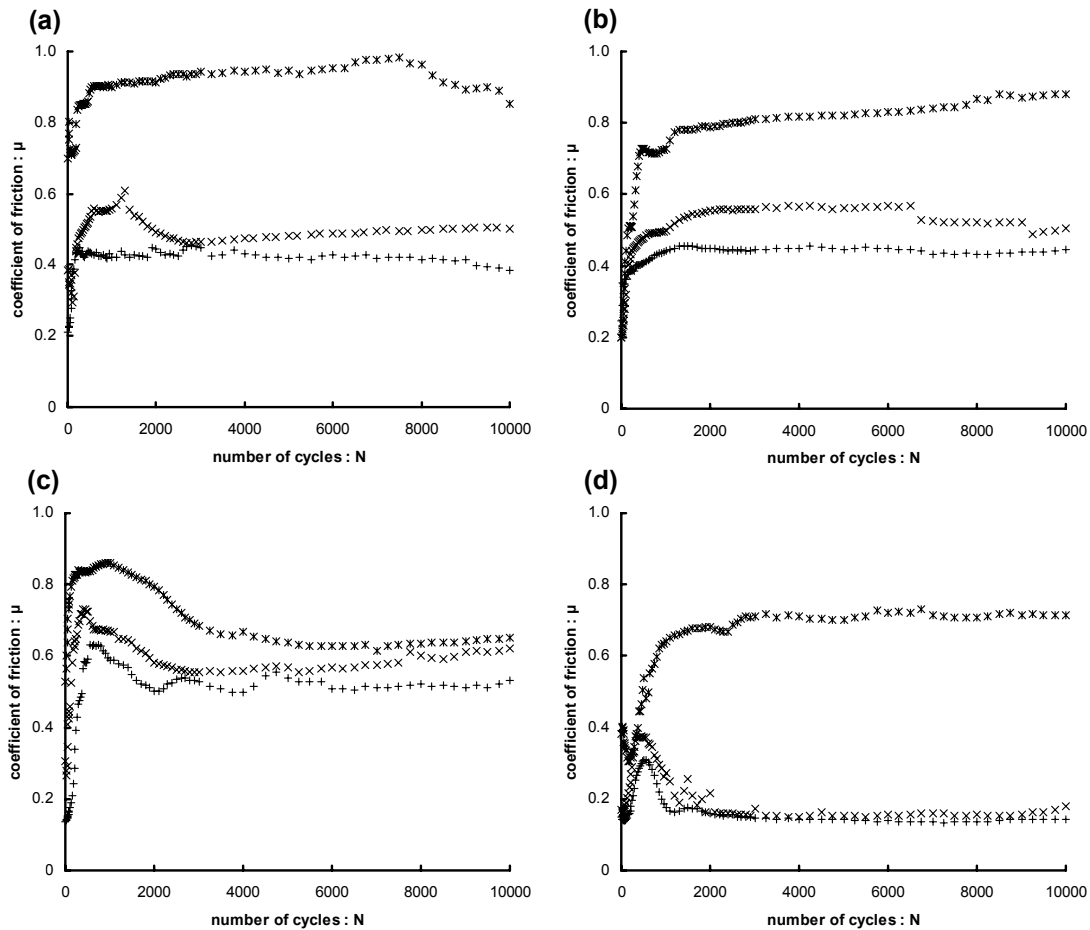


Figure 69. Evolution of friction coefficient as a function of the number of fretting cycles for four different coatings ((a) TiC, (b) VC, (c) TiN, (d) TiCN) and at three different values of the relative humidity (* 5%, x 50%, + 90%).

Table 11. Wear volume and wear depth of the coatings from Figure 70 at different environmental conditions.

Coating	Wear volume : W_v ($10^5 \mu\text{m}^3$)			Wear depth : h (μm)		
	RH 5%	RH 50%	RH 90%	RH 5%	RH 50%	RH 90%
TiC	11.001	1.024	0.059	7.27	1.81	0.59
VC	0.994	0.024	0.077	0.85	0.24	0.31
TiN	2.769	5.277	5.267	1.74	3.26	2.60
TiCN	2.230	0.946	0.711	1.80	0.84	1.71

The TiN coating behaviour under different relative humidity conditions has been widely described, among others, by: Mohrbacher H. et al. (1995a), Wei J. et al. (1997a), Wu. P.Q. et al. (2000) or Fu Y. et al. (2000). It has been established that the degradation of the TiN coating proceeds by oxidation wear, as the debris generated during the fretting wear form the layer of TiO_{2-x} and these oxides play a lubricating role within the contact area. High RH accelerates the reactions between TiN coating and the oxygen from the atmosphere, during fretting and is conducive to easier formation of TiO_{2-x} which decreases the COF. This effect has been proved for all the hard coatings under investigation and indicates the significant lubricating action of oxides for other coatings than the TiN one. The decrease of friction coefficient at high relative humidity decreases the fretting wear rates for TiC, VC and TiCN coatings. Only for the TiN coating the wear rate is greater at low RH. This different behaviour of TiN coating can be justified by the poor tribological properties of this coating, which has been depicted in Chapter 4. In this case the main wear mechanism could be cracking with spalling, which leads to coating failure independently of friction forces.

The results and observations completed in this part depict the significant role of the relative humidity conditions in the fretting wear process. It is evident that the effect of the environmental conditions should be considered separately for each superficial layer, as the reaction of each coating for variable RH is unique. Some more complex analysis and investigations are required to bring into light and interconnect the particular physical and chemical phenomena and reactions proceeding within a contact area with determined wear rates.

3.4. MORPHOLOGY OF DAMAGED SURFACES

In order to visualize clearly the morphology of the fretting wear scars, the 3D surface analysis has been carried out. Some of the results have been presented earlier in this Chapter (§ 3.2 *Fretting Wear of Hard Coatings under Investigation*) and an example of typical wear scar has been depicted for each one of the investigated coatings. Nevertheless, in this part the evolution of the fretting wear scar as a function of the test duration is more profoundly analysed and some additional features of the 3D surface morphology are taken into consideration.

In order to quantify the evolution of the surface morphology, the tactile topometer *Surfascan S-M2 Somicronic-Hommel* (France) has been used. To visualize and calculate different surface parameters *Surfascan 2.6.2.4* package has been applied, as this particular program offers complex 3D morphological analysis. Tactile *Somicronic-Hommel Surfascan* and its software was selected for few scientific, metrological and industrial reasons:

- standardized stylus techniques for manufacturing industry (ISO 3274, 4287, 4288, 5436, 11562, 12085, 12179, 13565-1 &-2);
- various (convex and concave) forms of measured surfaces;
- horizontal measuring range offering up to 200 mm;
- resolution of 6 nm.

Software enables different kinds of surface morphology analysis as well as of data treatments and the wear volume (removed and/or transferred) can be easily and accurately determined. The morphologies of wear scar of TiN coated specimens are depicted in Figure 70 for applied number of cycles from 1000 up to 18000. As it has been mentioned earlier, the wear scars have the maximum wear depth at the border and the minimum one at the centre of the contact area which leads to a typical W-shape of the longitudinal section of the fretting wear scar in case of the TiN coating.

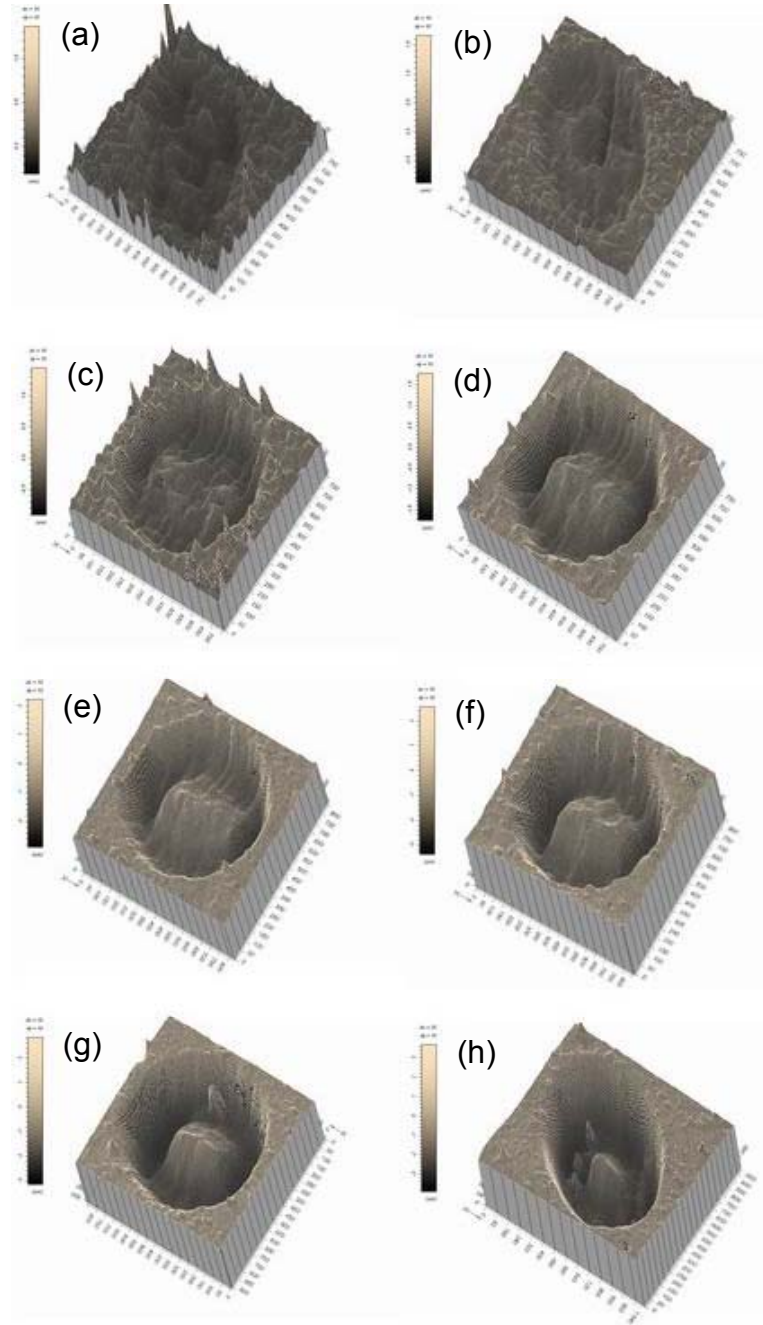


Figure 70. Progressive changes of the fretting wear scar volume with increasing number of the fretting cycles: (a) 1k; (b) 2k; (c) 3k; (d) 6k; (e) 9k; (f) 12k; (g) 15k; (h) 18k.

Worn surface of the counter-body alumina ball has been subjected to surface measurements as well (Figure 71). To estimate the volume of the material transferred onto the surface of the alumina ball a particular separation procedure has been carried out (Figure 71b). For the number of fretting cycles 15k this volume is equal to $1.011 \cdot 10^6 \mu\text{m}^3$. If we compare it with the wear volume of the scar ($1.859 \cdot 10^6 \mu\text{m}^3$), the ratio of

the transferred material (m_t) can be introduced: $m_t = \frac{T_V}{W_V} = \frac{1.011}{1.859} = 0.54$, where: T_V is the volume of the transferred material onto the surface of the alumina ball (in μm^3) and W_V wear volume of the wear scar in the TiN coating (in μm^3).

Hence, it is deduced that near half of the removed material is transferred in this case into the debris and ejected outside the contact area, while the second half is transferred onto the counter-body surface.

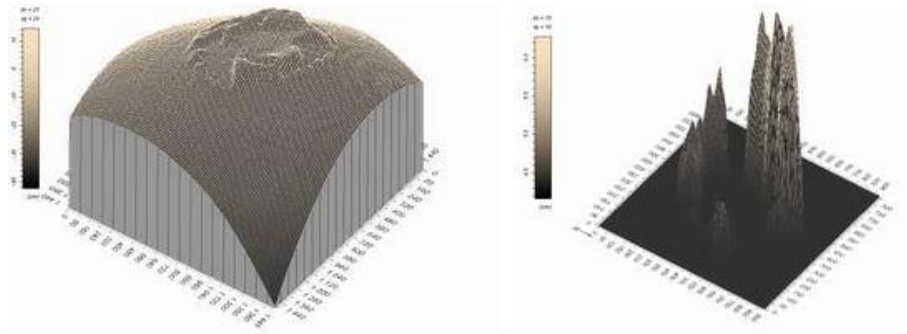


Figure 71. Alumina ball surface morphology after the number of 15k of the fretting cycles: (a) global 3D view; (b) isometric plot of separated volume of the material transferred onto ball surface.

CHAPTER 4



HARD COATINGS TRIBOLOGICAL EVALUATION

CHAPTER 4: HARD COATINGS TRIBOLOGICAL EVALUATION

In this last Chapter the studied hard coatings are compared in terms of their fretting wear resistance. The classical Archard's law is applied at the beginning. Then surface treatments are classified by means of global dissipated energy analysis. Finally, hard coatings durability approach is introduced and its endurance is estimated. The thesis of the work is proved in this Chapter.

4.1. COMPARISON OF INVESTIGATED HARD COATINGS WITH USE OF THE ARCHARD'S WEAR COEFFICIENT

The classical Archard's wear coefficient K previously defined in Chapter 1 [Eq. (7)] is considered to compare fretting wear resistance of investigated hard coatings. Wear volume extension is compared to the product of the normal force and the cumulated sliding distance. For fretting sliding, the Archard's expression is derived as follow:

$$K = \frac{W_v}{W} = \frac{W_v}{\sum_{i=1}^N 4 \cdot \delta_g(i) \cdot P(i)} \quad (\mu m^3/Nm) \quad (15)$$

where W is the product of the normal force and total displacement.

Experimental results obtained within the series of fretting tests under conditions described in Chapter 3 are depicted in Figure 72. As one can notice the VC coating has the highest wear resistance in contrast to the TiN one characterised by much less resistance to the fretting wear. The length of the linear functions is related to the coatings total thickness and their resistance to wear. The Archard's wear coefficient values together with the corresponding correlation parameters calculated for all the coatings from Figure 72 are listed in Table 12.

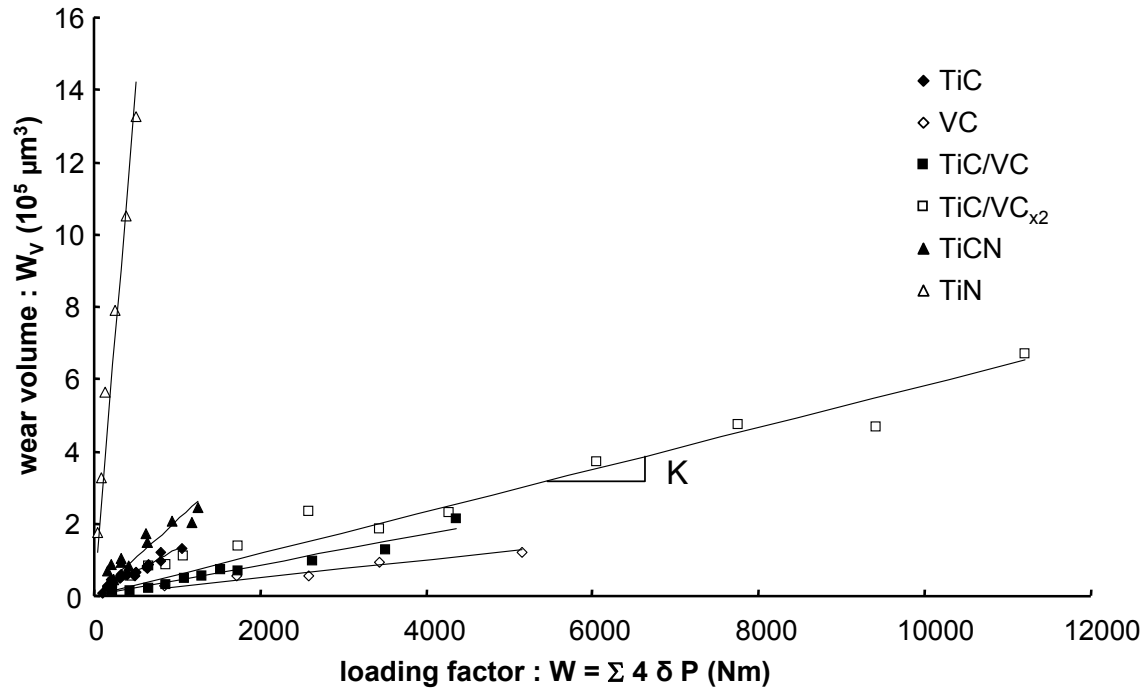


Figure 72. Evolution of the wear volume versus the product of normal force and sliding total distance (Archard's load factor W): comparison of investigated hard coatings by means of the Archard's wear coefficient $K = W_v/W$.

Table 12. Wear coefficients (K) and correlation parameters (R^2) values for studied hard coatings.

Coating	Archard's wear coefficient K ($\mu\text{m}^3/\text{Nm}$)	Correlation parameter R^2
VC	24.6	0.93
TiC/VC	42.6	0.95
(TiC/VC) _{x2}	58.1	0.95
TiC	130.5	0.93
TiCN	207.9	0.83
TiN	2769.8	0.93

It has been demonstrated that there exists a correlation between the chemical composition of the coatings under consideration and the wear kinetics. A first step to explain the evolution of the kinetics was to compare the wear coefficients with the hardness of the relevant coatings. Indeed, a reduction of the wear kinetics with the increase of the material hardness of the frictional couple has been observed in numerous research works.

The evolution of the wear kinetics as a function of the hardness of the various coatings under consideration is given in Figure 73. One can distinguish two different trends of the kinetics as a function of the coatings hardness. If the TiC and VC systems

(mono and multilayer ones) are being considered the Archard's coefficient K decreases with the increase of the coatings hardness. Contrary to that is the behaviour of the Ti-C-N system. While the hardness numbers of the coatings in the system do not differ significantly, a very strong variation of the wear kinetics is being observed with the worst behavior of the TiN coating. One can say that for the Ti-C-N system there is no correlation between the resistance to wear and the hardness.

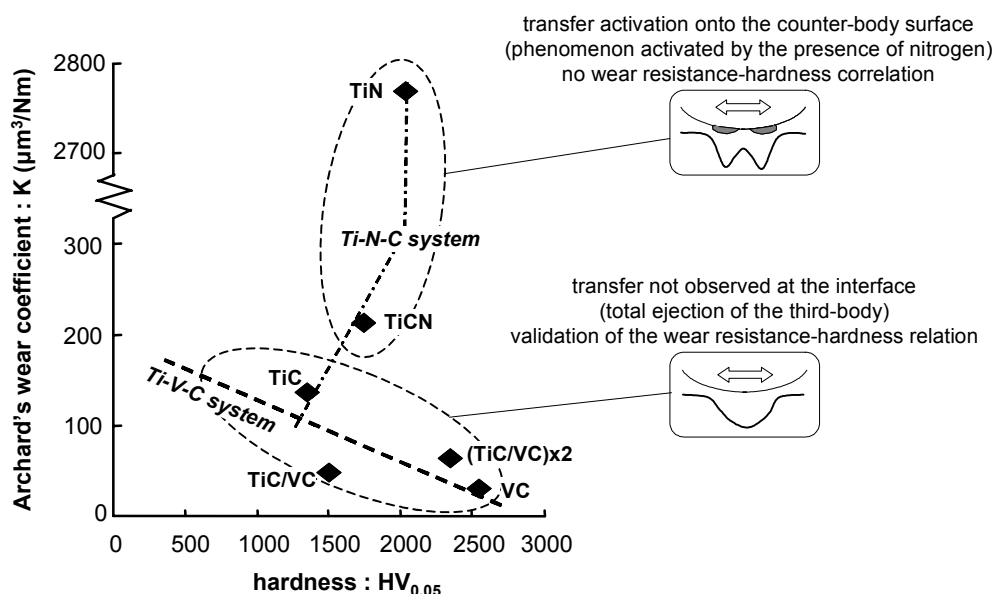


Figure 73. Illustration of the correlation between the coatings hardness and its resistance to wear: validation of the 3rd body impact associated with the chemical composition of the systems under consideration.

This research allowed to demonstrate that the hardness of the coating is not the crucial parameter which predetermines the resistance of the coating to wear at least in the case of the fretting wear in the Ti-C-N system (of one metal and two different metaloids). Contrary to that the correlation seems to be valid for the Ti-V-C system of two different metals and only one light element (C). It looks like that the nitrogen atoms in the coating modify the tribological system in the manner that the correlation wear resistance – hardness fails. To explain this behavior the investigations of the interfaces of the fretting bodies have been performed in order to draw out the effect the third-body. It has been noticed that in the case of the Ti-V-C system there were no debris on the surface of the counter-body and a conventional *U-shape* wear scar was observed in this case (Fig. 49, 50, 57, 58). Contrary to that, in case of the Ti-C-N system the third-body was remaining on the surface of the alumina ball and a modified *W-shape* wear scar was observed in this case (Fig. 52, 53). Finally, one can postulate that the correlation wear

resistance – hardness is valid as long as the third body and especially the adhesion phenomena on the counter-body do not influence (or to a small extent) the tribological system. The latter concerns the Ti-V-C system. On the other hand, since the third body plays a crucial role at the interface, then in the case of the systems including nitrogen the correlation wear resistance – hardness does not seem to be valid any longer.

This is well coherent with a physical interpretation of the tribological behavior of the fretting contact. If there is no third-body the energy dissipated in the interface is being transferred directly to the first-bodies. On the other hand, the third-body agglomerated at the interface modifies to a great extent the energy processes and thus invalidate the wear – hardness relation. It has been shown as well that activation of the third-body phenomena is directly related to the nitrogen atoms in the interface. Finally, one can notice that the third-body does not imply the systematic decrease of the wear kinetics. Indeed, the highest wear rate has been observed for the TiN coating for which the intensity of the material transfer was the greatest. A future research will have to concentrate on explanation why the nitrogen atoms supports the adhesion of the debris to the alumina counter-body and why does it modify the wear mode. This research, implying the very fine chemical analyses, including those of various components such as oxides and hydrates formed during the fretting processes, was not possible in the frame of the present work.

4.2. PREDICTION OF THE WEAR VOLUME EVOLUTION

Although the most common wear model proposed in tribology is the Archard's one, it has been found in a great number of works that for the same friction couple the wear coefficient K and friction coefficient, strongly depend on the parameters like contact geometry, wear mode or displacement amplitude. Fouvry S. et al. (2001b) demonstrated that the Archard's wear coefficient increases to a great extent when the elastic shakedown boundary is crossed and to quantify the fretting wear rate the coefficient of friction has to be integrated. Hence, in this paragraph the attention is paid to evaluate the coatings wear resistance by means of the dissipated energy approach.

4.2.1. Global dissipated energy analysis

This approach links the total wear volume with the total dissipated energy [Qiu X. et al. (1991), Rodkiewicz C.M. et al. (1994), Mohrbacher M. et al. (1995a), Fouvry S. et al. (1996)]. The dissipated energy during one fretting cycle is defined as the area of the sliding hysteresis (Figure 74). This characteristic fretting loop is a function of tangential force and applied displacement amplitude. The cumulated quantity of energy dissipated through the test duration is simply defined as the total area of the fretting cycle:

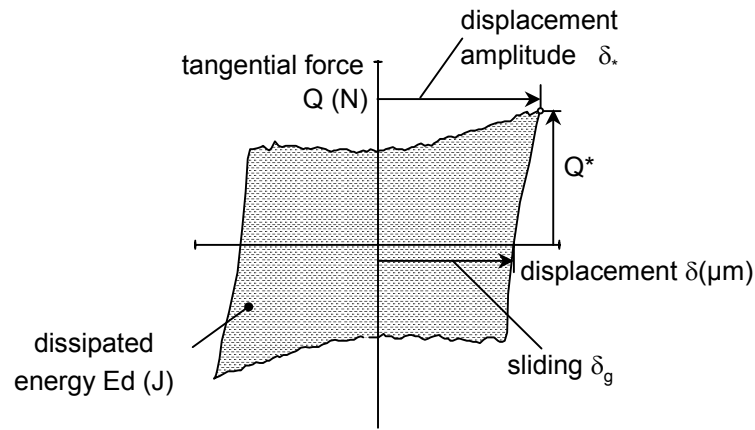


Figure 74. Characterisation of the fretting cycle.

$$\sum E_d = \sum_{i=1}^N E_d(i) \quad (J) \quad (16)$$

A mean value of friction coefficient defined over the whole fretting cycle appears more pertinent to quantify the wear. Therefore an energy friction coefficient is introduced:

$$\mu_e = \frac{E_d}{4 \cdot P \cdot \delta_g} \quad (17)$$

Its average value over the whole test duration is defined as:

$$\bar{\mu}_e = \frac{1}{N} \sum_{i=1}^N \frac{E_d(i)}{4 \cdot \delta_g(i) \cdot P(i)} \quad (18)$$

where N denotes the total number of fretting cycles.

4.2.2. Energy wear coefficient

According to this global energy approach, in which the wear volume of the degraded material is related to the shear work (i.e. cumulated dissipated energy) in the contact area, the analysis of the TiC coating/alumina ball tribo-system has been carried out at two different values of constant displacement amplitudes: 50 and 100 μm . The plot of wear volume as a function of cumulated dissipated energy results in a common linear representation for all the test conducted under both displacement amplitudes (Figure 75b) as distinct from evolution of wear volume as a function of the number of fretting cycles (Figure 75a), where two different linear plots have been obtained (each one for a particular displacement amplitude).

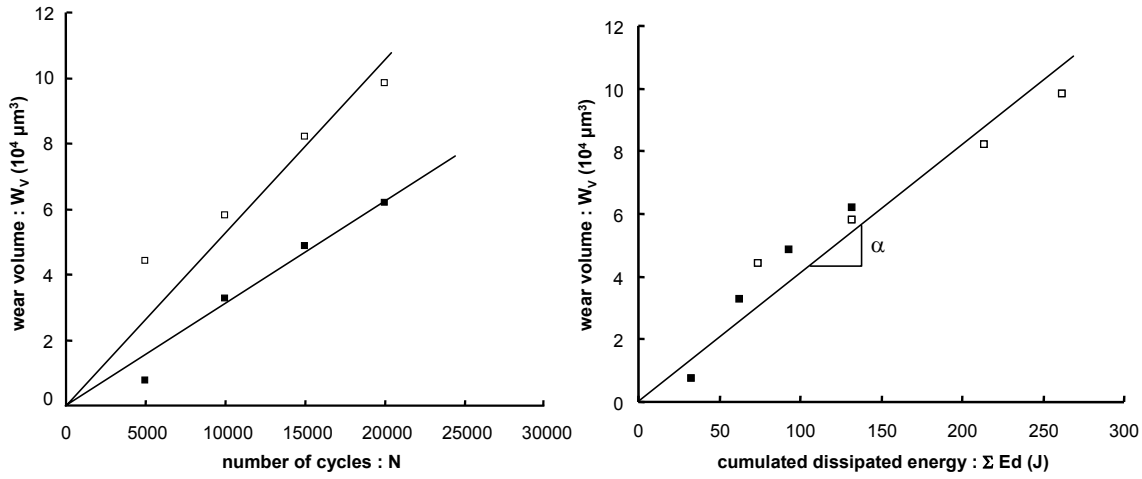


Figure 75. Evolution of the wear volume of the TiC coating as a function of: (a) number of fretting cycles; (b) cumulated dissipated energy for two different displacement amplitudes: ■ 50 μm , □ 100 μm . Fretting test conditions: TiC/alumina, RH=50%, $f=5\text{Hz}$, $P=100\text{N}$.

When the wear volume of the removed material becomes a function of the cumulated dissipated energy ($\sum E_d$), the resistance of the material to wear can be expressed by the energy wear coefficient:

$$\alpha = \frac{W_v}{\sum E_d} \quad (\mu\text{m}^3/\text{J}) \quad (19)$$

For the TiC coating investigated at two different displacement amplitudes the wear volume as a function of the cumulated dissipated energy is a single linear plot and its slope $\alpha=411\mu\text{m}^3/\text{J}$ is a unique common characteristic of the friction couple corresponding to its resistance to wear independently of the applied displacement amplitude.

4.2.3. Stability of the approach under variable loading conditions

The displacement between adjacent surfaces is generally caused by a machine motion or oscillations or vibrations. To study such phenomena, fretting tests are carried out at different displacement amplitudes [see e.g.: Ko P.L. et al. (2001), Fouvry S. et al. (1996, 2001a), Liu Q.Y. (2000)], but usually under constant loading conditions. Such a situation is very different from real operating conditions of mechanical devices, where elements are working with various speeds or frequencies or at different thermal stresses and under different loads. All these parameters can influence the fretting displacement amplitude. Hence, the author of this thesis has undertaken the problem of variable displacement amplitudes within duration of a single fretting test [Liśkiewicz T. et al. (2003)].

Investigations at various loads (constant or variable) confirm that there exists a correlation between the wear volume extension of TiC coating and the applied displacement amplitudes. For any particular numbers of cycles, fretting at the amplitude 100 μm provokes the greatest wear volume while the one at 50 μm provokes the smallest one. For all the three different loading conditions previously defined in Chapter 1, the rates of the wear volume as a function of the number of fretting cycles have some intermediate values (Figure 76a). As distinct from this behaviour, when the energy approach is applied all the five loading conditions are represented by one and only linear plot from which an unique global wear energy coefficient α can be derived (Figure 76b). In the case under consideration $\alpha = 415\mu\text{m}^3/\text{J}$.

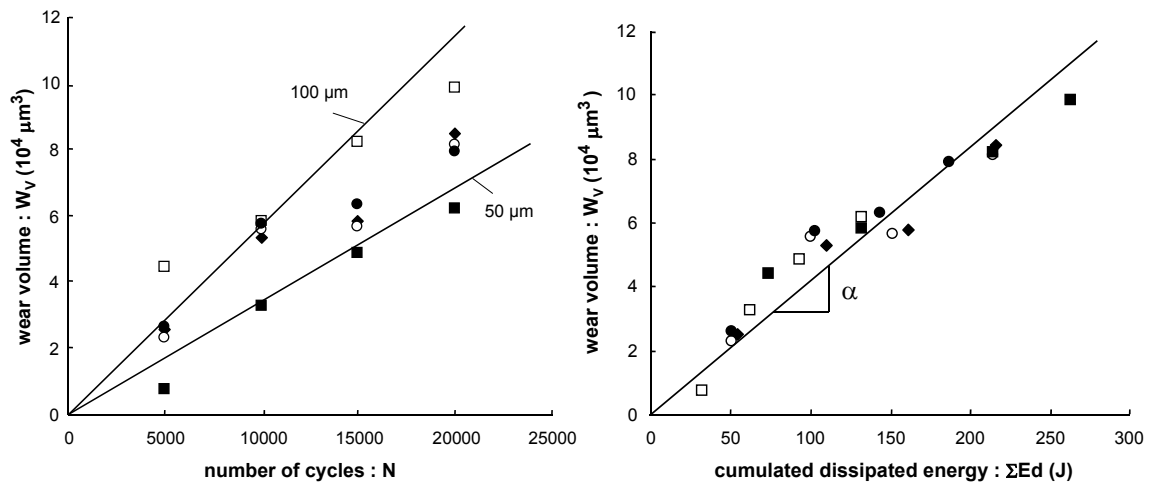


Figure 76. Evolution of the wear volume of the TiC coating as a function of: (a) number of fretting cycles; (b) cumulated dissipated energy for variable displacement amplitudes: ■ 50 μm , □ 100 μm , ♦ $(50/100)\mu\text{m}_{x1}$, ○ $(50/100)\mu\text{m}_{x2}$, ● $(50/100)\mu\text{m}_{x4}$. Fretting test conditions: TiC/alumina, RH=50%, $f=5\text{Hz}$, $P=100\text{N}$.

The global wear energy approach permits to consider the wear volume removal as a function of the cumulated dissipated energy which can be used to predict the durability of the coating independently of a particular displacement amplitude which will be used at the working conditions.

4.2.4. Hard coatings comparison

The global energy approach has been applied for all the hard coatings under investigation in agreement with the loading conditions discussed in Chapter 3. The results of the approach are depicted in Figure 77.

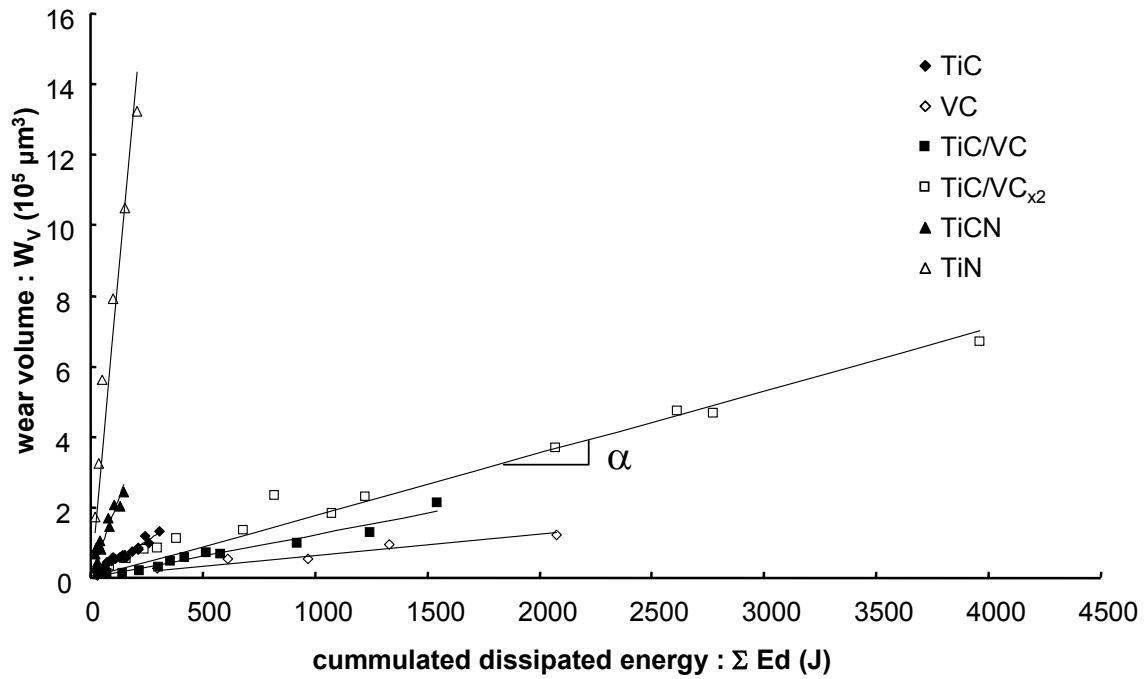


Figure 77. Linear evolution of the wear volume as a function of the cumulated dissipated energy for all the investigated hard coatings.

One can notice the same order of wear resistance for the investigated hard coatings, as the one previously obtained on the ground of the Archard's law (Table 13) and again the VC coating has the highest resistance to wear. However, some differences can also be noticed, concerning the differences of wear resistance between TiN and TiCN coatings. In case of the wear coefficient K the ratio $K_{TiN} / K_{TiCN} = 13.4$, while the ratio of $\alpha_{TiN} / \alpha_{TiCN}$ is equal to 3.9. This is a clear impact of integration of coefficient of friction in case of the energy approach formulation as the mean value of the COF for TiN coating was specified to 0.6 and for TiCN it was 0.2.

Table 13. Energy wear coefficients (α) and correlation parameters (R^2) values for studied hard coatings.

Coating	Energy wear coefficient α ($\mu\text{m}^3/\text{J}$)	Correlation parameter R^2
VC	62.5	0.90
TiC/VC	121.8	0.95
(TiC/VC) _{x2}	176.4	0.97
TiC	415.1	0.92
TiCN	1764.8	0.87
TiN	6918.6	0.93

4.3. HARD COATINGS DURABILITY APPROACH

The results presented in the previous section demonstrate that the global energy concept allows the wear volume of the TiC coating under various loading conditions to be described with a single value of the energy wear coefficient. The value of this coefficient characterises the wear resistance of the coating. Nevertheless, in thin film applications, the main difficulty in describing the durability of the components is not the evolution of the wear volume but evolution of the wear depth rather and the parameter that determines the lifetime of a particular coating is its thickness. It is expected that the wear depth is proportional to the dissipated energy density per unit area and this concept introduced by Fouvry S. et al. (1996) will be examined and developed in the next section. The methodology of this novel hard coatings durability approach will be applied at first for the TiC coating and next for other tribo-systems under investigation.

4.3.1. Local dissipated energy analysis

If the cumulated dissipated energy is the crucial parameter of wear, one should expect that the wear depth is related to the surface density of the cumulated dissipated energy. Figure 78 illustrates such a correlation considering a Hertzian shear stress field distribution. In the first approximation the Hertzian shear work distribution could be utilised but due to rapid wear of the interface and its constant extension a mean pressure (p_m) appears to be more representative. The general expression for the density of the energy dissipated at the contact centre during the i^{th} fretting cycle is expressed as:

$$\text{if } r(i) > \delta_g(i) \quad \text{then} \quad E_{dh}(i) = 4 \cdot \delta_g(i) \cdot \mu_e(i) \cdot p_m(i) \quad (J/\mu\text{m}^2) \quad (20)$$

else,

$$E_{dh}(i) = 4 \cdot r(i) \cdot \mu_e(i) \cdot p_m(i) \quad (J/\mu m^2) \quad (21)$$

with $r(i)$ defined as a scar radius and the mean pressure $p_m(i)$ equal to

$$p_m(i) = \frac{P(i)}{A_r(i)} \quad (22)$$

where $A_r(i)$ is the contact area for the i^{th} fretting cycle.

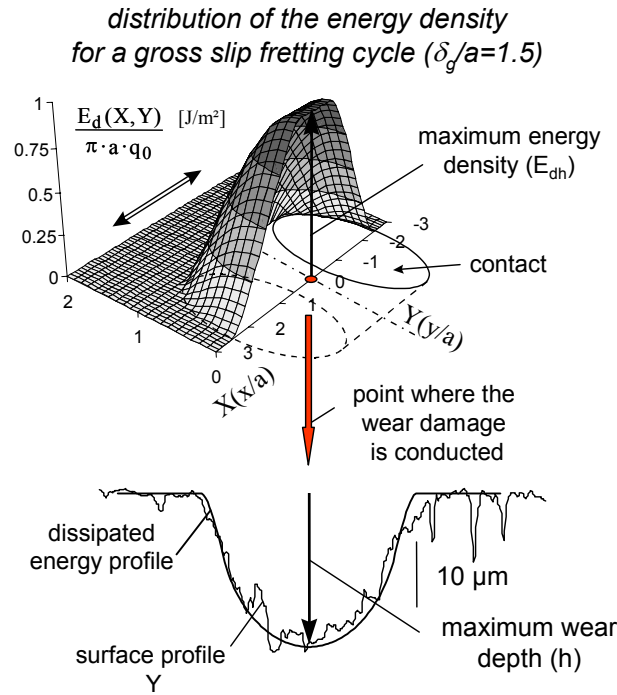


Figure 78. Illustration of the energy density approach to quantify the wear depth evolution in case of the sphere/plane contact geometry (a – Hertzian contact radius, q_0 – maximum Hertzian shear) [Sauger E. et al. (2000)].

For each test the local energy density is summed up, in order to obtain the cumulated dissipated energy density at the centre of the contact area:

$$\sum E_{dh} = \sum_{i=1}^N E_{dh}(i) \quad (J/\mu m^2) \quad (23)$$

4.3.2. Contact area evolution

One should notice that the normal force, the sliding amplitude, as well as the friction coefficient in equations (20-22) are continuously recorded and can be easily used for on-line calculations. A major difficulty arises with extrapolation of the contact area evolution.

Assuming the fretting wear cap to be spherical, the surface of contact area (S_a) is then introduced and the wear volume can be expressed as follows (the relative notations are referred to in Figure 79):

$$S_a = 2\pi Rh \quad (24)$$

$$W_v = \frac{1}{3}\pi h^2 (3R - h) \quad (25)$$

combining (24) and (25) one obtains:

$$W_v = \frac{1}{3}\pi \frac{S_a^2}{(2\pi R)^2} R \left(3 - \frac{h}{R} \right) \quad (26)$$

Taking into account that $h \ll R$, it can be deduced:

$$W_v = K S_a^2 \quad \text{with} \quad K = \frac{1}{4\pi R} \quad (27)$$

The dependence of the dissipated energy on the wear scar radius extension is, in fact – direct consequence of the wear volume increase with the cumulated dissipated energy. Hence, the wear scar radius can be defined from the measured cumulated dissipated energy.

The equation (27) can be substituted into equation (19) to determine the following expression:

$$S_a = \left(\frac{\alpha}{K} \right)^{1/2} \cdot (\Sigma E_d)^{1/2} \quad (28)$$

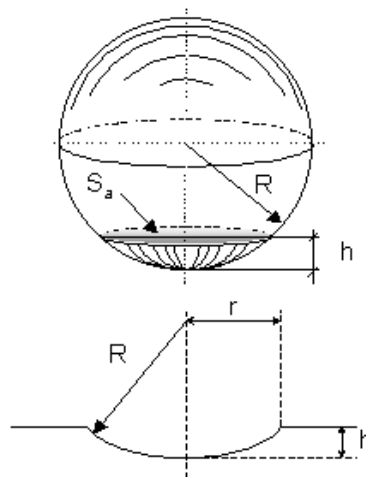


Figure 79. Illustration of the spherical cap shape hypothesis of the fretting wear scar.

It is evident that the surface of contact area is not equal to zero at the beginning of the test, and the formulation needs to consider the incipient Hertzian contact area.

Therefore for the sphere/plane configuration the contact surface extension is assumed to fulfil the following simple expression:

$$S_a = A \cdot \Sigma E_d^{1/2} + B \quad (29)$$

Figure 80 confirms the reliability of this approximation and the corresponding linear regression constants found with use of the least squares fit turned out to be $A = 5300 \mu\text{m}^2/\text{J}$ and $B = 98500 \mu\text{m}^2$.

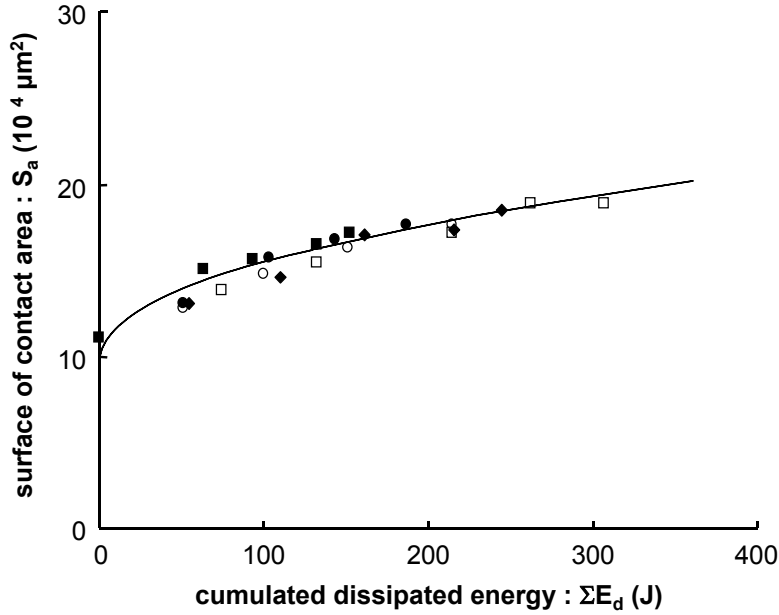


Figure 80. Evolution of the surface of contact area defined from optical measurements as a function of the cumulated dissipated energy for variable displacement amplitudes: ■ $50 \mu\text{m}$, □ $100 \mu\text{m}$, ◆ $(50/100) \mu\text{m}_{x1}$, ○ $(50/100) \mu\text{m}_{x2}$, ● $(50/100) \mu\text{m}_{x4}$, — Theoretical evolution defined from Eq. (29) with $A = 5300 \mu\text{m}^2/\text{J}$ and $B = 98500 \mu\text{m}^2$. Fretting test conditions: TiC/alumina, $RH = 50\%$, $f = 5\text{Hz}$, $P = 100\text{N}$.

One interesting aspect of this simple fretting scar dimensional analysis is that it permits also energy wear parameters to be rapidly identified. Indeed assuming on the ground of Eq. (29) that:

$$\alpha \approx K \cdot A^2 \quad (30)$$

where $K = (4\pi R)^{-1}$ and R is the ball radius, the energy wear parameter α can adequately be estimated.

A numerical application for the case of TiC coating and alumina counter-body under investigation gives $\alpha = 176 \mu\text{m}^3/\text{J}$. This value is significantly smaller than the value given by more precise surface profiles ($\alpha = 415 \mu\text{m}^3/\text{J}$). However, the simplicity of this reverse approach may provide a rapid and low cost estimation of energy wear parameters to compare different surface coatings. Further investigations should be

conducted to evaluate how the optimization of such an area of quantification, widely employed to characterise wear under abrasion tests, could be applied to fretting wear.

By quantifying the surface of contact area evolution as a function of the cumulated dissipated energy, it is finally possible to determine the energy density properly. Hence, the energy density dissipated during the i^{th} fretting cycle is represented by:

$$E_{dh}(i) = 4 \cdot \delta_g(i) \cdot \mu_e(i) \frac{P(i)}{A \sum E_d(i)^{1/2} + B} \quad (J/\mu m^2) \quad (31)$$

where

$$\sum E_d(i) = \sum_{j=1}^i E_d(j) \quad (J) \quad (32)$$

It should be indicated, that the surface of contact area evolution for a given hard coating has to be established for fretting tests within a coating thickness. As only the substrate is reached the contact area extension change rapidly due to the modification of tribological properties of a system.

4.3.3. Energy density wear coefficient

This above formula derivation at first seems intricate and complex. However, only linear expressions and regular sums are considered which can easily be implemented in any data post treatment. Automatic procedures developed to this approach have been extensively applied to analyse each fretting test. A linear evolution between the wear depth and the cumulated energy density is observed, confirming the stability of the energy approach to quantify the wear process of such a hard coating. Figure 81 presents results for two constant displacement amplitudes.

Once again wear coefficient can be obtained relating wear depth whit the cumulated dissipated energy density. In this case the coefficient is defined as energy density wear coefficient and is expressed by:

$$\beta = \frac{h}{\sum E_{dh}} \quad (\mu m^3/J) \quad (33)$$

For the studied TiC coating and two different displacement amplitudes the linear regression of the results from Figure 81 gives a value of energy density wear coefficient equal to $\beta = 488 \mu m^3/J$.

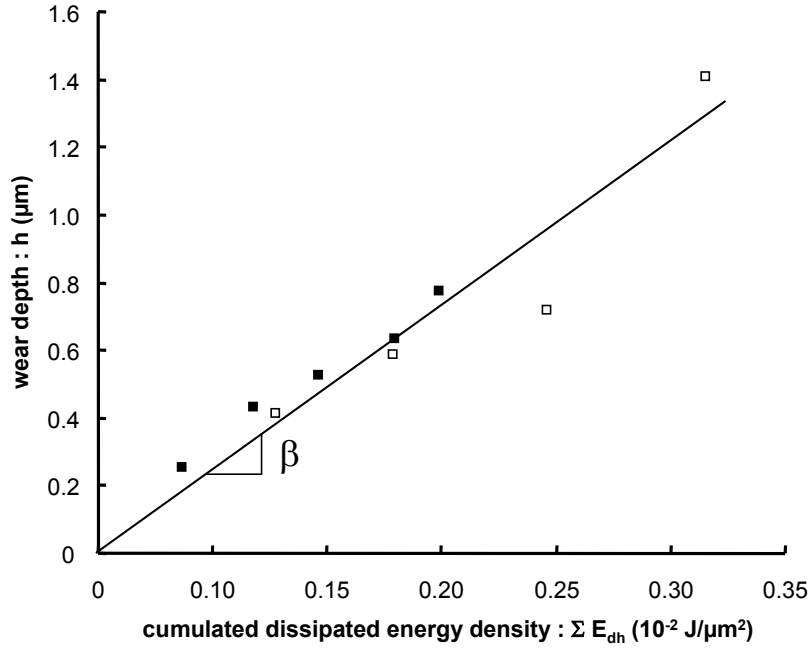


Figure 81. Evolution of the wear depth in the TiC coating as a function of cumulated dissipated energy density for two different displacement amplitudes: ■ 50 μm , □ 100 μm . Fretting test conditions: TiC/alumina, RH=50%, $f=5\text{Hz}$, $P=100\text{N}$.

4.3.4. Application of the approach under variable loading conditions

The stability of the local approach has been examined under variable displacement amplitudes as well. As shown in Figure 82a, the evolution of the dissipated energy density during a fretting test is related to changes in displacement amplitude and to the evolution of the surface of contact area during the test. The decrease of the dissipated energy density is related to the extension of the contact area and the decrease of the shear field distributions. As expected, the variable amplitude condition induces discontinuities in the energy density evolution. An increase of the sliding amplitude leads to a proportional increase of the dissipated energy density. For each test performed under variable loading conditions, cumulative dissipated energy density was calculated in the same manner as described above. Subsequently, the values of the wear scar depth measured in each test were plotted against the corresponding cumulated dissipated energy density calculated for that test (Figure 82b).

It confirms once again the reliability of the dissipated energy density approach to predict the evolution of the wear depth of the coating under investigation. Linear regression of the experimental data gives the β value equal to $474\mu\text{m}^3/\text{J}$ for the studied TiC/alumina contact.

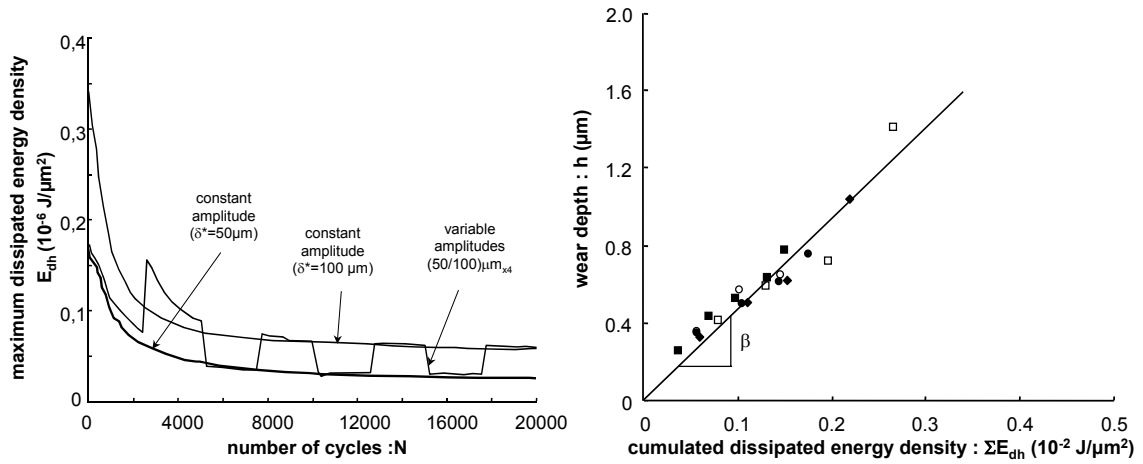


Figure 82. (a) Evolution of the dissipated energy density as a function of the number of fretting cycles for three different sliding conditions; (b) Local wear analysis: determination of the energy density wear coefficient β as a slope of the wear depth in the function of the cumulated dissipated energy density for different displacement amplitudes: \blacksquare $50\mu\text{m}$, \square $100\mu\text{m}$, \blacklozenge $(50/100)\mu\text{m}_{x1}$, \circ $(50/100)\mu\text{m}_{x2}$, \bullet $(50/100)\mu\text{m}_{x4}$. Fretting test conditions: TiC/alumina, RH=50%, $f=5\text{Hz}$, $P=100\text{N}$.

4.3.5. Coatings endurance: ‘Energy-Wöhler’ wear chart

The former local wear depth analysis supports the idea that the coating lifetime could be predicted. Hence, for a given coating thickness (t), we can identify the critical dissipated energy density (E_{dhc}) related to the moment when the substrate is reached:

$$E_{dhc} = \frac{t}{\beta} \quad (34)$$

One fundamental conclusion of this relationship is that the coating endurance is simply related to a critical energy density delivered to the tribo-system. As can be noticed in Figure 83 for the investigated TiC coating the critical energy value has been identified and it is equal to $E_{dhc} = 3.4 \cdot 10^{-3} \text{ J}/\mu\text{m}^2$.

Thus, for a constant energy density per fretting cycle the critical number of cycles to reach the substrate (N_c) can be determined:

$$N_c = \frac{E_{dhc}}{E_{dh}} \quad (35)$$

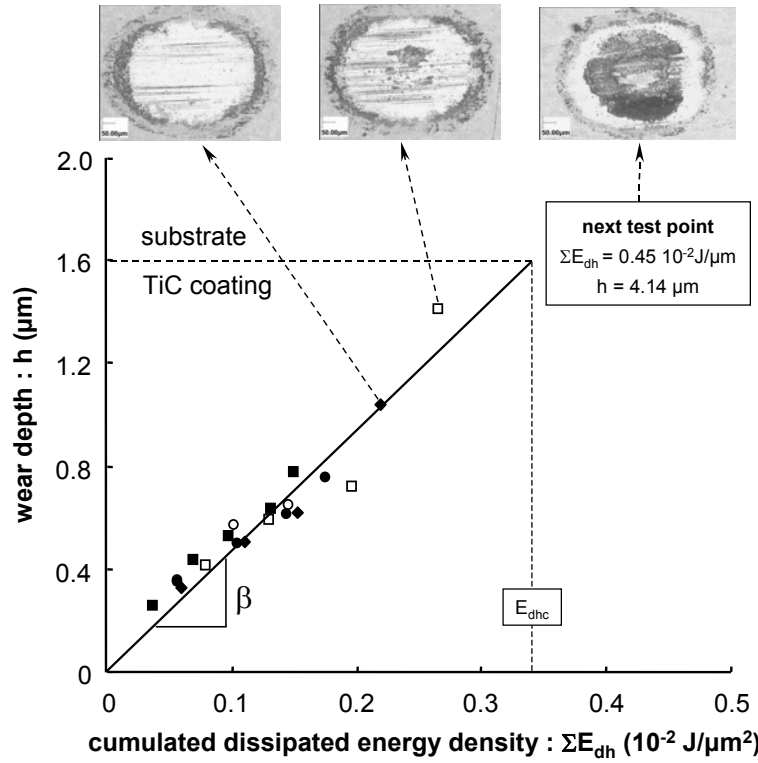


Figure 83. Plot of the wear depth versus the cumulated dissipated energy density and determination of the critical energy density for a given coating thickness. Displacement amplitudes: ■ $50\mu\text{m}$, □ $100\mu\text{m}$, ◆ $(50/100)\mu\text{m}_{x1}$, ○ $(50/100)\mu\text{m}_{x2}$, ● $(50/100)\mu\text{m}_{x4}$. Fretting test conditions: TiC/alumina, $RH=50\%$, $f=5\text{Hz}$, $P=100\text{N}$.

However, whatever the sliding condition (constant or variable), the energy density is never constant. An increase of the contact area and/or a variation of the sliding amplitude influence the energy density (Figure 84a) which suggests that an averaged energy density value should be considered:

$$\bar{E}_{dh} = \frac{\Sigma E_{dh}}{N} \quad (36)$$

therefore,

$$N_c = \frac{E_{dhc}}{\bar{E}_{dh}} \quad (37)$$

By inserting this mean value into equation (35), an energy density–coating endurance chart (i.e. \bar{E}_{dh} - N curve), equivalent to the Wöhler’s fatigue one can be developed. It was proposed by Langlade C. et al. (2001) to compare different surface treatments by means of Wöhler curves. However the authors consider in their work the endurance of a coating as a function of maximum pressure. The introduced energy concept appears more “universal” as integrates most of the loading variables with of the imposed mean energy density.

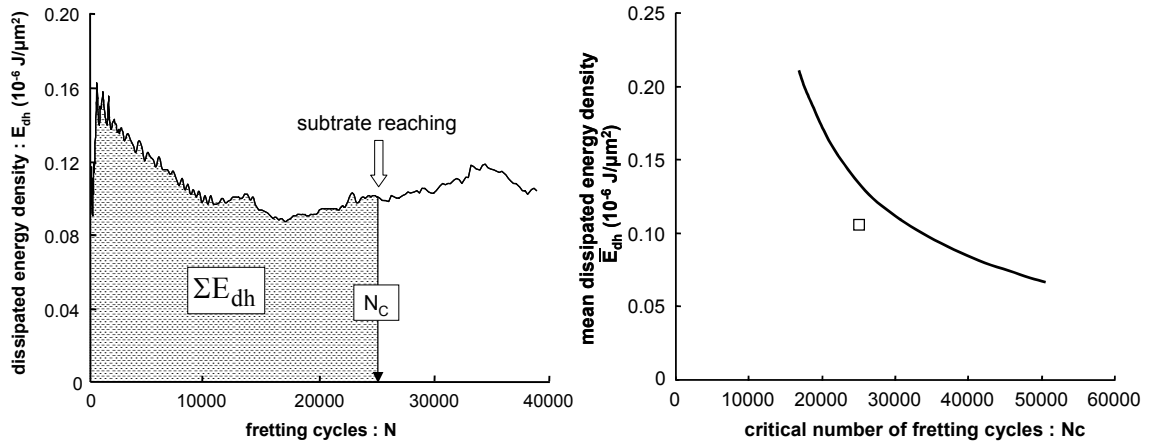


Figure 84. (a) Evolution of energy density as a function of number of fretting cycles and determination of the substrate reaching condition ($N_c = 24500$ cycles); (b) Introduction of the energy density coating endurance chart: — Theoretical coating lifetime based on the energy wear depth prediction (TiC/alumina, $E_{dhc} = 3.4 \cdot 10^{-3} \text{ J}/\mu\text{m}^2$); \square - experimentally determined number of fretting cycles to reach the substrate at the fretting conditions: TiC/alumina, $\delta = 100 \mu\text{m}$, $RH = 50\%$, $f = 5 \text{ Hz}$, $P = 100 \text{ N}$.

Figure 84b presents the theoretical endurance of the TiC coating derived from the critical energy density $E_{dhc} = 3.4 \cdot 10^{-3} \text{ J}/\mu\text{m}^2$ determined previously in Figure 83. In the next step this theoretical value is being compared with a critical number of fretting cycles for a particular fretting test as depicted in Figures 84a and 84b. In practice a slightly shorter coating lifetime than the one predicted by the volumetric wear model is usually obtained. To experimentally validate such an assumption, substrate reaching conditions must be determined and compared with the model.

4.3.5.1. Determination of the critical number of fretting cycles

Substrate reaching condition for hard coatings is usually indicated by the friction discontinuity resulting from severe ceramic (alumina) ball/metal interactions (Figure 85). However, not always this moment can be clearly pointed out by this method. Some problems with critical number of fretting cycles determination can occur in the case of good adhesion of coating to the substrate material. Also some spalling of the coating can appear when the coating is almost worn through, which generates large coating debris and influences the system kinetics.

Due to the diffusion process involved in elaboration of the TiC hard coating investigated in the work, no clear friction discontinuity has been observed. Therefore in order to determine the coating endurance, the critical number of fretting cycles was

established by numerous interrupted tests where the substrate reaching conditions were confirmed by surface profiles and optical observations.

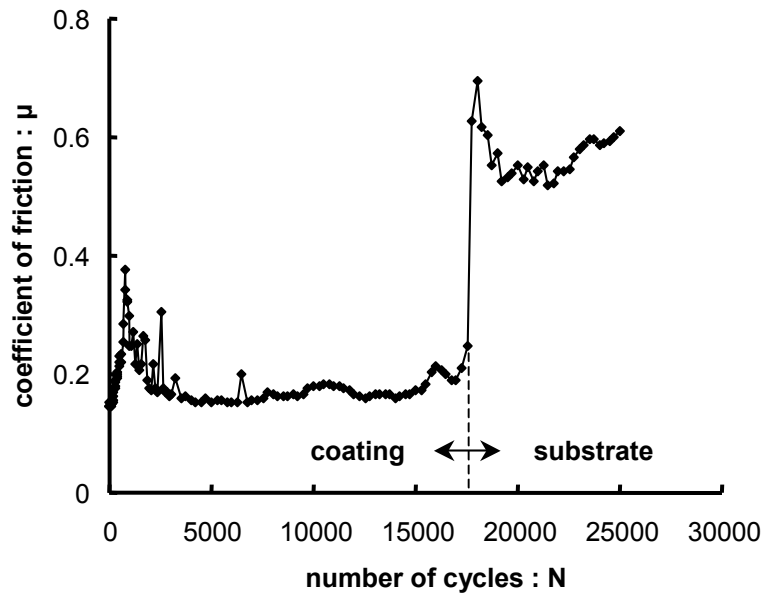


Figure 85. Determination of the substrate reaching condition by means of the discontinuity of the friction coefficient observation. Fretting test conditions: TiCN/alumina, RH=50%, $\delta = 100\mu\text{m}$, $f=5\text{Hz}$, $P=100\text{N}$.

Another way to undoubted determination of the critical number of fretting cycles is observation of fretting loop evolution (Figure 86). It can be realised during the test duration or afterwards working with acquired experimental data. The evolution of a loop shape is due to increase of a friction force during the sliding motion. The maximum value of this force is observed in the centre of a contact as it was a place where the substrate material was reached and coefficient of friction locally increased. For the examined case the coating was worn through after 14000 of fretting cycles.

To sum up there are three ways to determine the substrate reaching condition:

- COF discontinuity analysis,
- interrupted tests;
- fretting loop analysis.

Second method is the most time-consuming as large number of tests has to be completed and some post-treatment is required. The other ones are much faster, however not always possible to apply. To be convinced to the experimental results all the three methods should be employed simultaneously whenever it is possible.

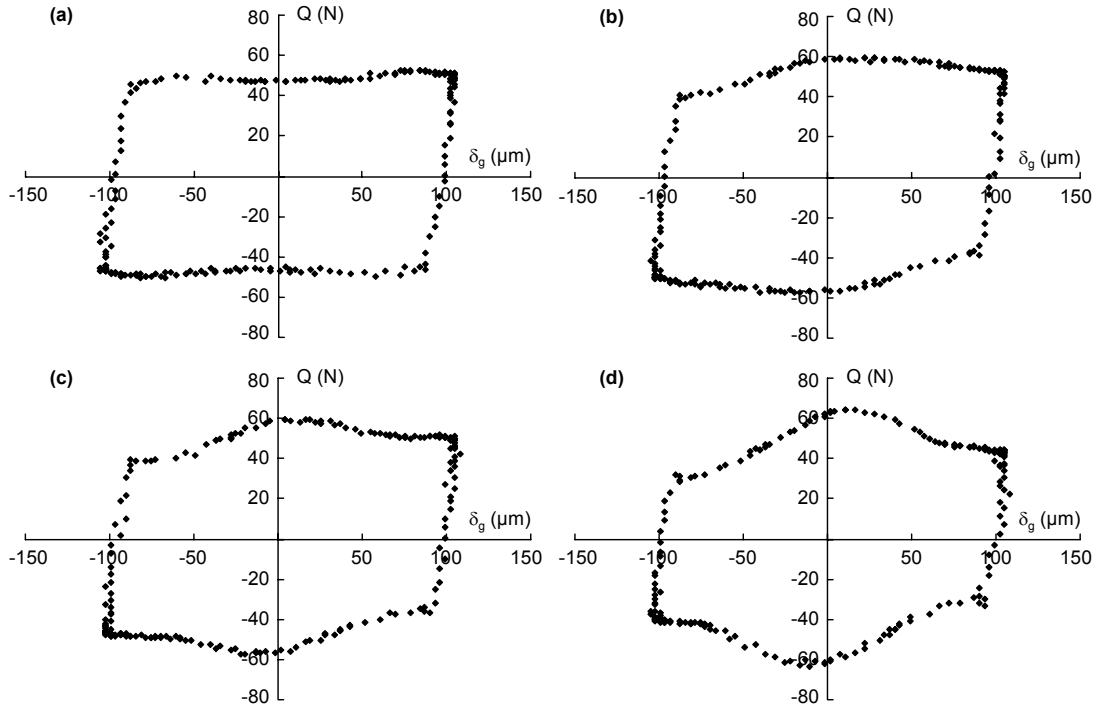


Figure 86. Shape changes of the fretting loop with the number of fretting cycles: (a) 5k; (b) 11,8k; (c) 13k; (d) 15k. Fretting test conditions: TiN/alumina, RH=50%, $\delta = 100 \mu\text{m}$, $f=5\text{Hz}$, $P=100\text{N}$. Note: the coating has been worn through after 14000 fretting cycles.

4.3.6. Introduction of the effective coating thickness concept

The experimental lifetime reduction has been confirmed for all the studied loading conditions. Figure 87 (next page) shows that the coatings endurance evolution (dotted curve) is similar to the one of the theoretical curve (bold curve) but for smaller number of fretting cycles.

This indicates that the coating lifetime is not only related to the progressive wear mechanisms but is also a function of more severe mechanisms which ultimately reduce the coating lifetime. As previously mentioned, when the substrate is almost reached, spalling phenomena associated to coating decohesion are frequently observed. On the ground of these observations the following scenario can be displayed. As wear progresses and the coating becomes thinner, the cyclic stresses imposed through the substrate/coating interface are increased [Gupta P.K. et al. (1974)]. Above a threshold stress value (i.e. below a critical residual coating thickness), a severe decohesion is activated inducing a general failure. According to this hypothesis, damage evolves as progressive wear controlled by the friction energy, followed by a quasi instantaneous decohesion controlled by a critical overstressing of the substrate interface (Figure 88).

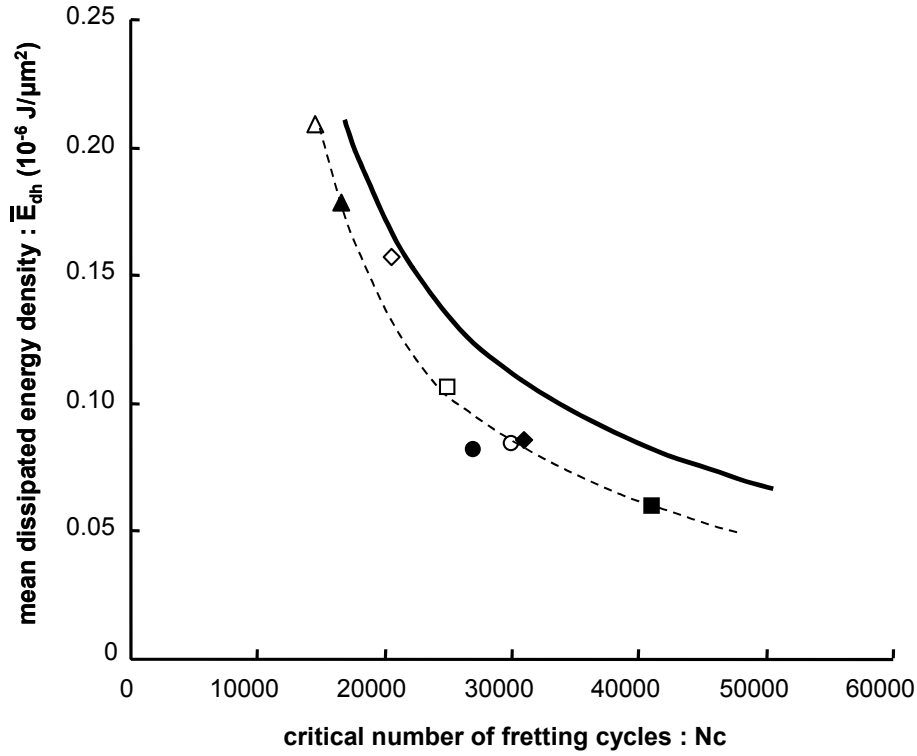


Figure 87. Comparison between experimentally and theoretically predicted coating endurance for different sliding amplitudes: Δ 200 μm , \blacktriangle (150/200) μm_{x1} , \diamond 150 μm , \blacksquare 50 μm , \square 100 μm , \blacklozenge (50/100) μm_{x1} , \circ (50/100) μm_{x2} , \bullet (50/100) μm_{x4} . — Theoretical curve defined from the energy wear depth analysis (Eq. (34), $E_{dhc} = 3.4 \cdot 10^{-3} \text{ J}/\mu\text{m}^2$). Fretting test conditions: TiC/alumina, RH=50%, $f=5\text{Hz}$, $P=100\text{N}$.

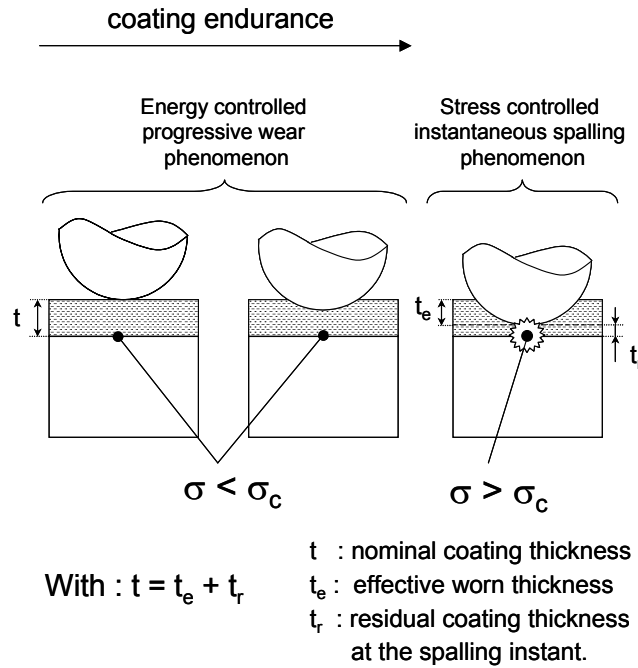


Figure 88. Illustration of the coating damage scenario involving first a progressive wear mechanism followed by an instantaneous decohesion of the coating (σ_c – critical stress).

This tendency is quantified by plotting the ratio between the experimental endurance and the theoretical one defined from the wear depth progression (Nc_{exp}/Nc_{th}), as a function of the coating endurance Nc_{exp} (Figure 89). A scattered distribution is observed, characterizing the spalling instability. However a constant tendency can be defined and a mean value around 0.8 can be approximated.

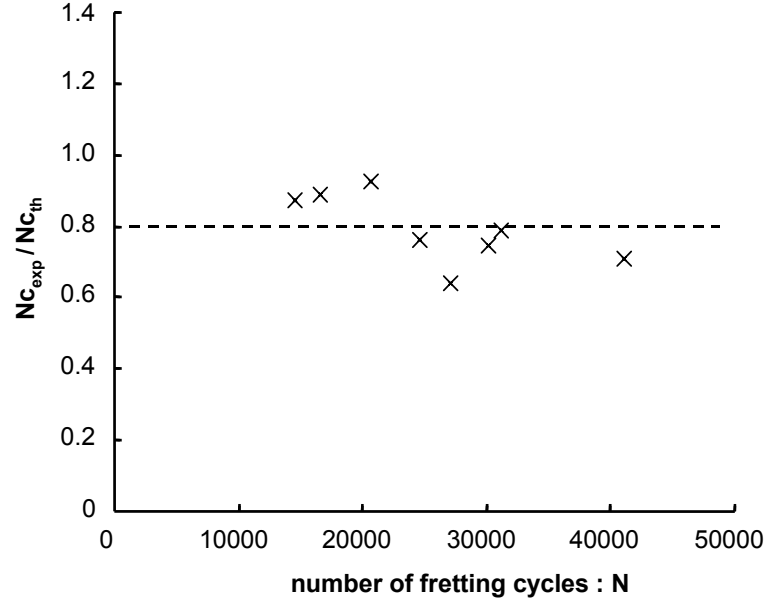


Figure 89. Evolution of the ratio between the experimental coating lifetime and the theoretically predicted endurance deduced from the wear depth modelling.

This confirms that the decohesion phenomena seems to be activated for a constant residual coating thickness:

$$t_r = t \left(1 - \frac{Nc_{exp}}{Nc_{th}} \right) \approx 0.3 \mu m \quad (38)$$

Hence considering that similar friction and normal loadings have been applied, we can deduce that this critical residual thickness is in fact related to a constant threshold interface stress (Figure 88). The results suggest that two damage mechanisms need to be considered to properly predict the coating endurance.

Considering that the coating decohesion is closely related to a threshold stresses associated with a critical residual coating thickness, the coating endurance can be estimated by introducing an effective critical dissipated energy density E_{dhe} so that:

$$E_{dhe} = \frac{t_e}{\beta} \quad \text{with} \quad t_e = t - t_r \quad (39)$$

where t_e is the effective coating thickness removed by the progressive wear process before decohesion (Figure 88).

Again a similar Wöhler description is derived and the coating lifetime is finally given by the following simple expression:

$$N_C = \frac{E_{dhe}}{E_{dh}} \quad (40)$$

Considering the calculated effective thickness, a numerical application gives $E_{dhe} = 2.7 \cdot 10^{-3} \text{ J}/\mu\text{m}^2$. The corresponding energy density–coating endurance chart (i.e. \bar{E}_{dh} -N curve) confirms the stability of the approach (Figure 90), outlining the fact that the contribution of each damage process to the coating lifetime reduction could be formalized through an equivalent consumed coating thickness approach, as previously illustrated in Figure 88.

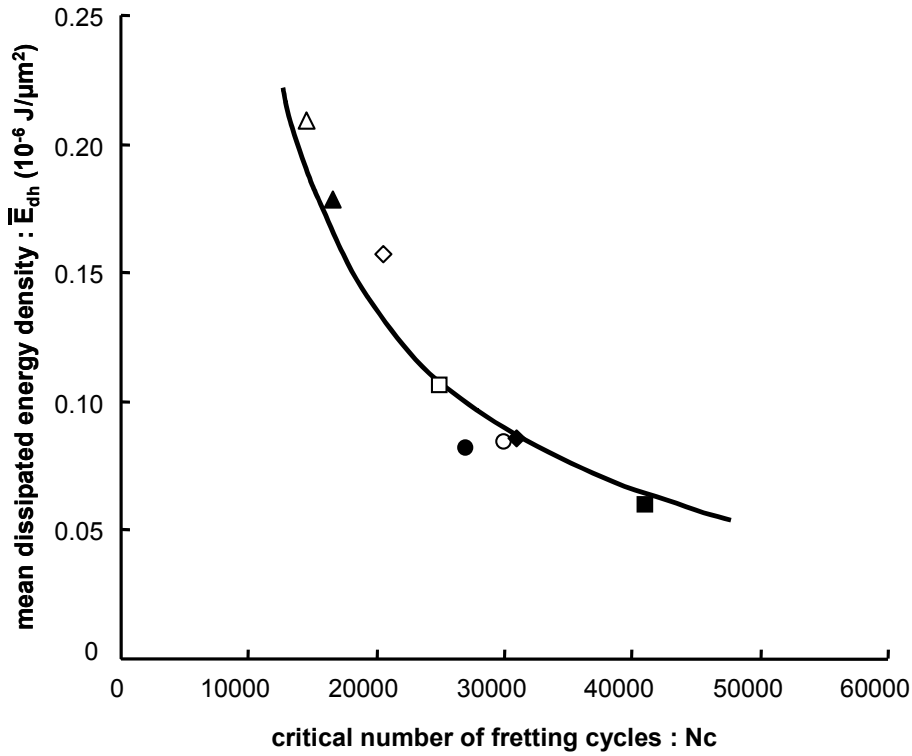


Figure 90. Prediction of the coating endurance, taking into account the lifetime reduction due to spalling for different displacement amplitudes: Δ 200 μm , \blacktriangle (150/200) μm_{x1} , \diamond 150 μm , \blacksquare 50 μm , \square 100 μm , \blacklozenge (50/100) μm_{x1} , \circ (50/100) μm_{x2} , \bullet (50/100) μm_{x4} . — Practical curve defined from effective coating thickness approach (Eq. (40), $E_{dhe} = 2.7 \cdot 10^{-3} \text{ J}/\mu\text{m}^2$). Fretting test conditions: TiC/alumina, RH=50%, $f=5\text{Hz}$, $P=100\text{N}$.

4.3.7. Cumulative damage approach

It is important to point out that the stability of this wear model is linked to the additive property of the energy variable and to the associated linear correlation with the

wear damage evolution. To illustrate such a cumulative damage principle a parallel can be drawn with the science of fatigue of materials. Hence considering the additive principle of the energy density, a linear damage accumulation, equivalent to the Miner's fatigue expression [Miner M.A. (1945)] could be derived. The substrate is reached when the following relationship is verified:

$$\sum \frac{N_i}{N_{Ci}} = 1 \quad (41)$$

where:

N_i – number of cycles under the i^{th} energy density level;

N_{Ci} – number of cycles to reach the substrate under the i^{th} energy density level.

The linearity and the damage accumulation are enclosed in the energy density average and the cumulated energy parameter. To illustrate this principle an incremental analysis is depicted in Figure 91.

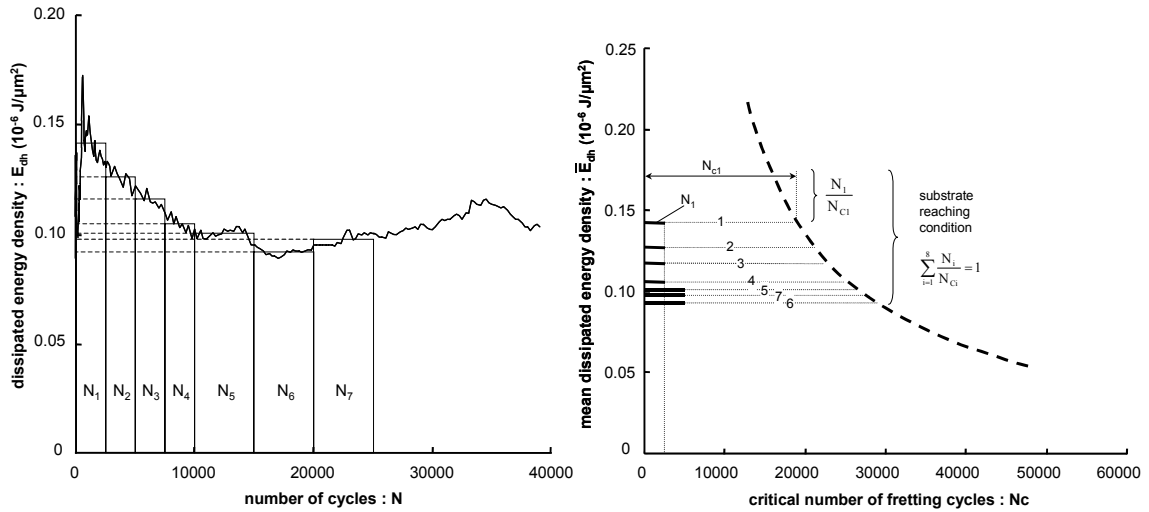


Figure 91. Illustration of linear cumulative wear damage approach associated to the energy density concept (Miner's Fatigue analogy): (a) block segmentation of the energy density evolution (7 intervals); (b) prediction of the coating endurance based on the energy density description (Eq. (40), $E_{dhe} = 2.7 \cdot 10^{-3} \text{ J}/\mu\text{m}^2$). Fretting test conditions: TiC/alumina, $\delta = 100 \mu\text{m}$, $RH = 50\%$, $f = 5 \text{ Hz}$, $P = 100 \text{ N}$.

Splitting the 25000 cycles of the coating endurance into 7 appropriate intervals, it is deduced:

$$\sum_{i=1}^7 \frac{N_i}{N_{iC}} = \frac{2500}{17000} + \frac{2500}{19000} + \frac{2500}{21000} + \frac{2500}{24000} + \frac{5000}{26000} + \frac{5000}{28500} + \frac{5000}{26500} = 1.058 \quad (42)$$

The received value is coherent with the result obtained from globally averaging the energy density (Figure 84) and confirms that such an approach is useful to quantify coating endurance under variable loading conditions.

4.3.8. Durability assessment of hard coatings under investigation

4.3.8.1. Comparison of TiC, TiCN and TiN coatings

In the preceding section the hard coatings durability approach based on dissipated energy density was developed for the TiC coating. The research procedure of this approach is as follows:

1. Fretting test programme carried out within a coating thickness;
2. Determination of two important factors characteristic for each coating:
 - surface of contact area evolution,
 - energy density wear coefficient,
 (on the grounds of the results of the experiments);
3. Calculation of theoretical critical energy density from equation (34);
4. Carrying out of the fretting test programme in order to specify the substrate reaching condition;
5. Estimation of the effective thickness of studied coatings and associated effective energy density;
6. Prediction of the coating endurance by means of an energy Wöhler-like chart.

The same procedure has been employed for TiN and TiCN coatings and the results are presented below.

The experimental test programme carried out in order to characterise the coatings properties has delivered an interesting relation: three values of normal load applied in a test programme for the TiCN coating result in three surface of contact area evolutions characteristic for each loading condition (Figure 92b). Furthermore, if we consider the coefficients A and B (Table 14) it can be noticed that with increase of normal load only coefficient B (related to curve position on y -axis) increases, while coefficient A (related to the curve slope) remains constant.

Hence, it is evident that the slope of contact area evolution refers to the particular coating wear kinetics and remains constant independently of loading conditions, while y -position of this curve is a function of applied normal load.

According to the obtained evolution of the contact area, the energy density wear coefficient and the theoretical value of the critical dissipated energy density have been identified for TiN and TiCN coatings (Table 14).

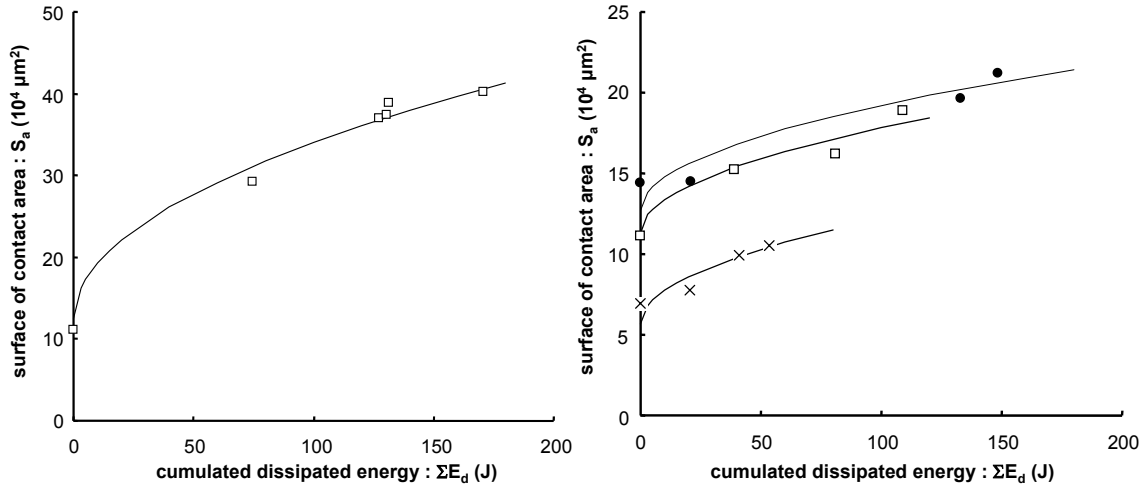


Figure 92. Evolution of the surface of contact area as a function of the cumulated dissipated energy; (a) TiN/alumina, $RH=50\%$, $f=5Hz$, $\delta=50-100\mu m$; (b) TiCN/alumina, $RH=50\%$, $f=5Hz$, $\delta=50-200\mu m$; normal load: x 50N, □ 100N, ● 150N.

Table 14. Surface of contact area evolution coefficients, energy density wear coefficient and critical value of dissipated energy density for TiN and TiCN coatings.

Coating		Coefficients related to surface of contact area evolution*		Energy density wear coefficient** $\beta (\mu m^3/J)$	E_{dhc} theoretical*** ($10^{-3} J/\mu m^2$)
		A ($\mu m^2/J$)	B (μm^2)		
TiN		21500	125000	5034.4	0.79
TiCN	P=50N	6500	57000	2267.4	1.10
	P=100N		113000		
	P=150N		127000		

* from Eq. (29); ** from Eq. (33); *** from Eq. (34).

In order to define the substrate reaching condition for each coating, the successive fretting test programmes have been carried out. To indicate clearly the moment when the coating is worn through, all the results of interrupted tests are presented in Figure 93 for TiN coating and in Figure 94 for TiCN coating. An averaged curve, which separates the tests in which the coating has been worn through from those in which the coatings were still not damaged has been drawn as well.

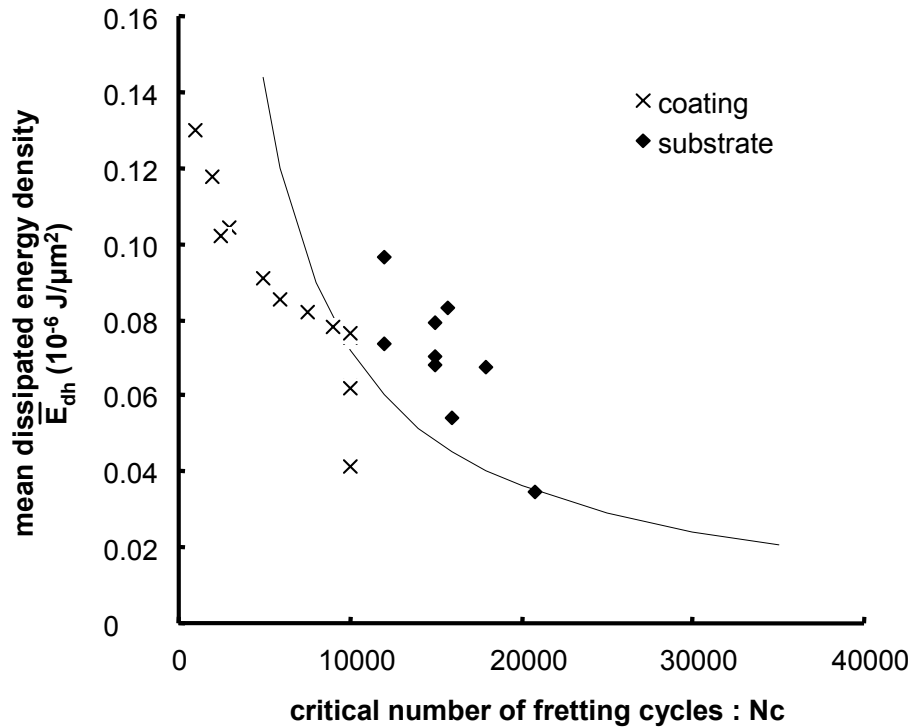


Figure 93. Determination of substrate reaching for TiN coating by means of interrupted tests. Solid line corresponds to the mean practical coating endurance. Fretting test conditions: $P=100\text{N}$, $\delta=50\text{-}100\mu\text{m}$, $RH=50\%$, $f=5\text{Hz}$.

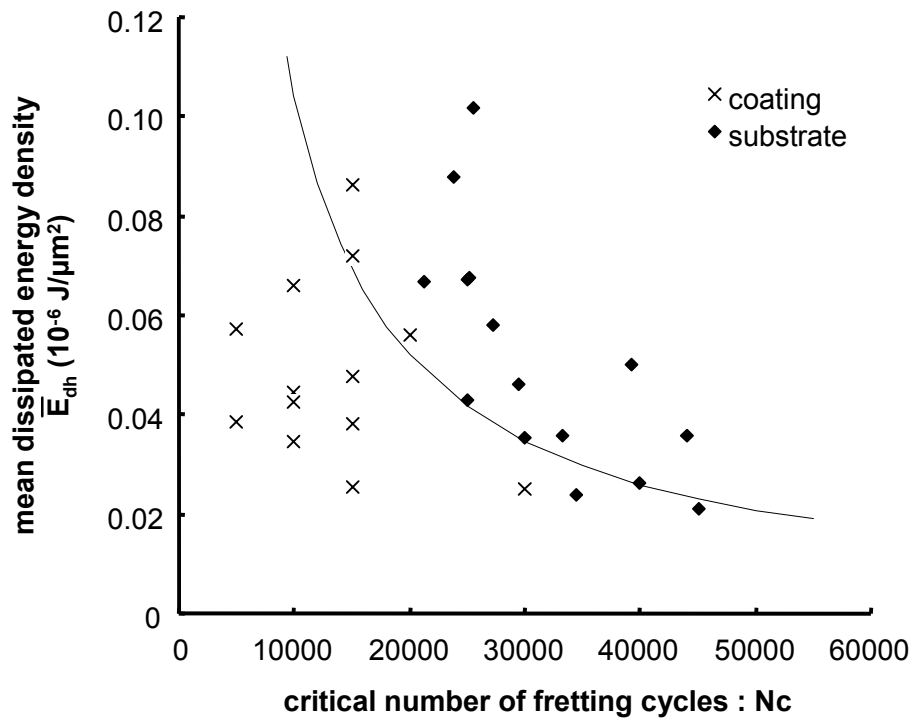


Figure 94. Determination of substrate reaching for TiCN coating by means of interrupted tests. Solid line corresponds to the mean practical coating endurance. Fretting test conditions: $P=50\text{-}150\text{N}$, $\delta=50\text{-}200\mu\text{m}$, $RH=50\%$, $f=5\text{Hz}$.

Making use of the mean practical coating endurance represented in Figures 93 and 94 and the theoretical one defined by the critical value of dissipated energy density (Table 14), the ratio between experimental and theoretical endurance can be determined (Table 15). Estimation of the effective critical dissipated energy density of the coatings is realised by several simple computations based on equations (38) and (39), as it has been previously done for TiC coating. Results of these calculations are given in Table 15.

Table 15. Ratio between experimental and theoretical endurance, residual coating thickness and effective critical dissipated energy density for TiN and TiCN coatings.

Coating	Ratio between experimental and theoretical endurance* $N_{c_{exp}}/N_{c_{th}}$	Residual coating thickness** t_r (μm)	Effective critical dissipated energy density*** E_{dhe} ($10^{-3} \text{ J}/\mu\text{m}^2$)
TiN	0.90	0.40	0.71
TiCN	0.95	0.12	1.04

*from Eq. (38); ** according to Fig.88; ***from Eq. (39).

When the effective critical dissipated energy density is defined, the endurance of the studied coatings can be compared with use of an energy Wöhler-like chart (Figure 95). For a given coating thickness TiC coating appears to have the highest fretting wear resistance.

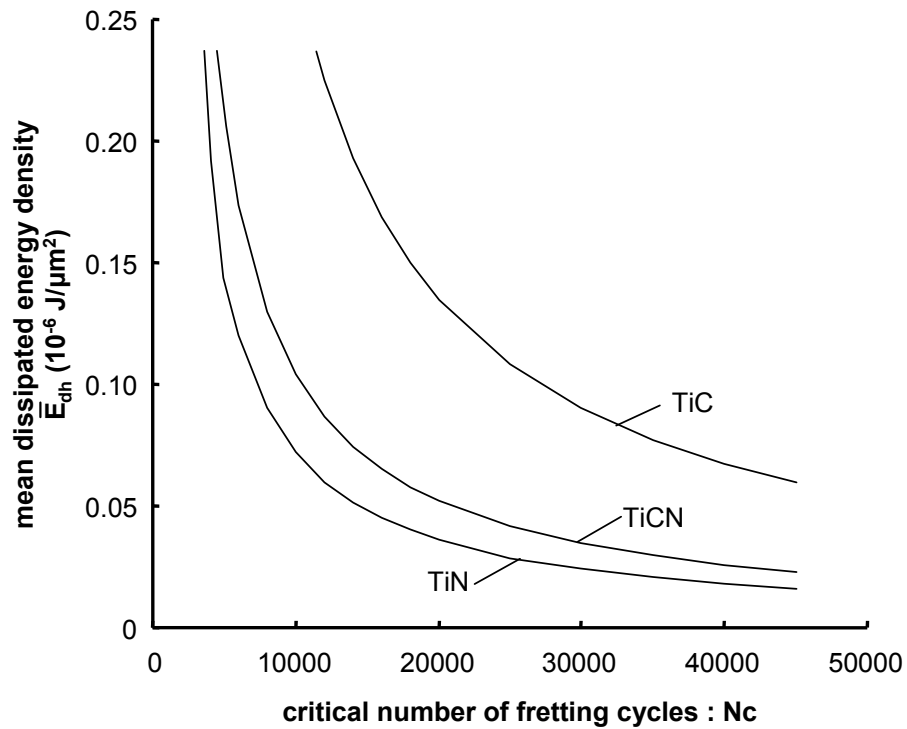


Figure 95. Durability of hard coatings as a function of the critical number of fretting cycles for three different coatings with different thickness: TiC – $1.6 \mu\text{m}$, TiCN – $2.5 \mu\text{m}$, TiN – $4 \mu\text{m}$.

The Figure above can be used for the practical prediction of studied coatings lifetime. However, to assess clearly the tribological properties of the system under investigation, durability prediction can not be related to a particular coating thickness. Hence, in order to compare the resistance to wear of the investigated surface treatments independently of the material volume, a unitary mean dissipated energy density is introduced as a ratio of the mean dissipated energy density to the coating thickness: $\sum \bar{E}_{dh} / t$ (Figure 96). One can see that in this case there is a greater difference between the thicker coating (TiN) and the thinner one (TiC).

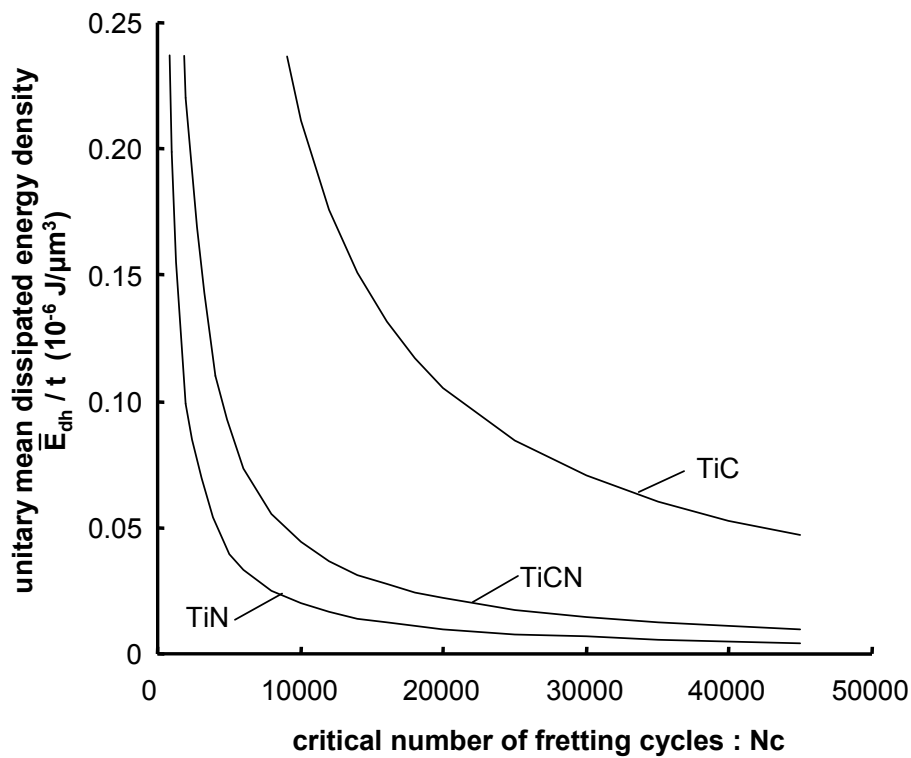


Figure 96. Durability of hard coatings as a function of unitary mean dissipated energy density versus critical number of fretting cycles independently on the coating thickness.

The foregoing assessment of hard coatings gives a distinct visualisation of surface treatments durability under fretting wear regime on the ground of the energy density – coating endurance chart. According to equation (31) it is evident that increasing the pressure in the contact or the displacement amplitude, more energy is dissipated within a contact area and the coating failure can take place after a smaller number of fretting cycles. This aspect is clearly displayed in Wöhler-like endurance chart and the critical number of fretting cycles can be easily predicted. A confrontation of different surface treatments can also be realised quickly and easily.

Referring to calculations of the effective coating thickness, the fraction of residual thickness (t_r) for each coating under investigation has been estimated: TiC-20%, TiN-10% and TiCN-5%. The damage mechanisms at the substrate/coating interface are complex and not fully understood. The differences between the residual coating thicknesses can be related to a number of mechanical and physico-chemical factors, nevertheless the most important ones seems to be: nominal coating thickness, coating morphology, normal load and adhesion forces. To explain the damage mechanism the coating/substrate interface needs further studies including the effect of stress distribution at the interface.

4.3.8.2. Confrontation of all the hard coatings under investigation

Hard coatings durability approach has been introduced for a TiC coating and successively verified for the others systems with TiN and TiCN coatings. The stability of the proposed methodology has been proved for a wide range of displacement amplitudes (50-200 μ m), normal loads (50-150N) and under variable loading conditions. Thus, a simplified version of the developed approach can be applied to compare durability of all the hard coatings investigated in this work, where simplification is related to the determination of the effective worn thickness.

To complete this confrontation a number of fretting tests has been carried out to characterise different tribo-systems by means of the energy density wear coefficient β (Table 16 and Figure 97).

Table 16. Energy density wear coefficients (β) and correlation parameters (R^2) calculated from Figure 96 for all the hard coatings under investigation.

Coating	Energy density wear coefficient β ($\mu\text{m}^3/\text{J}$)	Correlation parameter R^2
VC	52.387	0.66
TiC/VC	124.69	0.94
(TiC/VC) _{x2}	173.41	0.86
TiC	474.01	0.91
TiCN	2267.4	0.80
TiN	5034.4	0.90

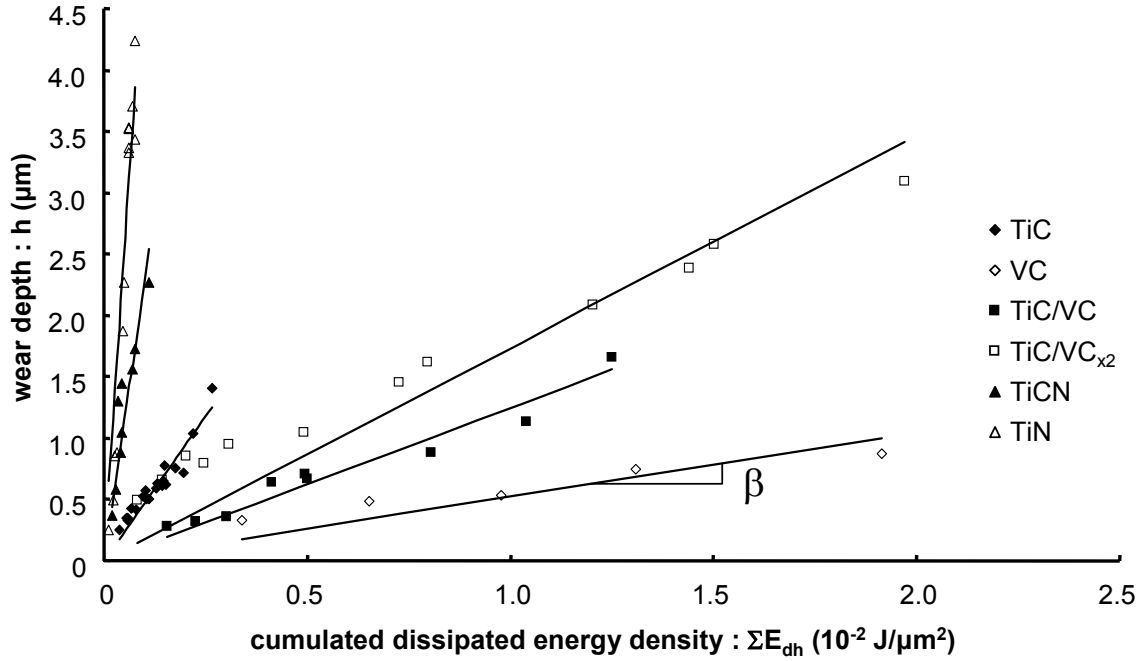


Figure 97. Plots of the wear depth versus the cumulated dissipated energy density: comparison of all the investigated hard coatings by means of the energy density wear coefficient β .

To estimate the exact value of an effective critical dissipated energy density numerous and long-lasting fretting tests need to be carried out in which the relative coating has to be worn through several times (one should compute a mean critical value). It is a highly expensive and time-consuming procedure especially when hard coatings with a good wear resistance are being examined. Hence, the value of the critical dissipated energy density (obtained with β coefficient) should be reduced by some safety factor related to an effective coating thickness. This can be realised by introduction of a safety coefficient (s): $E_{dhc} \cdot s$, where $s < 1$. In case of pure tribological applications the value of the coefficient can be fixed at 0.8, as it has been proved for the TiC and the ratio Nc_{exp}/Nc_{th} [see Eq. (38)]. However, when some chemical properties of a coating are used, as e.g. diffusion barrier, the s value should be decreased. This distinction results from a failure mechanism: if only mechanical coating properties are concerned some spalling can appear but the loads are still transmitted by a coating, while in case of diffusion barriers first cracks are conducive to catastrophic failure.

Comparison of durability of all the hard coatings investigated in the work has been carried out at uniform test conditions ($P=100\text{N}$, $\delta=100\mu\text{m}$, $f=5\text{Hz}$) and under a safety coefficient $s = 0.8$. The results are displayed for two different cases: for a particular coating thickness (in Figure 98) and independently of the coating thickness (in Figure 99).

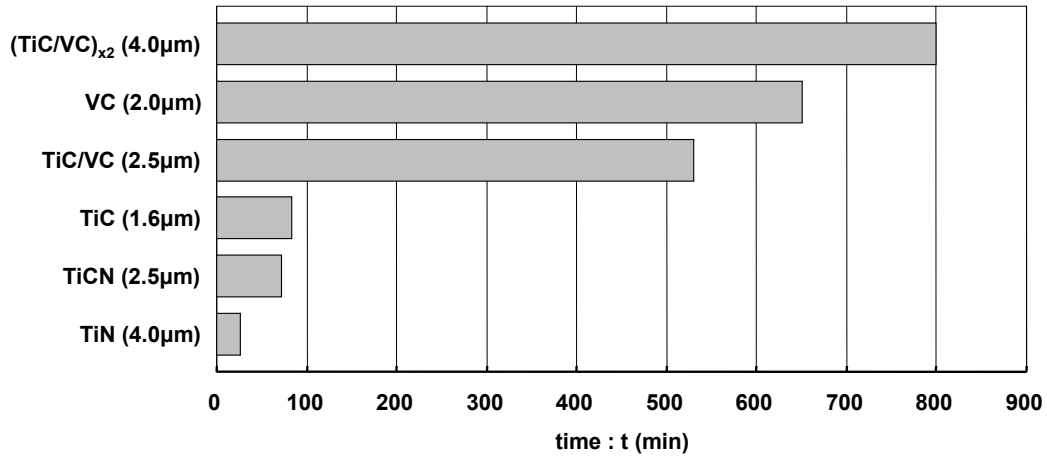


Figure 98. Durability under fretting regime of hard coatings under investigation for a particular coating thickness. Fretting test conditions: $P=100N$, $\delta=100\mu m$, $f=5Hz$.

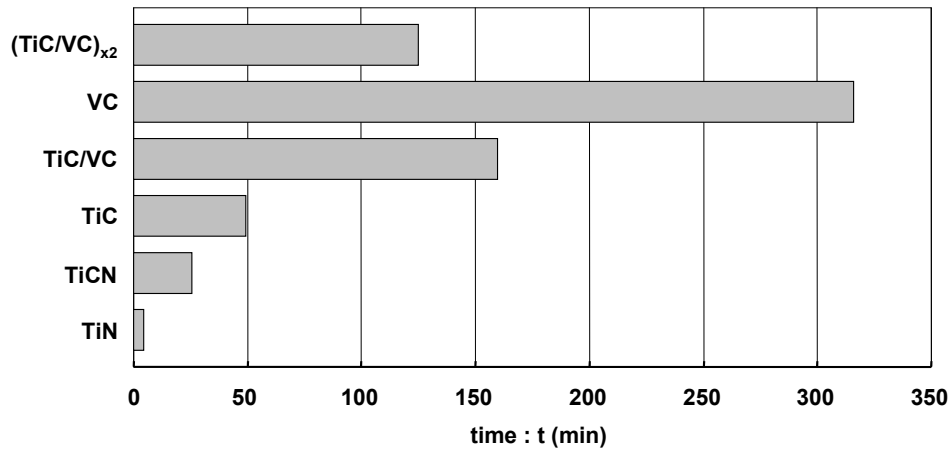


Figure 99. Durability under fretting regime of hard coatings under investigation for a unitary coating thickness. Fretting test conditions: $P=100N$, $\delta=100\mu m$, $f=5Hz$.

4.4. SYNTHESIS OF THE CHAPTER

Three methods of evaluation of hard coatings tribological properties have been set forth in this Chapter. Two of them: Archard's wear law and global dissipated energy approach permit determination of the wear volume evolution. However, as it was previously highlighted, the loss of coating volume is not an adequate parameter to predict the surface treatment endurance. In order to estimate properly the component lifetime, it is essential to recognise the resistance of the coatings to wear depth evolution.

That was the reason for introducing hard coatings durability approach, in which the critical value of the dissipated energy density is defined for any studied coating. It has been shown that the increase of the wear depth under reciprocating, and adequately fretting sliding conditions can be expressed as a function of the friction energy capacity

approach. It has been outlined that the increase of the surface of contact area has to be defined in an analytical form in order to describe properly the wear depth extension. However, a significant difference between the experimental coating lifetime and the endurance deduced from this formal description of the wear depth has been observed. This demonstrates that the coatings endurance is related to a friction energy controlled progressive wear phenomenon which can be interrupted by a stress controlled instantaneous decohesion of the coating/substrate interface.

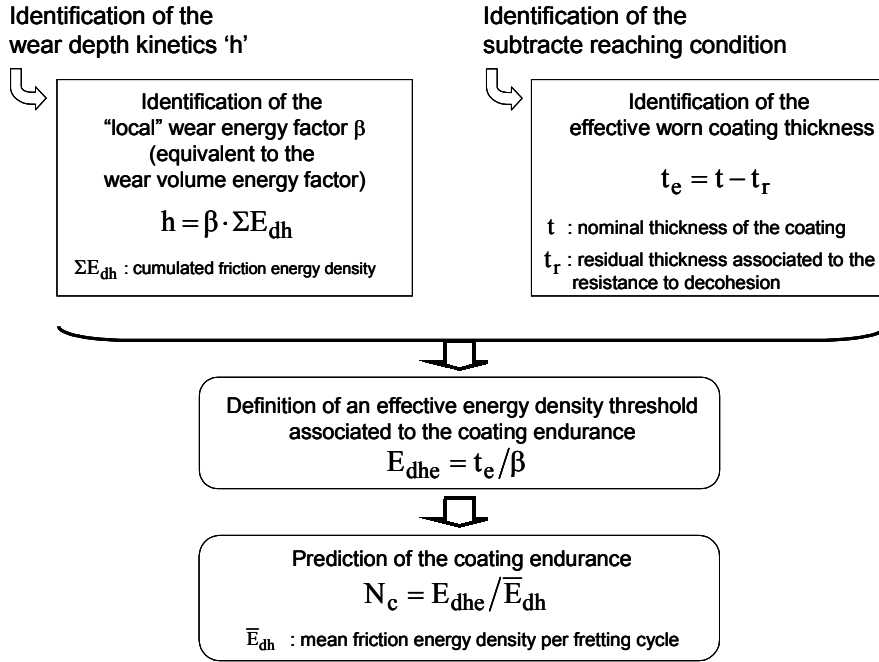


Figure 100. Flow chart of the friction energy capacity approach to predict coating endurance. The model integrates both the intrinsic wear resistance of the coating (i.e. wear depth kinetics) and the strength of the substrate/coating interface (i.e. identification of the residual coating thickness).

As illustrated in Figure 100, two damage processes must be quantified to obtain a reliable prediction of the coating lifetime. When an “effective worn coating thickness” concept is introduced, an effective energy density threshold is derived which allows a stable and reliable prediction of the coating endurance. This endurance is then simply related to a friction energy capacity (i.e. effective energy density threshold) whereas the coating lifetime is related to a ratio between this energy and the mean energy density dissipated per fretting cycle. Making use of the additive property of the energy variable, a wear damage law is defined, in the frame of which the coating endurance can be rationalized from constant to variable sliding conditions by means of an energy density–coating endurance chart (i.e. \bar{E}_{dh} -N curve).

It is important to note that if one takes into account different damage processes, it should be possible to explain and perhaps quantify the classical gap existing between industrial loading conditions and laboratory wear tests [Imbeni V. et al. (2001)]. Indeed the coating endurance is not only related to its intrinsic wear resistance properties: it is a function of the strength of the coating/substrate interface as well. These two aspects have been taken into account, respectively, by an energy wear coefficient and the effective worn coating thickness. The weaker is the interface, the smaller the effective worn thickness and the shorter the coating lifetime.

Finally, this global damage description makes it possible to formalize a classical result concerning the difference between the observed wear increase of a coated system (i.e. here the wear depth) and the expected coating response. By introducing an effective energy density threshold, this aspect is resolved or at least explained.

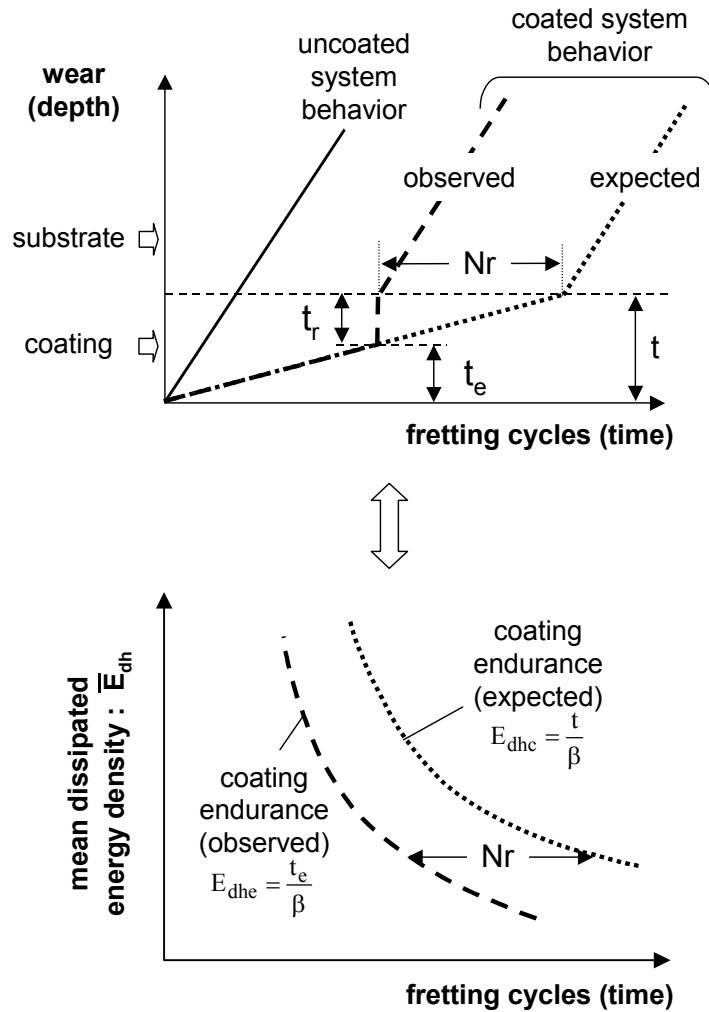


Figure 101. Illustration of the wear generalized coating endurance approach (N_r – number of cycles related to difference between expected and observed coating endurance).

Considering this wear generalized coating endurance approach (Figure 101) there is a gap between the expected coating wear kinetics and the observed response. Indeed, only a part of the nominal thickness is being worn due to the fretting wear process. Below a critical residual thickness, a severe decohesion mechanism is being activated. This phenomenon is formalized and quantified for any sliding conditions by means of an energy density coating endurance chart (i.e. \bar{E}_{dh} -N curve). The coating endurance is associated to a specific energy density and the corresponding lifetime deduced from an energy ratio: $Nc = E_{dhe} / \bar{E}_{dh}$. It has been shown that, considering an effective worn coating thickness t_e , and deducing an effective threshold energy density E_{dhe} , the coating endurance is well predicted and both the energy-controlled progressive wear and the stress-controlled instantaneous spalling phenomenon are formalized. Finally the safety coefficient s is introduced to determine the coating durability on the adequate level to a particular engineering application.

GENERAL CONCLUSIONS

The following conclusions can be drawn from the presented research work:

- It has been proved that it is possible to predict the wear depth increase under fretting sliding conditions through the *hard coatings durability approach* introduced in the work.
- This approach allows to compare the surface treatments under investigation in relation to the substrate reaching condition, which strictly corresponds to the coating endurance.
- The critical value of the dissipated energy density has been proposed as a factor indicating the specific quantity of energy that has to be delivered to the coating in order to worn through its total thickness.
- Energy-Wöhler wear chart has been introduced, in which the dissipated energy density description corresponds to the moment when the substrate is reached after an exact number of fretting cycles.
- It has been outlined that the increase of the wear surface contact area must and can be formalized to describe properly the wear depth extension.
- Coating endurance is not only related to its wear resistance properties but is also controlled by the stress field distribution at the substrate/coating interface. An effective coating thickness concept has been developed to derive an energy density threshold, which allows a stable and reliable prediction of the coating endurance.
- The following order of the fretting wear resistance of hard coatings under investigation (starting from the one with the highest resistance) has been found in the work: VC, TiC/VC, (TiC/VC)_{x2}, TiC, TiCN, TiN. One can see that this order of the fretting wear resistance does not correlate with the hardness order, which is as follows: VC, (TiC/VC)_{x2}, TiN, TiCN, TiC/VC, TiC.

GENERAL CONCLUSIONS

- It has been verified that the global energy approach as well as the local one are able to predict the wear volume removal and the wear depth extension even under variable displacement amplitudes.
- There is strong impact of the relative humidity of the experimental environment on the friction and wear of the coatings under investigation. This complex problem has to be treated separately for each tribo-system, as for different hard coatings the physical and chemical reactions provoked due to environmental conditions are unique.
- It has been demonstrated that Ti interlayer deposited between the substrate and the TiN coating does not influence significantly the fretting wear properties of the TiN coating.
- The introduced mixed carbide layer approach in the multilayer TiC/VC coatings allows to explain a very peculiar resistance to wear observed in the experiments.

Finally the application boundaries and perspectives of the introduced hard coatings durability criterion should be assigned. The proposed methodology has been developed for a particular set of materials and experimental conditions that limit the application area of the criterion, these are:

- alumina ball counter-body,
- steel substrate with a high hardness,
- constant value of 50% relative humidity,
- constant value of 5Hz frequency oscillatory motion.

It is expected that change of any of these parameters will lead to different tribological behaviour of a coated system and the criterion will not indicate the surface treatments lifetime properly. Hence, the further studies should consider impact of the above factors.

There are also some more open questions and interesting aspects worth additional work. The possible studies can develop the following areas:

- stress field distribution at the interface (by means of numerical simulations in order to control the spalling phenomena and predict the effective thickness of a coated component);

GENERAL CONCLUSIONS

- determination of the substrate reaching condition (deeper work is required for a clear indication of the coating perforation to determine unequivocally related effective dissipated energy density);
- mechanism of 3rd body transfer (this transfer of the debris onto the counter-body surface has been found as a main reason for an accelerated coating damage due to contact pressure field modification. Further analysis of debris/counter-body adhesion are necessary including impact of different elements from the coating, e.g. nitrogen);
- titanium interlayer (effect of the Ti-buffer layer on the stress field distribution at the interface);
- safety wear coefficient (the effort can be undertaken to estimate the coefficient range for different groups of tribo-systems related e.g. to coating type, deposition technique or applied substrate material);
- other contact geometries (verification of the developed methodology with other geometries by means of finite elements calculations).

Summarizing, the hard coatings durability criterion concept allows not only to compare the tribological properties of the surface treatments but also to indicate and formalize the lifetime under wide range of loading conditions. The concept allows also to physical analysis of the damage and this way to develop the thermodynamic approach of wear. The energy density is a intrinsic value and identified for a given contact conditions can be easily transferred on more complex industrial components.

GENERAL CONCLUSIONS

NOTATIONS

Materials properties

E	Young's modulus
ν	Poisson's ratio
H	hardness
σ_{pl}	yield point
Ra	surface roughness

Contact mechanics

P	normal load
Q	tangential force
Q_s	static tangential force
Q_k	kinetic tangential force
P_r	rotation load
μ	coefficient of friction
μ_s	static coefficient of friction
μ_k	kinetic coefficient of friction
p_0	maximal Hertzian pressure
p_m	mean pressure
σ	stress
σ_c	critical stress
τ_{max}	maximal tangential stresses
a	Hertzian contact radius
r	contact radius
c	stick zone radius
l	length of contact
A_r	real contact area
δ	relative displacement amplitude
δ_g	sliding displacement amplitude
δ_0	sliding aperture
f	frequency
e	sliding ratio ($e = d_g / a$)
A, B, C	transition criteria of fretting sliding
N	number of cycles
t	time

NOTATIONS

Wear models

W_v	wear volume
h	wear depth
K	wear coefficient
Δm	weight loss
V	sliding speed
S	sliding distance
W_r	wear resistance
W	loading factor ($W = P \cdot S$)
T_v	is a volume of the transferred material
m_t	ratio of transferred material ($m_t = T_v / W_v$)
p_f	flow pressure
E_r	erosion resistance
ε	erosion rate
f	fraction of volume loss due to spalling
ρ_t	target density
ρ_p	particle density
V_p	particle velocity
d	particle diameter
K_c	fracture toughness
R	counter-body ball radius
α	energy wear coefficient ($\alpha = W_v / \Sigma E_d$)
w	flow of debris
h_d	thickness of the debris screen
u	gradient of debris ejecting velocity

Hard coatings deposition

T	temperature
ΔG^0_T	free enthalpy
t	coating's thickness
M_r	atomic weight of sprayed metal
t_d	deposition time
R_v	radius-vector

Hard coatings durability criterion

E_d	dissipated energy
ΣE_d	cumulated dissipated energy
E_{dh}	dissipated energy density

NOTATIONS

ΣE_{dh}	cumulated dissipated energy density
\bar{E}_{dh}	mean dissipated energy density
E_{dhc}	critical dissipated energy density
E_{dhe}	effective critical dissipated energy density
μ_e	energy coefficient of friction
β	energy density wear coefficient ($\beta = h / \Sigma E_{dh}$)
S_a	surface of contact area
A, B	coefficients related to evolution of the surface of contact area
N_c	critical number of cycles
N_f	number of cycles to material failure
N_r	number of cycles related to difference between expected and observed coating endurance
t_e	effective worn thickness
t_r	residual coating thickness
s	safety coefficient

Abbreviations

COF	coefficient of friction
HSS	high speed steel
RH	relative humidity
EDS	energy-dispersive spectrometry
SEM	scanning electron microscopy
GDOS	glow discharge optical spectroscopy
ML	mixed layer
PSR	partial slip regime
GSR	gross slip regime
MFR	mixed fretting regime
RCFM	running condition fretting map
MRFM	material response fretting map
TTS	tribologically transformed structure
PVD	physical vapour deposition
CVD	chemical vapour deposition
PACVD	plasma assisted chemical vapour deposition
LPCVD	low pressure chemical vapour deposition
MOCVD	metal-organic chemical vapour deposition
LCVD	laser chemical vapour deposition

NOTATIONS

REFERENCES

To find the adequate publication the last name of the first author and publication year is given in the text. The references are listed in alphabetic order by first author last name.

Arai T., Fujita H., *Plasma-assisted CVD of TiN and TiC on steel*, Proc. of 6th Int. Conf. on Ion and Assisted Techniques, Brighton (1987), p. 196-200.

Archard J.F., *Contact and rubbing of flat surfaces*, Journal of Applied Physics 24 (1953), p. 981-988.

Arkel van A.E., Boer de J.H., Zs. Anorg. Chemie 148 (1925), p. 345.

Barwell J.T., *Wear of Machine Element. Fundamentals of Tribology*, Proc. of Int. Conf. MIT Press., London (1980).

Berger, M., Wiklund, U., Eriksson, M., Engqvist, H., Jacobson, S., *The multilayer effect in abrasion - optimising the combination of hard and tough phases*, Surface and Coatings Technology 116-119 (1999), p. 1138-1144.

Berthier Y., Columbié C., Lofficial G., Vincent L., Godet M., *Corrosion et corrosion de contact*, 7th Congrès Européen de Corrosion, Fédération Européenne de la Corrosion, 19-24 Nov., Nice, France (1985).

Berthier Y., Vincent L., Godet M., *Fretting fatigue and fretting wear*, Tribology International 22 (1989), p. 235-242.

Berthier Y., Vincent L., Godet M., *Velocity accommodation in fretting*, Wear 106 (1988), p. 25-38.

Bhushan B. (Ed.), *Modern Tribology Handbook*, CRC Press (2000).

Blanchard P., Colombie C., Pellerin V., Fayeulle S., Vincent L., *Material effects in fretting wear: Application to iron, titanium and aluminium alloys*, Metallurgical Transactions A 22 (1991), p. 1535-1544.

Blanchard P., *Usure induite en petits débattements: TTS d'alliages de titane*, Thèse Ecole Centrale de Lyon, N° 91-32 (1991).

Blanpain B., Celis J.P., Roos J.R., Ebberink J., Smeets J., *A comparative study of the fretting wear of hard carbon coatings*, Thin Solid Films 223 (1993), p. 65-71.

Blau P.J., *The significance and use of the friction coefficient*, Tribology International 34 (2001), p. 585-591.

REFERENCES

- Bromark M., Larsson M., Hedenqvist P., Hogmark S.,** *Wear of PVD Ti/TiN multilayer coatings*, Surface and Coatings Technology 90 (1997), p. 217-223.
- Bull S.J., Jones A.M.,** *Multilayer coatings for improved performance*, Surface and Coatings Technology 78 (1996), p. 173-184.
- Bunshah R.F.,** *Deposition Technologies for Films and Coatings*, New Jersey, Noyes Publications (1982).
- Burakowski T., Mazurkiewicz A., Miernik K., Smolik J., Walkowicz J.,** *Current state and directions of the development of anti-wear technologies*, Tribologia 5 (2000), p. 877-899.
- Burakowski T., Miernik K., Walkowicz J.,** *Zastosowanie fizykochemicznych technologii wspomaganych plazmą do wytwarzania cienkich powłok odpornych na zużycie*, Metaloznawstwo, Obróbka Ciepła, Inżynieria Powierzchni 130-132 (1995).
- Burakowski T., Wierzchoń T.,** *Inżynieria Powierzchni Metali*, Warszawa, WNT (1995).
20. **Chen G.X., Zhou Z.R.,** *Study on transition between fretting and reciprocating sliding wear*, Wear 250 (2001), p. 665-672.
- Chin J.,** *CVD and PECVD*, in "Advanced Surface Engineering", Sproul W.D., Legg K.O. (Eds.), Lancaster-Basel, Technomic Publ. Comp. (1993).
- Chu X., Barnett S.A.,** *Model of superlattice yield stress and hardness enhancements*, Journal of Applied Physics 77 (1995), p. 4403-4411.
- Collins J.A.,** *Failure of Materials in Mechanical Design*, New York, J.Wiley (1981).
- Crossland B.,** *Effect of large hydrostatic pressures on the torsional fatigue strength of an alloy steel*, Proc. of Intr. Conf. on Fatigue of Metals, London (1956), p. 138-149.
- Czichos H.,** *Tribology*, Elsevier, Amsterdam (1978).
- Dang Van K.,** *Macro-micro approach in high-cycle multiaxial fatigue*, Advances in Multiaxial Fatigue, ASTM STP 1191 (1993), p. 120-130.
- Del Puglia A., Pratesi F., Zonfrillo G.,** *Experimental procedure and involved parameters in fretting-fatigue test*, ESIS 18, Edited by R.B. Waterhouse and T.C. Lindley, Mechanical Engineering Publication, London, (1994), p. 219-238.
- Deriagin B.V.,** *Tchto takoe trenie?*, Moskva, Izd. AN SSRR (1952).
- Dobrzański L.A.,** *Metaloznawstwo*, Warszawa, WNT (1999).
30. **Endo K.,** *Initiation and propagation of fretting-fatigue cracks*, Wear 38 (1976), p. 311-324.

REFERENCES

Evans A.G., Marshall D.B., in Rigney D.A. (Ed.), *Fundamentals of Friction and Wear of Materials*, American Society for Metals, Metals Park, OH (1981), p. 439.

Fleischer W., Schulze D., Wilberg R., Lunk A., Schrade F., *Reactive ion plating (RIP) with auxiliary discharge and the influence of the deposition conditions on the formation and properties of TiN films*, Thin Solid Films 63 (1979), p. 347-356.

Forsyth P.J.E., *A two stage fatigue fracture mechanisms*, Proc. Cranfield Symposium on Fatigue, (1961), p. 76.

Fouvry S., Kapsa Ph., *An energy description of hard coating wear mechanisms*, Surface and Coatings Technology 138 (2001a), p. 141-148.

Fouvry S., Kapsa Ph., Vincent L., *An elastic plastic shakedown analysis of fretting wear*, Wear 247 (2001b), p. 41-54.

Fouvry S., Kapsa Ph., Vincent L., *Analysis of sliding behaviour for fretting loadings: determination of transition criteria*, Wear 185 (1995), p. 35-46.

Fouvry S., Kapsa Ph., Vincent L., *Fretting-Wear and Fretting-Fatigue: Relation through a mapping concept*, Fretting fatigue: current technology and practices, D.Hoeppner, V.Chandrasekaran, C.B.Elliott, Eds. ASTM STP 1367 (2000), p. 49-64.

Fouvry S., Kapsa Ph., Vincent L., *Quantification of fretting damage*, Wear 200 (1996), p. 186-205.

Fouvry S., Kapsa Ph., Zahouani H., Vincent L., *Wear analysis in fretting of Hard coatings through a dissipated energy concept*, Wear 203-204 (1997), p. 393-403.

Fouvry S., Liśkiewicz T., Kapsa Ph., Hannel S., Sauger E., *An energy description of wear mechanisms and its applications to oscillating sliding contacts*, Wear 255 (2003), p. 287-298.

Fouvry S., Wendler B., Liśkiewicz T., Dudek M., Kołodziejczyk Ł., *Wear analysis of TiC-VC multilayers: Experiments and modeling approaches*, Wear 257 (2004), p. 641-653.

Fu Y., Wei J., Batchelor A.W., *Some considerations on the mitigation of fretting damage by the application of surface-modification technologies*, Journal of Materials Processing Technology 99 (2000), p. 231-245.

Godet M., *The third-body approach: a mechanical view of wear*, Wear 100 (1984), p. 437-452.

Godfrey D., Bailey J.M., Lubr. Engr. 10 (1952), p. 155.

Gordelieen S.C., Stallings L., ASTM Spec. Tech. Publ. 780 (1982), p. 30-48.

REFERENCES

- Gordelier S.C., Chivers T.C.**, *A literature review of palliatives for fretting fatigue*, Wear 56 (1979), p. 177-190.
- Goryacheva I.G., Rajeev P.T., Farris T.N.**, *Wear in Partial Slip Contact*, Journal of Tribology 123 (2001), p. 848-856.
- Gupta P.K., Walowit J.A.**, *Contact stresses between an elastic cylinder and a layered elastic solid*, Journal of Lubrication Technology 79(2) (1974), p. 250-257.
- Guzowski S.**, *Effect of contact interaction in clamped joints on fretting wear development*, Tribologia 5 (1998), p. 698-707.
50. **Halliday J.S., Hirst W.**, *The fretting corrosion of mild steel*, Proc. Roy. Soc. A 236 (1956), p. 411-425.
- Halling J.**, *The tribology of surface coatings, particularly ceramics*, Proc. Inst. Mech. Engrs. Vol. 200, No C1 (1986), p. 31-40.
- Harris S.J., Overs M.P., Gould A.J.**, *The use of coatings to control fretting wear at ambient and elevated temperatures*, Wear 106 (1985), p. 35-52.
- Haś Z., Kula P.**, Proc. 2nd Int. Conf. *Carburising and nitriding with atmospheres*, Cleveland, USA, 6-8 Dec. 1995, Grosch J., Morral J., Schneider M (Eds.), ASM Int., Materials Park, Cleveland OH (1995), p. 227-231.
- Hauert R., Patscheider J.**, *From alloying to nanocomposites – improved performance of hard coatings*, Advanced Engineering Materials 5 (2000), p. 247-259.
- Hebda M., Wachal A.**, *Trybologia*, Warszawa, WNT (1980).
- Helmersson U., Todorova S., Barnett S.A., Sundgren J.E., Market L.C., Greene J.E.**, *Growth of single-crystal TiN/VN strained-layer superlattices with extremely high mechanical hardness*, Journal of Applied Physics 62 (1987), p. 481-484.
- Hertz H.R.**, *On the contact of elastic solids*, In Jones Schott (Eds.), *Miscellaneous Papers by H. Hertz*, London, Macmillan (1882).
- Hills D.A., Nowell D., Sackfield A.**, *Mechanics of Elastic Contacts*, Butterworth-Heinemann (1993).
- Hinterman H.E.**, *Verschleiss und Korrosionsschutz durch CVD- und PVD Überzüge*, VDI Berichte No. 333, Düsseldorf (1979), p. 53.
60. **Hitchman M.L., Jensen K.F.**, *Chemical vapour deposition*, London, Acad. Press (1993).
- Hodor K., Zięba P., Olszowska-Sobieraj B.**, *Materiały gradientowe jako nowe możliwości współczesnej techniki*, Inżynieria Materiałowa 6 (1999), p. 595-600.

REFERENCES

- Hoepfner D.W.**, *Mechanisms of fretting fatigue*, ESIS 18, Edited by R.B. Waterhouse and T.C. Lindley, Mechanical Engineering Publication, London, (1994), p. 3-19.
- Hollahan J.L., Bell A.T.**, *Techniques and applications of plasma chemistry*, New York, John Wiley and Sons (1974).
- Holm R.**, *Electric Contacts*, Almqvist & Wiksells Boktryckeri, Uppsala (1946).
- Holmberg K., Matthews A.**, *Tribological properties of metallic and ceramic coatings*, in: Bhushan B. (Ed.), *Handbook on Modern Tribology*, Boca Raton, CRC Press (2000), p. 827-870.
- Hornbogen E.**, *The role of fracture toughness in the wear of metals*, Wear 33 (1975), p. 251-259.
- Hutchings I.M.**, *Tribology: Friction and Wear of Engineering Materials*, CRC Press (1992), Boca Raton.
- Imbeni V., Martini C., Lanzoni E., Poli G., Hutchings I.M.**, *Tribological behaviour of multi-layered PVD nitride coatings*, Wear 251 (2001), p. 997-1002.
- Johansson L.**, *Model and numerical algorithm for sliding contact between two elastic half-phase with frictional heat generation and wear*, Wear 160 (1993), p. 77-93.
- Johansson S., Ericson F., Schweitz J.**, *Solid particle erosion – a statistical method for evaluation of strength properties of semiconducting materials*, Wear 115 (1987), p. 107-120.
- Johnson K.L.**, *Contact Mechanics*, Cambridge, University Press (1985).
- Jost P.** (Chairman), *Lubrication (Tribology) Education and Research – A report on the present position and industry needs*, Her Majesty's Stationery Office, London, (1966).
- Keles O., Aykac G., Inal O.T.**, *The role of parameters in plasma assisted vapor deposition of tin/tin-oxide coatings*, Surface and Coatings Technology 172 (2003), p. 166-175.
- Kennedy P.J., Stallings L., Petersen M.B.**, *A study of surface damage at low amplitude slip*, Proc. of Conf. "ASLE-ASME Lubrication Conf.", Hartford (1983).
- Klaffke D., Skopp A.**, *Are thin hard coatings (TiN, DLC, diamond) beneficial in tribologically stressed vibrational contacts? – Effects of operational parameters and relative humidity*, Surface and Coatings Technology 98 (1998), p. 953-961.
- Klaffke D.**, *Tribological behaviour of Me:CH coating on steel against steel in the case of oscillating sliding motion at room temperature*, Diamond Films and Technology 3 (1994), p. 149-165.
- Ko P.L., Taponat M.-C., Pfäifer R.**, *Friction-induced vibration — with and without external disturbance*, Tribology International 34 (2001), p. 7-24.

REFERENCES

Kosteckij B.I., *Trienije, smazka i iznos w mashinach*, Kiev (1970).

Kragielskij I.V., Dobytchin M.N., Kombalov V.S., *Osnovy rastchetov na trenie i iznos*, Moskva, Mashinostroenie (1977), p. 321.

80. **Kula P.**, *Inżynieria Warstwy Wierzchniej*, Wydawnictwo Politechniki Łódzkiej (2000), Łódź.

Labeledz J., *Metal Treatments against Wear, Corrosion, Fretting Fatigue*, Oxford, Pergamon Press (1988), p. 87-98.

Langlade C., Vannes B., Taillandier M., Pierantoni M., *Fretting behavior of low-friction coatings: contribution to industrial selection*, Tribology International (2001), p. 49-56.

Li J.F., Liao H., Normand B., Cordier C., Maurin G., Foct J., Coddet C., *Uniform design method for optimization of process parameters of plasma sprayed TiN coatings*, Surface and Coatings Technology 176 (2003), p. 1-13.

Lindley T.C., Nix K.J., *The role of fretting in the initiation and early growth of fatigue cracks in turbo-generator materials*, Conference: multiaxial fatigue, ASTM, Philadelphia, USA, (1985), p. 340-360.

Liśkiewicz T., Fouvry S., Wendler B., *Impact of variable loading conditions on fretting wear*, Surface and Coatings Technology 163-164 (2003), p. 465-471.

Liu Q.Y., Zhou Z.R., *Effect of displacement amplitude in oil-lubricated fretting*, Wear 239 (2000), p. 237-243.

Łunarski J., *Obróbka powierzchniowa*, Praca Zbiorowa pod Red. Łunarski J., Politechnika Rzeszowska (1989).

Matthews A., Teer D.G., Thin Solid Films 80 (1981), p.41.

Mattox D.M., J. Vac. Sci. Technol. 10 No.1 (1973), p. 47.

90. **McDiarmid D.L.**, *A general criterion for high-cycle multiaxial fatigue failure*, Fatigue Fract. Engng Mater. Structs, 14 (1991), p. 429-453.

McDowell O.J., *Fretting corrosion tendencies of several combinations of materials*, Symposium on fretting corrosion, ASTM, Philadelphia, USA, (1953), p. 40-53.

Meng H.C., Ludema K.C., *Wear models and predictive equations: their form and content*, Wear 181-183 (1995), p. 443-457.

Miernik K., *Magnetronowe osadzanie powłok*, Inżynieria Powierzchni 3 (1996a), p. 22-27.

REFERENCES

- Miernik K.**, *Magnetronowe urządzenia rozpylające*, Inżynieria Powierzchni 2 (1996b), p. 15-22.
- Miernik K.**, *Podstawy fizyczne rozpylania magnetronowego*, Inżynieria Powierzchni 1 (1996c), p. 66-74.
- Miernik K., Ruta R., Trzos M.**, *Matematyczne modelowanie rozkładu grubości powłok osadzanych przy użyciu magnetronów planarnych*, Problemy Eksploatacji 13 (1994), p. 153.
- Mindlin R.D.**, *Compliance of elastic bodies in contact*, Trans. ASME Ser. E, J. Appl. Mech. 16 (1949), p. 259-268.
- Miner M.A.**, *Experimental verification of cumulative fatigue damage*, Automot. Avia Ind. 93 (1945), p. 20-24.
- Mohrbacher H., Blanpain B., Celis J.-P., Roos J.R., Stals L., Van Stappen M.**, *Oxidational wear of TiN coatings on tool steel and nitrided tool steel in unlubricated fretting*, Wear 188 (1995a), p. 130-137.
100. **Mohrbacher H., Celis J.-P., Roos J.R.**, *Laboratory testing of displacement and load induced fretting*, Tribology International 28 (1995b), p. 269-278.
- Moll E., Daxinger H.**, Patent USA Nr 4 197 175 (1980).
- Münster A., Ruppert W.**, Pat. BDN 1 142 261 (1952).
- Münster A., Ruppert W.**, *Zur Thermodynamik einiger Reaktionen des Tetrachlorids*, Zs. Elektrochemie Bd. 57 Nr 7 (1953), p. 558-564.
- Münz W.D.**, Surface and Coatings Technology 48 (1991), p. 81.
- Nakasawa K., Sumita M., Maruyaman N.**, *Effect of contact pressure on fretting fatigue of high strength steel and titanium alloy*, Standarization of fretting fatigue test methods and equipment, ASTM STP 1159, M.H. Attia and R.B. Waterhouse Eds., ASTM, Philadelphia (1992), p. 115-125.
- Neyman A.**, *Intensywoność zużycia w procesie frettingu, możliwość jej ograniczenia*, Proc. of Conf. XVIII Szkoła Tribologiczna, Radom (1992).
- Nordin M., Larsson M., Hogmark S.**, *Mechanical and tribological properties of multilayer PVD TiN/CrN, TiN/MoN, TiN/NbN and TiN/TaN coatings on cemented carbides*, Surface and Coatings Technology 106 (1998), p. 234-241.
- Ohmae N., Tzukizoe T.**, *The effect of slip amplitude on fretting*, Wear 27 (1974), p. 281-293.
- Pelczyński T.**, *Obróbka ciepło-chemiczna stali*, Białystok, Wyd. Polit. Białostocka, Ser. Rozprawy, Nr 10 (1991).

REFERENCES

110. **Qiu X., Plesha M.E.**, *A theory for dry wear based on energy*, Trans. ASME, J. Tribology 111 (1991), p. 442-451.
- Quinn T.F.J.**, *Oxidational wear*, Wear 18 (1971), p. 413-419.
- Rabinowicz E.**, *Friction and Wear of Materials*, Wiley (1995), New York.
- Rhee S.K.**, *Wear equation for polymers sliding against metal surfaces*, Wear 16 (1970), p. 431-445.
- Rie K.T., Gebauer A.**, *Plasma-assisted CVD of hard coatings with metallo-organic compounds*, Materials Science Engineering A 139 (1991), p. 61-66.
- Rigney D.A., Chen L.H., Naylor M.G.S., Rosenfield A.R.**, *Wear processes in sliding systems*, Wear 100 (1984), p. 195-219.
- Rodkiewicz C.M., Wang Y.**, *A dry wear model based on energy consideration*, Tribology International 27 (1994), p. 145-151.
- Sato K., Kodoma S.**, *Effect of TiN coating by the CVD and PVD processes on fretting fatigue characteristics in steel*, ESIS 18, Edited by R.B. Waterhouse and T.C. Lindley, Mechanical Engineering Publication, London, (1994), p. 513-526.
- Sato K., Stolarski T.A., Iida Y.**, *The effect of magnetic field on fretting wear*, Wear 241 (2000), p. 99-108.
- Sauger E.**, *Contribution à l'étude de la transformation tribologique superficielle en fretting*, Thèse Ecole Centrale de Lyon, N° 97-25 (1997).
120. **Sauger E., Fouvry S., Ponsonnet L., Kapsa Ph., Martin J.M., Vincent L.**, *Tribologically transformed structure in fretting*, Wear 245 (2000), p. 39-52.
- Schouterden K., Blanpai B., Celis J.-P., Vingsbo O.**, *Fretting of titanium nitride and diamond-like carbon coatings at high frequencies and low amplitude*, Wear 181-183 (1995), p. 86-93.
- Shaw M.C.**, *Dimensional analysis for wear systems*, Wear 43 (1977), p. 263-266.
- Shima M., Suetake H., McColl I.R., Waterhouse R.B., Takeuchi M.**, *On the behaviour of an oil lubricated fretting contact*, Wear 210 (1997), p. 304-310.
- Singer I.L., Fayeulle S., Ehni P.D.**, *Friction and wear behaviour of TiN in air: the chemistry of transfer films and debris formation*, Wear 149 (1991), p. 375-394.
- Smith K.N., Watson P., Topper T.H.**, *A stress-strain function for the fatigue of metals*, J. Mater. (1970), 5(4), p. 767-778.
- Snaper A.A.**, Patent USA Nr 3 625 848 (1971).
- Solski P., Ziemba S.**, *Zagadnienia tarcia suchego*, Warszawa, PWN (1965).

REFERENCES

- Sproul W.D.**, *PVD tool coatings*, Surface and Coatings Technology 81 (1996), p. 1-7.
- Stachowiak G.W.**, *Particle angularity and its relationship to abrasive and erosive wear*, Wear 241 (2000), p. 214-219.
130. **Stock H., Mayr P.**, *Hartstoffbeschichtungen mit dem Plasma-CVD-Verfahren*, Härtereitechnische Mitteilungen 41 No. 3 (1986), p. 145-152.
- Tomlinson G.A.**, *The rusting of steel surfaces in contact*, Proc. of Royal Society A 115 (1927), p. 427-483.
- Tyrkiel E., Dearnley P.**, *A guide to Surface Engineering Technology*, Tyrkiel E. (Ed.), London (1995).
- Vaessen G.H.G., Commissaris C.P.L., De Gee A.W.J.**, Proc. Inst. Mech. Eng. 183, London (1968-1969), p. 125.
- Varenberg M., Halperin G., Etsion I.**, *Different aspects of the role of wear debris in fretting wear*, Wear 252 (2002), p. 902-910.
- Vincent L., Berthier Y., Dubourg M.C., Godet M.**, *Mechanisms and materials in fretting*, Wear 153 (1992a), p. 135-148.
- Vincent L., Berthier Y., Godet M.**, *Testing methods in fretting fatigue: a critical appraisal*, ASTM STP 1159, M.H. Attia and R.B. Waterhouse, Eds, ASTM, Philadelphia (1992b), p. 33-48.
- Vingsbo O., Soderberg S.**, *On fretting maps*, Wear 126 (1988), p. 131-147.
- Waterhouse R.B.**, *Fretting Corrosion*, Oxford, Pergamon (1972).
- Waterhouse R.B.**, *Fretting Fatigue*, London, Applied Science (1981).
140. **Waterhouse R.B.**, *Metal Treatments against Wear, Corrosion, Fretting Fatigue*, Oxford, Pergamon Press (1988), p. 31-40.
- Wei J., Fouvry S., Kapsa Ph., Vincent L.**, *Fretting behaviour of TiN coatings*, Surface Engineering 13 (1997a), p. 227-232.
- Wei J., Fouvry S., Kapsa Ph., Vincent L.**, *Tribological behaviour of DLC coating during fretting*, Proc. of Processing and Fabrication of Advanced Materials, Singapore (1997b).
- Wendler B.**, *Simultaneous surface and bulk hardening of HSS steels*, Surface and Coating Technology 100-101 (1998), p. 276-279.
- Wendler B., Chejchman Z.**, *Wpływ powłoki z węgliku TiC wytwarzanego metodą pośrednią na trwałość narzędzi ze stali szybko tnących*, Proc. of 6th Int. Conf. on Tool Materials, Pieczyska, Poland (1997), p. 94.

REFERENCES

Wendler B., Danielewski M., Jachowicz M., Kaczmarek Ł., Rylski A., Proc. Int. Conf. Advances in Mechanics and Materials Engineering AMME-2003 in Zakopane, Poland, L. Dobrzanski (Ed.), Silesian University of Technology, Gliwice, Poland **(2003)**, p. 1033-1040.

Wendler B., Jakubowski K., Haś Z., Patent Pl Nr 167632 B1 **(1995)**.

Wendler B., *Wykorzystanie reakcyjnej, odrdzeniowej dyfuzji węgla w procesach uszlachetniania powierzchni*, Łódź, Zeszyty Naukowe Politechniki Łódzkiej 873 **(2001)**.

Westwood W.D., *Reactive sputter deposition*, in “Handbook of plasma processing technology”, Rossnagel S.M., Cuomo J.J., Westwood W.D. (Eds.), New York, Noyes Publ. **(1990)**.

Wu P.Q., Chen H., Van Stappen M., Stals L., Celis J.-P., *Comparision of fretting wear of uncoated and PVD TiN coated high-speed steel under different testing conditions*, Surface and Coatings Technology 127 **(2000)**, p. 114-119.

150. **Yashar P.C., Sproul W.D.,** *Nanometer scale multilayered hard coatings*, Vacuum 55 **(1999)**, p. 179-190.

Zhou Z.R., Fayeulle S., Vincent L., *Cracking behaviour of various aluminium alloys during fretting wear*, Wear 155 **(1992)**, p. 317-330.

152. **Zhou Z.R., Vincent L.,** *Lubrication in fretting - a review*, Wear 225-229 **(1999)**, p. 962-967.

AUTORISATION DE SOUTENANCE

Vu les dispositions de l'arrêté du 25 avril 2002,

Vu la demande du Directeur de Thèse

Monsieur S. FOUVRY

et les rapports de

Monsieur J-P. CELIS
Professeur - KU Leuven - Dept. MTM - Kasteelpark Arenberg 44 - B-3001 LEUVEN - Belgique

et de

Monsieur S. MISCHLER
Docteur - EPFL - Département DMX/LMCH - CH-1015 LAUSANNE - SUISSE

Monsieur LISKIEWICZ Tomasz

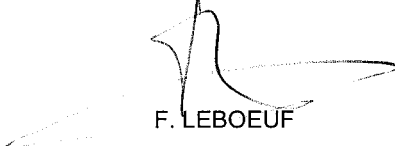
est autorisé à soutenir une thèse pour l'obtention du grade de **DOCTEUR**

Ecole doctorale MATERIAUX

Fait à Ecully, le 25 novembre 2004



P/Le Directeur de l'E.C.L.
Le Directeur des Etudes


F. LEBOEUF

